博士論文（要約）

ADDITIVE MANUFACTURING OF CELL FIBER BASED 3-D TISSUE CONSTRUCT

（細胞ファイバから構成される
3 次元組織の積層造形）

Nie Minghao

聶 銘昊

Contents

Chapter 1
Introduction

1.1 Objective and significance

Additive manufacturing (a.k.a. 3-D printing) refers to the technology that manufacture 3-D objects by depositing materials/inks in a layer-by-layer fashion. With 3-D printing, manufacturers can make existing products more efficiently—and create ones that weren't possible before[1], [2], such as printing human tissues/organs. The loss or failure of an organ or tissue is one of the most frequent, devastating and costly problems in human health care[3]. 3-D printing tissues/organs is one of the technologies that hold great potentials to manufacture replacement tissue rapidly and cost-effectively for the clinical needs around the globe. With years of research and development efforts, there has been some early successes such as 3-D printed skins[4]–[6], cartilages[7]–[9], etc. What these early successes share in common is that they aimed at printing loosely cellularized tissues/organs such as skins, cartilages, etc. However, amongst the many kinds of tissues/organs of clinical needs, densely cellularized tissues/organs (such as heart, liver, kidney, etc.) still remains difficult to be rapidly reconstructed *in-vitro*. Currently there are two major kinds of bioprinting methods: cell-printing[10]–[15] and tissue-printing[16]–[19].

Cell-printing utilize cell-ink (cell polymer mixture) to rapidly fabricate macroscopic porous cellular constructs, yet the cell density it can achieve is low ($<2\times10^7$ cells/mL); tissue-printing utilize tissue-ink (cell aggregates) to achieve high cell density, yet the fabrication time is long (generally more than 1 week).

To solve the problem, this thesis describes a bioprinter which is capable of printing high cell density multicellular microfiber (a.k.a. cell fiber[20]) based macroscopic, porous tissue construct. The creation of the bioprinter is based on the technical merging of two foundational techniques: cell fiber technology[20] and additive manufacturing technology[1], [2]. This work covers the detailed designs of the key components of the bioprinter (such as the microfluidic printhead, the syringe-vacuum substrate, etc.) as well as the practices to integrate these components as a system. Using this bioprinter, a one-step bioprinting of calcium alginate encapsulated HepG2 (a perpetual cell line consisting of human liver carcinoma cells) cell-laden collagen with high cell density ($>6\times10^7$ cells/mL) were achieved. With 4-5 days of post-printing culture, cells were able to proliferate, build cell-cell contacts and maturate into cell fibers, leading to *in-vivo* tissue-like morphologies and functions, such as human albumin secretions. The applicability of the HepG2 cell fiber based tissue construct as implantation graft for treating acute liver failure (ALF) is also tested. The 3-D shape of the printed tissue construct makes it highly handleable and easy to implant; cells were found to be alive after 3 days of implantation and human abumin was found out in mouse blood samples, showing it a promising method for maintaining blood albumin level without frequent albumin infusion.

1.2 Backgrounds and previous works

1.2.1 The “what” and “why” of 3-D bioprinting of tissue/organ

3-D bioprinting of tissue/organ leverages the power of 3-D printing (a.k.a. additive manufacturing) tool-sets to rapidly fabricate macro-sized biological tissues. 3-D bioprinting of tissue/organ could be categorized as one of the methods for modular/bottom-up tissue engineering. Modular/bottom-up tissue engineering aims to recreate biomimetic structures by designing structural features on the microscale

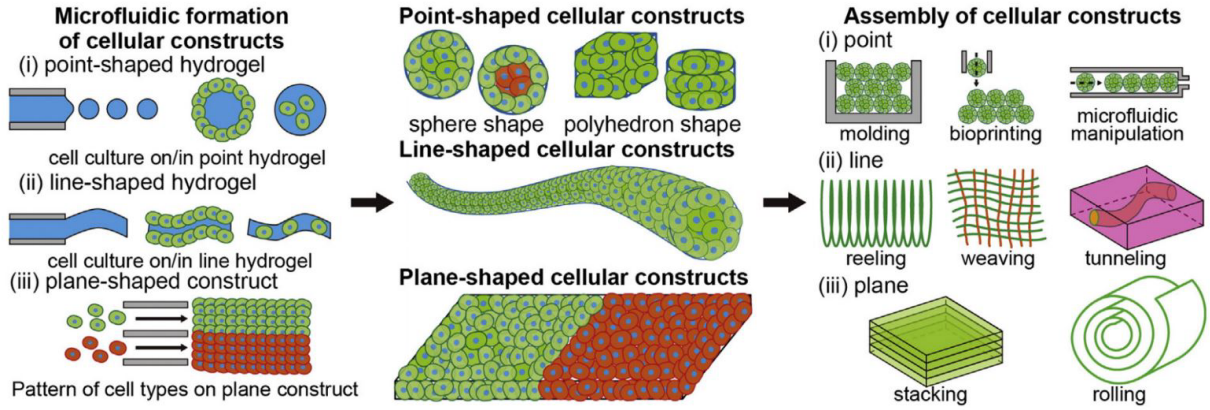

Fig. 1.1 Various types of microscale modular tissues categrorized as (1) point-shaped, (2) line-shaped and (3) plane-shaped cellular constructs. © 2015 Elsevier B.V.

to build modular tissues that can be used as building blocks to create larger tissues [21]. With the advancement of microfabrication technologies, which improves the ability of mimicking the intricate microstructural features of tissues, modular/bottom-up engineering has drawn many research attentions in recent years [22]–[25]. Now the field has evolved into a diverse one with various kinds of microscale modular tissues (μMTs) been proposed and investigated, such as point-shaped multicellular spheroids/ organoids[26], line-shaped cell-laden microfibers (CLMs)[23], [27] and plane-shaped cell-laden sheets[28], [29]. In accordance with the divergent types of μMTs, various kinds of assembling methods have also been proposed to build macro sized tissues using the μMTs as building blocks (Fig. 1.1)[24]. However, current assembling methods generally lacks flexibility, accuracy and efficiency. Many of the assembling methods are only applicable to some specific types of microscale building blocks, such as reeling/weaving to line-shaped μMTs, stacking/rolling to plane-shaped μMTs. Though molding method is both applicable to point-shaped and line-shaped μMTs, it is not capable to create heterogeneous structures and cannot place the μMTs with precise spatial control; in addition, the creation of molds is time- and labor- consuming. It is under this context that 3-D printing comes into play.

3-D printing refers to the processes which build 3-D object by depositing materials in a layer-by-layer

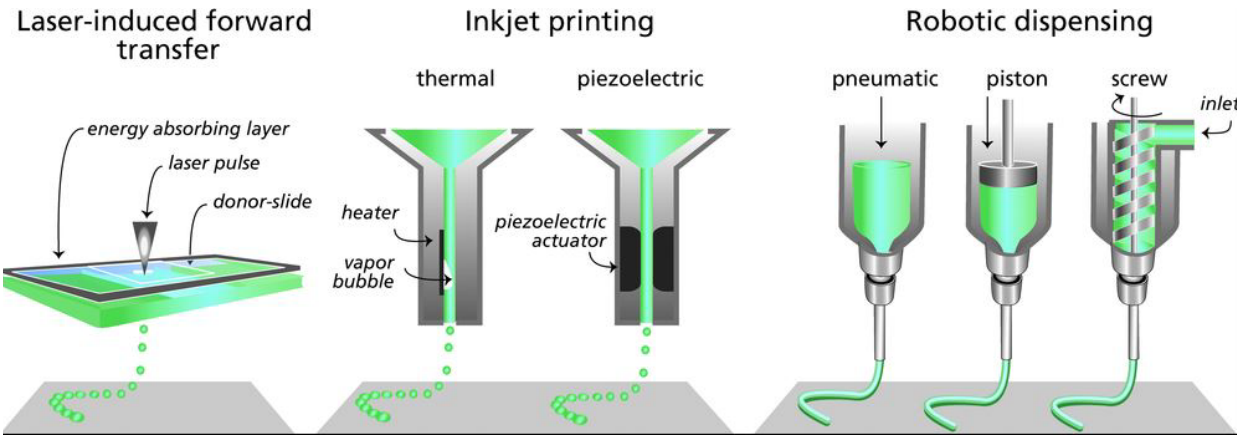

Fig. 1.2 Various types of bioprinting methods: laser-induced forward transfter genenrates laser pulse to form micro sized droplet for stacking up; inkjet printing generate local heating or peizo pressure to eject micro sized droplet for stacking up; robot dispensing use penmatic, piston or screw to push liquids forward to form strands for stacking up. © 2013 WILEY-VCH Verlag GmbH & Co. KGaA, Weinheim

fashion under computer control. After more than 40 years since the first valid patent filed by Chuck Hull in 1986[30], 3-D printing has already evolved into a series of powerful fabrication tool-sets thanks to the advancement of 3-D motion control systems as well as the development of highly automated computer-aided design (CAD) workflow; extremely complex objects with arbitrary shapes and compositions have been 3-D printed with a microscale level resolution.

With the shared philosophy of building objects from the “bottom-up”, the 3-D printing tool-sets were soon adopted by researchers in the field of modular/bottom-up tissue engineering, which eventually leads to the foundation of the field named “3-D bioprinting of tissue/organ”. Notably, the term “3-D bioprinting of tissue/organ” is different from another term called “3-D bioprinting”; “3-D bioprinting” is a more general terminology referring to all applications of 3-D printing technology in the biological/ medical fields. “3-D bioprinting of tissue/organ” focus on the fabrication of tissue/ogran using 3-D printing technology, and is the specific scope of interest in this thesis.

In 3-D bioprinting of tissue/organ, μMTs are assembled into arbitrary shaped 3-D macro tissues by

depositing and stacking up μMTs under computer control. As a proof of the applicability and versatility of the printing based approach, various types of printing systems have been implemented (Fig. 1.2)[31], such as inkjet/laser based systems to print point-shaped cell suspended droplets[32]–[35], extrusion based systems to print point-shaped tissue spheroids[17], [36] or line-shaped cellular filaments [18], [19], [37], and digital micromirror device (DMD) based systems to print patterned cellular sheets[38]–[40]. Using these printing systems, various kinds of μMTs can be assembled into macro-sized tissues efficiently with automatic computer control. In addition, the fabrication of tissue constructs with anatomical shape[10] or heterogeneous constitution[11], [13], [38], [41], [42] was also demonstrated.

To summarize, 3-D bioprinting of tissue/organ is the field created upon the technical merging of 3-D printing technology with modular/bottom-up tissue engineering technology. By taking advantage of 3-D printing tool-sets, it is possible to assemble the μMTs into macro sized 3-D tissues with beyond comparison shape/composition flexibility and spatial resolution.

1.2.2 Evaluation of existing methods for 3-D bioprinting of tissue/organ

As described in the previous section, there are various types of printing systems such as inkjet/laser based systems, extrusion based systems, digital micromirror device (DMD) based systems, etc. From a fabrication perspective, these printing system differs from each other in many aspects such as compatible material/ink types, material/ink preparation time, printing resolution, printing speed, viability, post-printing maturation time, etc. Each system has its own advantages and drawbacks, depending on the different angles posted for the purpose of comparison. This section strives to find a proper set of angles for the comparison between the existing systems; through these angles, we comment on the achievements of the existing systems, and propose the common issues/problems that are not yet well-resolved.

The prevalence of extrusion-based methods

Many kinds of additive manufacturing methods have been adapted for bioprinting of tissue/organ, such as inkjet/laser based systems, extrusion based systems, and digital micromirror device (DMD) based

Priniting method	Model name	Company	Country	Ref.
extrusion-based	3D-Bioplotter	EnvisionTEC	Germany	[44]
extrusion-based	NovoGen MMX	Organovo	USA	[44]
extrusion-based	3DDiscovery	RegenHU	Switzerland	[45]
inkjet-based & extrusion-based	Bio Factory	RegenHU	Switzerland	[45]
extrusion-based	FABION	3D Bioprinting Solution	Russia	[46]
extrusion-based	BioBot 1/2	BioBots	USA	[47, 48]

Table 1.1 A summary of the major commercial bioprinters for 3-D bioprinting of tissue/organ, their makers and the printing method they adopted.

systems. Amongst the three major types of printing methods, the extrusion based method is the most prevalent for the purpose of fast prototyping of macro-sized constructs.

Table 1.1 summarized the major bioprinters that are commercially available and the type of them, it can be found out that most of the commercial available bioprinters adopted the extrusion-based methods. The reasons is as follow. First, the extrusion based method is capable of printing sub-millimeter (several hundreds of microns) sized features, which is suitable for fast prototyping of macro-sized constructs. On the contrary, though the inkjet-based and DMD based methods can achieve high printing resolution (even up to single cell size), printing a tissue construct of clinical-relevant size takes too long time; considering that the viability of cells drops as time goes on, the task for printing macro-sized tissue is nearly impossible. Second, the extrusion-based method is gentle to cells comparing to inkjet-based and DMD-based method. The condition of thermal or laser energy needed for the generation of droplets for the inkjet-based method and the condition of strong light-exposure needed for planar patterning for the DMD-based methods are generally harmful for cells. In comparison, the extrusion-based methods relies on gentle shear forces which is less harsh for cells to survive through the fabrication process.

Since the purpose of this thesis is to create macro-sized tissue construct, we focus only on the comparison in between extrusion-based methods. Depending on type and number of the incorporated biomaterials/hydrogels, the extrusion-based methods can be further categorized into single bio- ink method and multiple bio- inks based method. In the single bio- ink based method, only one-type of bio-ink is used for additive manufacturing. The usage of only one-type of bio- ink simplified the printer system, leading to fast build-up of bioprinters. However, the mechanical strength of the material which is essential for layer-by-layer stacking up has to compromise with the bio- compatibility of the materials; currently there is yet not a good practice which finds the best balance between the need for mechanical strength and bio- compatibility at the same time. In comparison, the multiple bio- inks based method print hybrid constructs of both bio- compatible materials and mechanical supporting materials. The different materials works for two different purposes; the bio- compatible materials are generally mixed with cells to facilitate cell proliferation and phenotype expression, while the mechanical supporting materials provide the structural strength both during the layer-by-layer stacking up and after the additive manufacturing. In addition, a third type of bio- inks called fugitive inks can also be deposited in the hybrid constructs; after printing, the fugitive inks can be removed to create hollow structure to mimic blood vessels and provide perfusion culture compatibility[13], [42]. Due to the need for multiple nozzles to deposit multiple materials, nozzle switching system with precise alignment is necessary to perform multiple bio- inks based bioprinting; such requirements increases the complexity of the printer system with additional development costs, the printing time is also increased due to frequent switching of the depositing nozzles.

The emerging of microfluidics based approaches

Recently, another type of extrusion based method which utilizes a microfluidic device as the printhead emerges and draws many research attentions[11], [49]–[52]. Currently the major material that has been used for this method is alginate. Alginate is a natural seaweed derived polysaccharide which crosslinks reversibly; sodium alginate gel precursor crosslinks into alginate hydrogel upon mixing with cationic

aqueous solutions (such as Ca^{2+}, Ba^{2+} ions containing solutions); the alginate hydrogel could be de-crosslinked by chelating the cationic ions[53]. Microfluidic device featured with co-axial channel configuration is very suitable for delivering cations to sodium alginate precursors, which enables the fast prototyping of alginate fiber based 3-D constructs[49]. The reversible crosslinking property of alginate also makes it a useful templating material for 3-D bioprinting, by mixing the sodium alginate with other crosslinkable hydrogels such as GelMA, interpenetrated polymer network (IPN) can be created during the bioprinting process, after the IPN formation, alginate could be selectively removed effectively[11]. The major advantage of the microfluidics based approach is the low viscosity of the bio- inks, since the crosslinking of the hydrogel only happens at the very tip of the microfluidic printhead, the pressure drop on the whole tubing path along which the bio- inks are delivered can be drastically decreased; such decrease in pressure enables fast fluidic response and makes it possible to load higher density of cells inside comparing to the viscous bio- inks used for non-microfluidics based approaches.

Bio- ink formula: "cell-printing" and "tissue-printing"

Just as mentioned previously, the bio- ink used for bioprinting of tissue/organ is composed of biomaterials and living cells. For the extrusion-based bioprinting, currently there are two major types of bio- inks: cell spheroids/strands and cell suspension within biomaterials (mostly hydrogels). For simplicity of description, we name the cell spheroids/strands "tissue-ink" and the cell suspension with biomaterials "cell-ink"; the relative printing methods using "tissue-ink" or "cell-ink" is thus referred to as "tissue-printing" and "cell-printing" in this thesis (Fig. 1.3).

Tissue-inks are prepared based on the principle of self-assembly. The key to boost-up the process of self-assembly is to create a culture condition under which cells cannot attach to a biomaterials surface and are forced into contact with each other[26]. Cell spheroids can be prepared using practical techniques such as hanging-drop cultures[56], [57], micro-well condensations[58], [59], microfluidic droplet encapsulation[60] etc. Due to the high-throughput possibility of these methods, feasible spheroid generation platforms have been developed not only in labs but also commercialized. Cell strands can be

他者の著作権に関わる図版を使用しているため，本図を非公開とする.

Fig. 1.3 Different types of bio- inks and their relative printing methods and images of cellular constructs right after printing and after postprinting maturation. © 2009 Elsevier, © Ozbolat. et al. © 2015 WILEY-VCH Verlag GmbH & Co. KGaA, Weinheim, © Cho et al., © 2016 Elsevier.

prepared by collecting cell pellets (i.e. cell sediments after centrifugation) and injecting them into semi-permeable tubes, upon culture, the cell-cell contacts will be established to thus a handleable/printable strand-like structure[18], [19]. The major advantage of using the cell spheroids/strands as bio- inks is that: (1) since the cells are condensed in order to facilitate cell-cell contacts, the cell density of the bio-inks is generally high; (2) ECMs are secreted by the cells themselves, which could potentially cut the fabrication cost since ECMs are generally expensive. Preparation of the cell spheroids/strands takes from several days to more than a week.

Instead of forming tissue-inks, a more straight forward method for bio- ink preparation is to directly mix cells with other biomaterials to form the so-called “cell-inks”. Several advantages of this method is as follow. Firstly, it can drastically shorten the bio- ink preparation time, the process only involves recollecting of cells from dishes and simple mixing of cell pellets with other biomaterials. Secondly, the material properties of the bio- inks could be tailored for various purposes; mechanical property could be strengthened for improved printability and fidelity[61], rheological properties such as low intrinsic viscosity[11] or shear-thinning[41] could decrease cell damage during bio- ink extrusion, capability of preloading chemical cues (such as growth factors) controlled cell proliferation and differentiation[54], etc. The major drawback of this method is that most of the printed materials are stiff to facilitate layer-by-layer stackability, which will result in low cell density (Table 1.2) and restrained cell migration and cell-cell contacts.

Bio- ink type	Cell density (cells per mL)	Suspension Material	Ref.
cell-ink	1×10^6	1% (w/v) alginate, 10% (w/v) gelatin and 0.513, 0.615, 0.82, and 1.025mg/ml collagen	[15]
cell-ink	5.25×10^6	Sodium alginate 4% w/v	[12]
tissue-ink	2×10^6 *	2%, 4% and 6% sodium alginate	[8]
tissue-ink	2×10^8 **	N/A	[62]
tissue-ink	100% cellular	N/A	[37]
cell-ink	5×10^6	alginate	[63]
cell-ink	4×10^7	3 mg/mL hyaluronic acid, 35 mg/mL gelatin, and 25 mg/mL fibrinogenin	[64]
cell-ink	5×10^6 ***	35 or 45 or 35 mg/ml Gelation, 20 mg/ml Fibrinogen, 3 mg/ml HA, 10% v/v Glycerol	[10]
cell-ink	2×10^6 ****	7.5 wt/vol% gelatin and 10 mg/mL fibrinogen	[42]
cell-ink	1×10^7	4% w/v alginate, 4.5% w/v GelMA, 0.2% w/v photoinitiator, in water-HEPES-FBS	[11]
cell-ink	2×10^6	PEGX(polyethylene glycol(PEG) ending in two reactive groups), gelatin	[14]
tissue-ink	100% cellular	N/A	[18]

* cell concentration of 2×10^6, 4×10^6 and 8×10^6 are tested, most experiments were performed with 2×10^6.

** 2×10^8 is the cell concentration of the cell strands, while HUVECs of 1×10^7 is also used.

*** 5×10^6 for Human AFSCs, 4×10^7 for Rabbit ear chondrocytes, 3×10^6 for C2C12.

**** cell concentration of 0.1×10^6 to 10×10^6 are tested, most experiments were performed with 2×10^6.

Table 1.2 Summary of the bio-ink type, cell density and the material compostion of representative 3-D bioprinting of tissue/organ works.

Time schedule of the 3-D bioprinting of tissue/organ

Though the name of 3-D bioprinting of tissue/organ inherited the word “printing” from the traditional paper printing technology, there is apparently many differences between these two. One of the key difference is the time schedule of the printings decided by their workflows. The traditional workflow of paper printing starts from transmitting printing data to the printer, followed by the deposition of inks onto paper performed by the printer under computer control, and finally after a short time (less than a few seconds) for the inks to dry up, the printed paper is ready for use. In comparison, the workflow of the 3-D bioprinting of tissue/organ is different majorly in the following two aspects. First, unlike the ink/toner used for paper printing which is commercially available and can be stored for years, the bio-ink used for bioprinting of tissue/organ is composed of biomaterials and living cells, which have to be prepared freshly immediately before printing to maintain their biological activity and viability; the preparation time of the bio- ink takes from a few hours to weeks. Second, after the printing, the 3-D tissue construct has to undergo a post-printing maturation process in which the printed cells proliferate and build cell-cell/cell-ECM contact or the printed microscale tissues fuse together[65]; this process generally takes days to weeks, or even months. The post-printing maturation time is also dependent on the goal of application. For the recreation of loosely cellularized tissues/organs (such as bones, cartilages and skins), the post-printing time might be short or even negligible; for the recreation of densely cellularized tissues/organs (such as livers, kidneys and hearts), the post-printing time might take weeks or even desperately long.

1.3 Current challenges

By checking out the final cell density and fabrication time of the representative works in the field of bioprinting, a technical mapping summarizing these works could be found in Fig. 1.4. As shown, the cell-printing works appears in the region where the final cell density is low while the fabrication time is short; on the contrary, the tissue-printing works appears in the region where the final cell density is high while the fabrication time is long. For the purpose of rapid creation of high density tissue constructs,

methods which can fabricate high cell density in a short time is highly expected.

The reason that caused the current technical limitations is as shown in Fig. 1.5. For the purpose of printing tissue constructs with native tissue-like cell density, it is favorable that the initial cell density be as high as native tissues. Comparing the two major types of printing methods (i.e. cell-printing and tissue-printing), tissue-printing could achieve much higher cell density. However, the preparation time for cell spheroids/strands takes long time (from days to weeks). In addition, the cost to prepare cell spheroids/strands is also not negligible, since specially designed culture systems are needed. On the contrary, the step of ink preparation for cell-printing is both cost- and time- effective, the cell-inks could be prepared by collecting centrifuged pellets and simply mixing them with biomaterials using pipettes. The problem for the cell-printing method is as follow. First, the initial cell density is limited due to the generally high viscosity of the biomaterials. The static viscosity of the polymer is essential for maintaining the structure integrity of printed layers, since the polymer gelation is slow and generally takes long time. The high viscosity of the inks will demand high extrusion pressure, which is generally harmful for the cells. Second, the biomaterials needs to be stiff to provide mechanical strength during printing, yet the stiffness of the biomaterials generally hinders cell proliferation, migration and phenotype expression. Matrix stiffness is an important regulator for the proliferation, migration and phenotype expression of cells[66], [67]. Not specifically for the goal of bioprinting, many works have been conducted to find out the relationship of cell behaviour to matrix materials[68]. Some of the researches indicated that the increased matrix stiffness either facilitates or hinders the proliferation or migration of cells, depending on the type of cells and ECMs used for investigation. However, the stiffness range of these previous discussions is quite narrow (generally < 1 kP) and which is not the case when discussing the material stiffness for bioprinting. Practically for bioprinting, the material stiffness is generally tuned to be greater than 10-15 kPa[69]; in this stiffness range, the high polymer fractions can be debilitating to cells, preventing spreading, migration, and proliferation, and therefore, are not ideal candidates for cell-laden constructs[11], [14]. As a brief summary, the illustration on the fabrication window of current biofabrication technology can be found out in the inset of Fig. 1.5, which described the existing

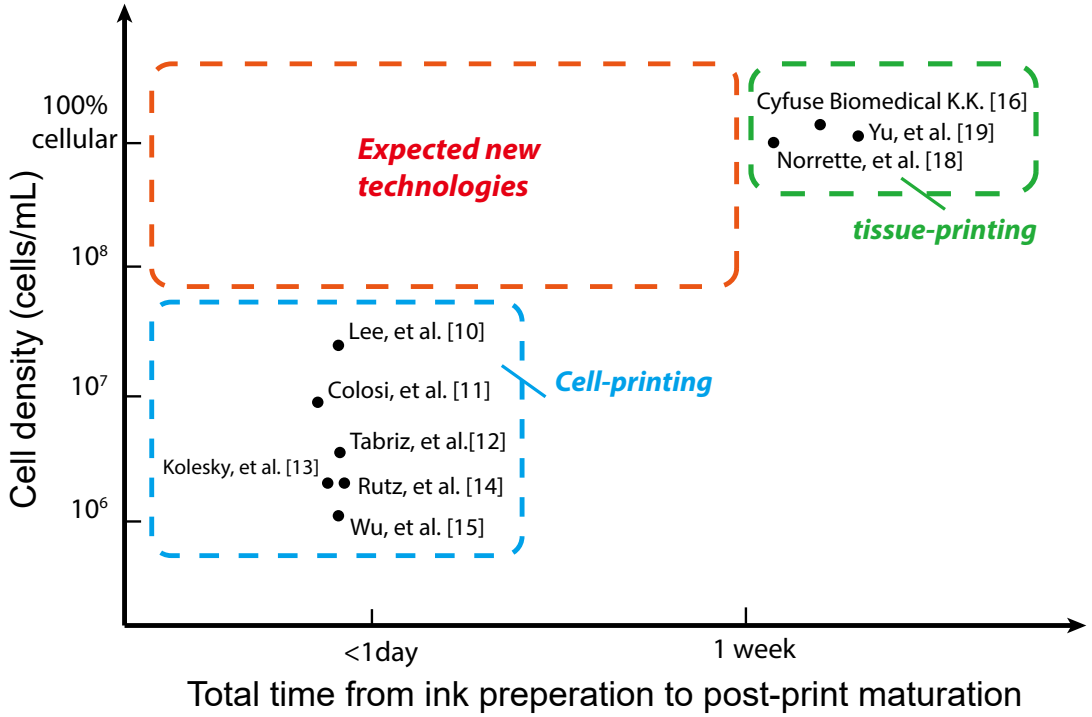

Fig. 1.4 Technical mapping of current bioprinting works in terms of the cell density and total fabrication time. The cell-printing and tissue-printing works appears in the region where either the final cell density is low or the fabrication time is long; new technologies for rapid creation of high density tissue constructs shall be expected.

contradiction between shape fidelity and material cell compatibility [31].

1.4 Proposed method and its application

1.4.1 Proposed method: cell fiber printing

This thesis propose to manufacture high density tissue construct by additively depositing cell fibers. Cell fiber (Fig. 1.6) is a thin (approximately 100 μm) and finely handleable cellular construct which exhibit tissue morphologies and functions[20]. Cell fiber is fabricated by first generating a core/shell cell-laden hydrogel microfiber using double co-axial microfluidic device; the core of the hydrogel microfiber is cell suspension (1×10^7~3×10^8 cells/mL) with collagen; the shell of the hydrogel microfiber is calcium alginate, a bio-inert polysaccharide with fine mechanical strength and semi permeability. Within culture,

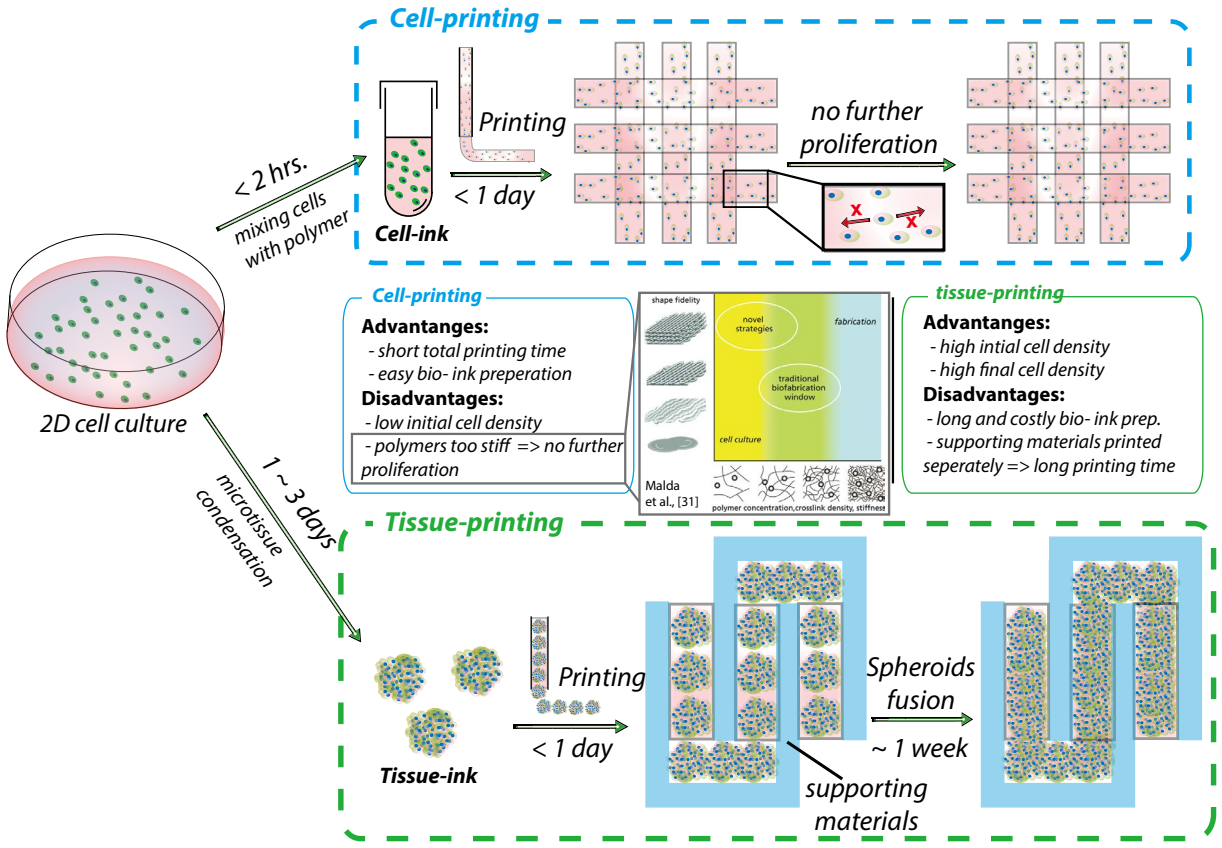

Fig. 1.5 The comparison between the cell-printing methods and tissue-printing methods: their detailed processes and relative disadvantages. © 2013 WILEY-VCH Verlag GmbH & Co. KGaA, Weinheim

nutrients and oxygens penetrate through the calcium alginate shell and reaches cells in the core; cells in the core proliferate, build cell-cell contacts and finally forms into cellular constructs; finally, the calcium alginate is removed by de-crosslinking. By printing the cell fiber, the current challenge described in the previous section can be addressed since: (1) short ink preparation time (< 1 day) can be achieved; (2) high cell density tissue construct can be created with tissue-like morphology and function.

To form the cell fiber, three kind of bio- inks will be used: cell/collagen mixture (> 6×10^7 cells per mL), sodium alginate aqueous solution and calcium chloride aqueous solution. Unlike the multi- nozzle approach which deposit multiple types of bio- inks separately, a microfluidic based approach is adopted to simultaneously print the three types of bio- inks in co-axial configuration. Upon the crosslinking of sodium alginate into calcium alginate, hydrogel microfibers with cell/collagen mixture as its core

encapsulated in calcium alginate shell will be formed during printing. Due to the low stiffness of collagen (2 mg/mL) and high initial cell density, the cells encapsulated in the core region of the microfibers are expected to maturate into densely cellularized cell fibers within several days upon culture. With the intensive cell-cell contacts reconstructed in the cell fibers, native tissue-like morphology and function will be achieved.

Currently, there is yet no commercial available bioprinter which is capable of printing cell fibers. This thesis plans to start from the construction of a bioprinter with the capability of printing cell fibers. To construct the bioprinter, several components of it will be originally designed, including the microfluidic printhead for the generation of core/shell hydrogel microfibers *on-a-fly*, and the syringe-

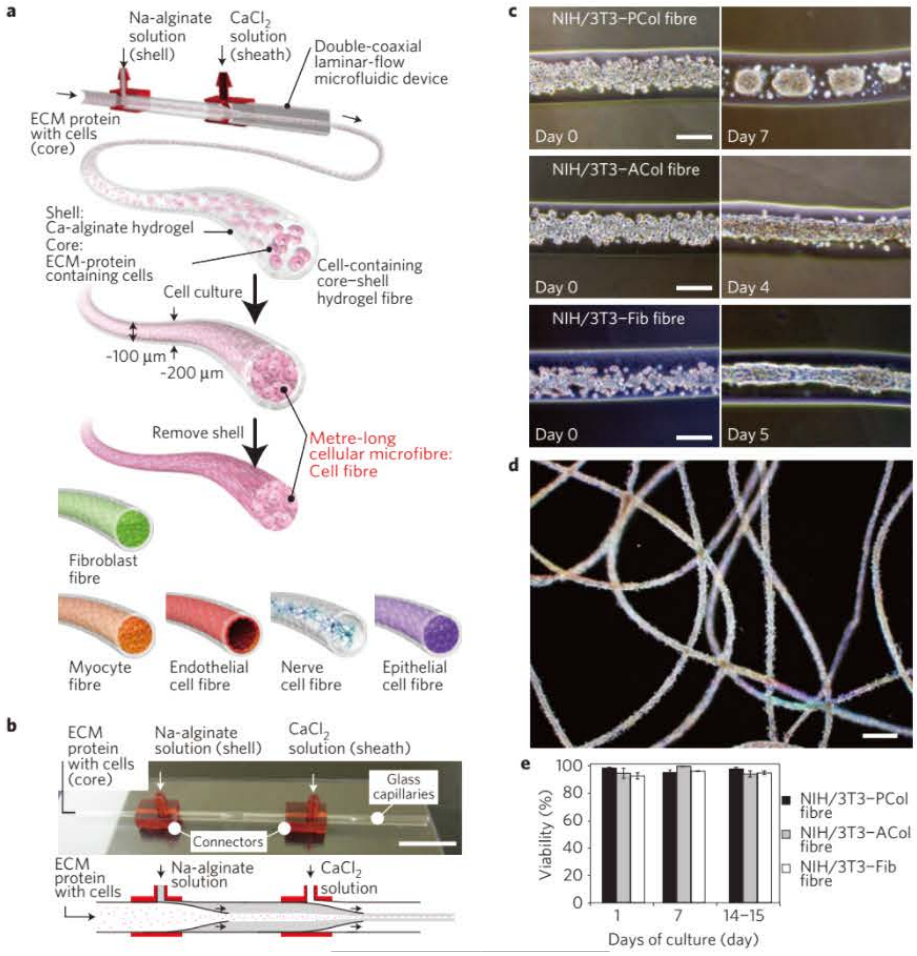

Fig. 1.6 The cell fiber technology. The cell fibers are created by first generationg cell-laden core/shell hydrogel microfibers, with cell/ECM mixture encapsulated in the core region of the microfibers. With cell culture, cells are able to proliferate and maturate into densely cellularized fiber shpaed tissues. © 2013 Macmillan Publishers Limited.

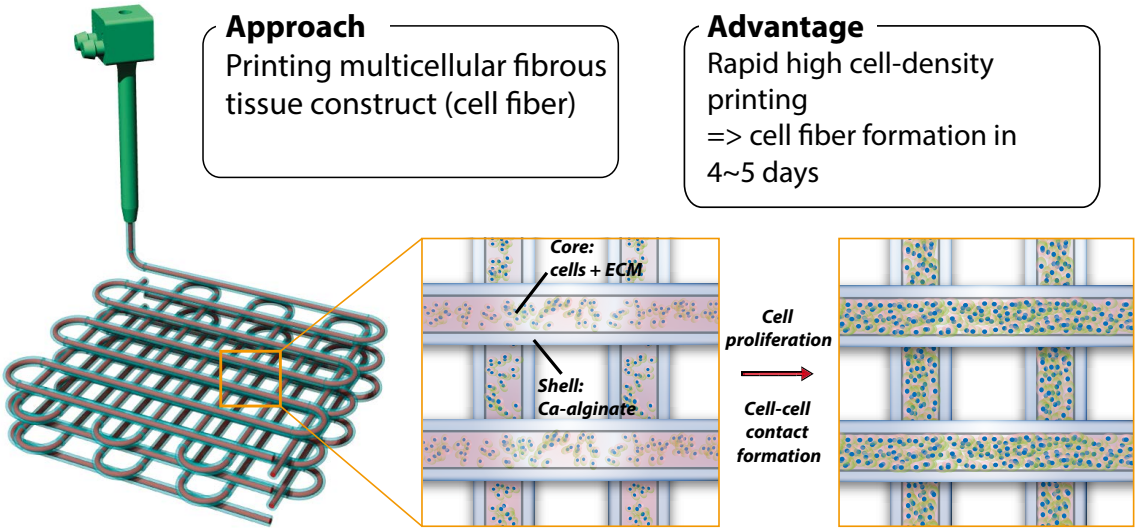

Fig. 1.7 A schematic illustration of the cell fiber printing technology. By printing cell fibers, rapid construction of highly densed tissue construct can be fabricated within 4~5 days.

vacuum substrate for the smooth and feasible deposition of the microfibers. Besides the microfluidic printhead and the syringe-vacuum substrate, commercially available motor stage and syringe pump will be adopted and installed. With all its components ready, the bioprinter for cell fiber printing will be finally assembled and tested. Using the bioprinter, optimized set of parameters for stable printing of core/shell hydrogel microfibers will be established. Then, we will demonstrate the printing of cell fibers and investigate the printed constructs in detail regarding its dimensional parameters and the ability of forming cell fibers upon culture.

1.4.2 The application of the cell fiber printing technology

As shown in Fig. 1.8, the cell fiber based macroscopic, dense and porous tissue construct is expected to have *in-vivo* tissue like high cell density with intensive cell-cell contacts, it has the potential of benefiting the pharmaceutical industry by providing *in-vitro* tissue samples for early stage drug screening[70]–[72]. Another possible application of the cell fiber based tissue construct is to use it as implantation graft for

treating organ-failure related diseases. Specifically, this thesis will target on proofing the potential of using HepG2 (a human liver cancer cell line) cell fiber based tissue construct as short-term implantation graft for treating acute liver failure disease. The fact that liver failure constitutes a life-threatening condition and can, in most cases, only be overcome by orthotopic liver transplantation, lead to the development of various artificial and bioartificial liver support devices[73]. Some of the liver disease such as fulminant hepatic failure (FHF) generally runs a rapid course with high mortality rate. The treatment of such diseases relies on liver transplantation within 72 hours[74], however, the waiting time for searching liver donors is generally longer. Here, we propose to use the hepatocytes cell fiber based tissue constructs as an implantable artificial organ to bridge the 72 hours vacancy until the transplantable liver is available. HepG2 cell pertains some specific liver functions, such as human albumin secretion. After checking the function of printed HepG2 cells for the proof-of-concept, other hepatocyte cell lines could be used in the future for printing hepatocyte cell fibers with various types of liver specific functions besides albumin secretion.

In experiment, we will print thick (i.e. 12 layers) HepG2 cell fiber based tissue construct with its size chosen as ca. 15mm×15mm×2mm. The thick tissue construct is supposed to contain higher amount of functional cells within a limited surface area for implantation; during implantation, an abdominal incision will be opened on the mouse body for the purpose of implantation, normally the length of this incision is smaller than 2~3 cm for laboratory mouses. Before implantation, the *in-vitro* albumin secretion of the printed tissue construct will be assessed by enzyme-linked immunosorbent assay (ELISA). Then, the HepG2 cell fiber based tissue like construct will be implanted into the abdomen of severe combined immunodeficiency (SCID) mouse for 3 days. The mechanical integrity of the cell fiber based tissue constructs will be evaluated during the implantation to find out whether it is easy to implant and retrieve with minimum cell leakages. The cell viability will be evaluated after 72 hours of implantation.

1.4.3 Development road map for cell fiber based printing technology

As apparent as it is literally, the ultimate goal for bioprinting of tissue/ogran is to reconstruct native-like functional organs. The development towards the final goal is as shown in Fig. 1.9. At the initial stage,

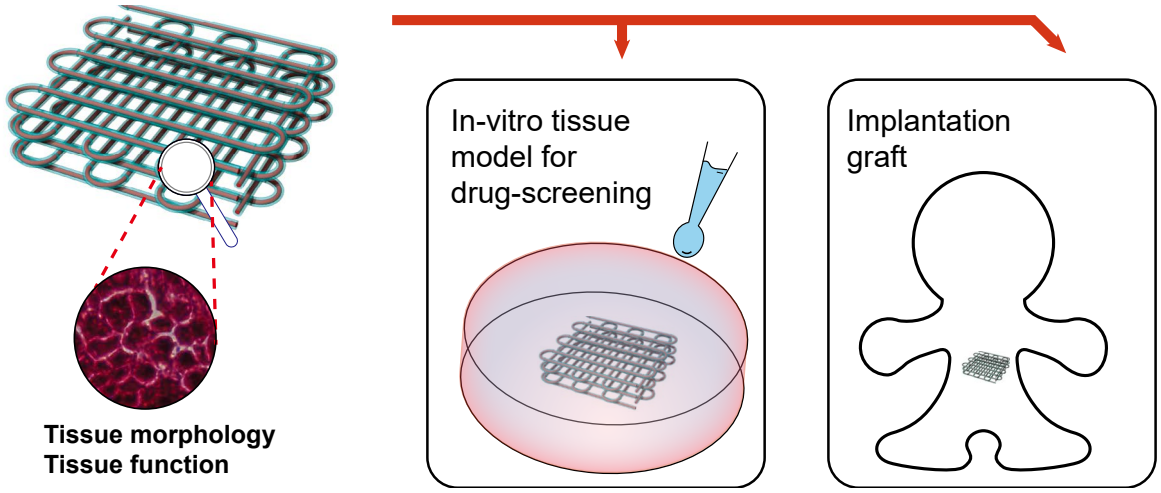

Fig. 1.8 The cell fiber based macroscopic, dense and porous tissue construct is potentially useful as in-vitro tissue model for drug-screening and implantation graft as functional substitute for damaged tissue.

technological developments are concentrated on enabling the printing of cells and maintain the viability of cells; at this stage, the cell density can be achieved is low and the printed constructs are almost homogeneous (i.e. with only one cell type). In the next stage, the focus is to enable the heterogeneous and high density printing of cells. Cell fiber printing technology developed in this work is the first substage with the goal of enabling high density printing of cells, the next substage is to develop methods for printing heterogenous structures. The following stage is the incorporation of vasculature inside the printed tissue. Then, at the final stage, efforts will be taken to further enhance to shape and size control to create artificial organs with anatomically correct shape and morphology.

Specifically, for the cell fiber based printing strategy, the cell fiber printing technology developed in this thesis will be the first and foundational step towards the ultimate goal of building densely cellularized tissues(Fig. 1.10). Based on the technology developed in this thesis, further developments on both the printing system and the relative culture system can be expected. Regarding the printing system: first, the ability to print hollow fibers with endothelial cells encapsulated in the core region will have the potential to enable lumen structure reconstruction in the cell fiber based tissue construct; second,

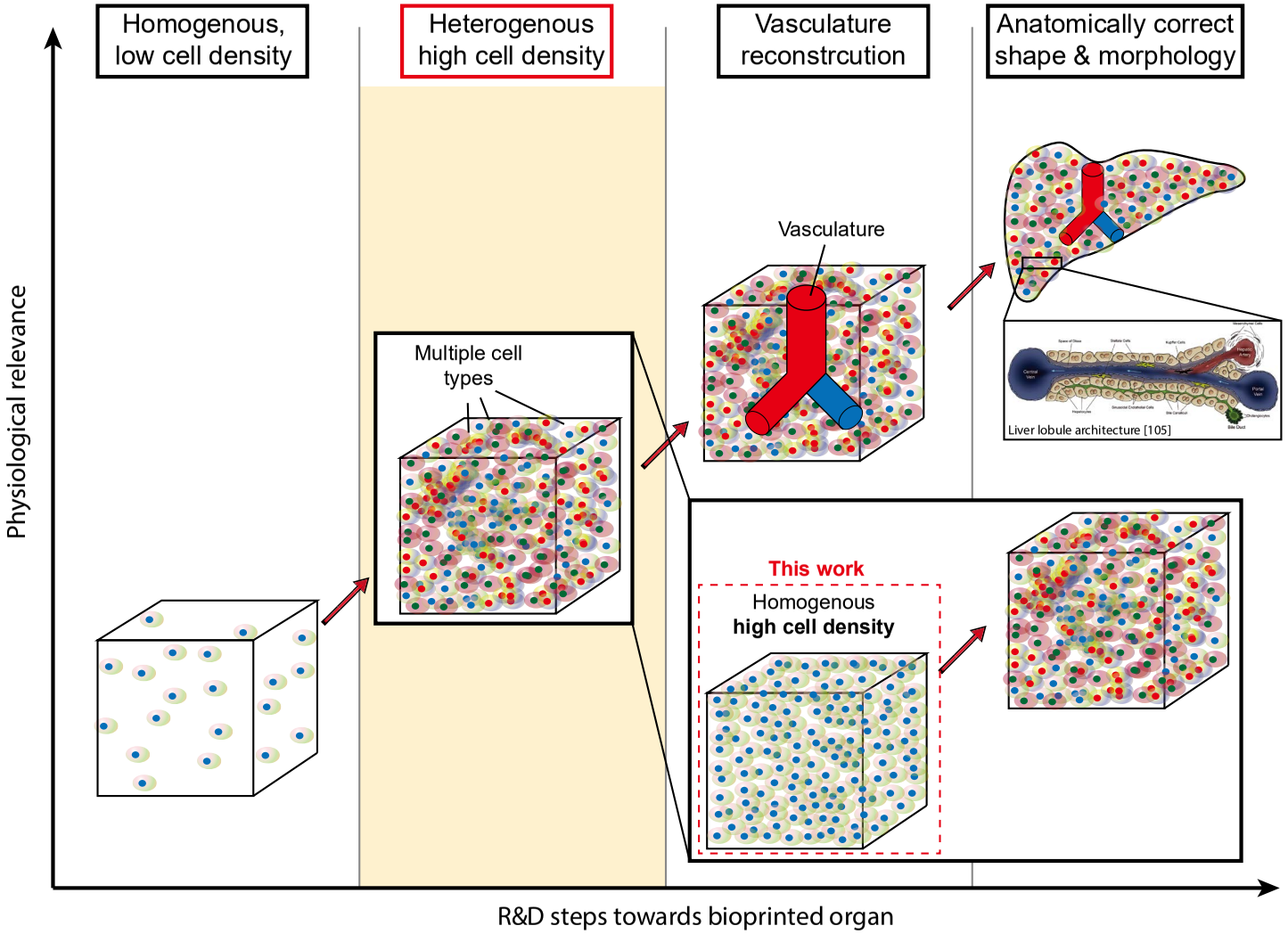

Fig. 1.9 Developement road map for bioprinting technology. Towards the bioprinted organ, repilcation of key physiological features such as cell density, heterogeneity, vasculature, anatomically correct shape and micro architecutre shall be achieved.

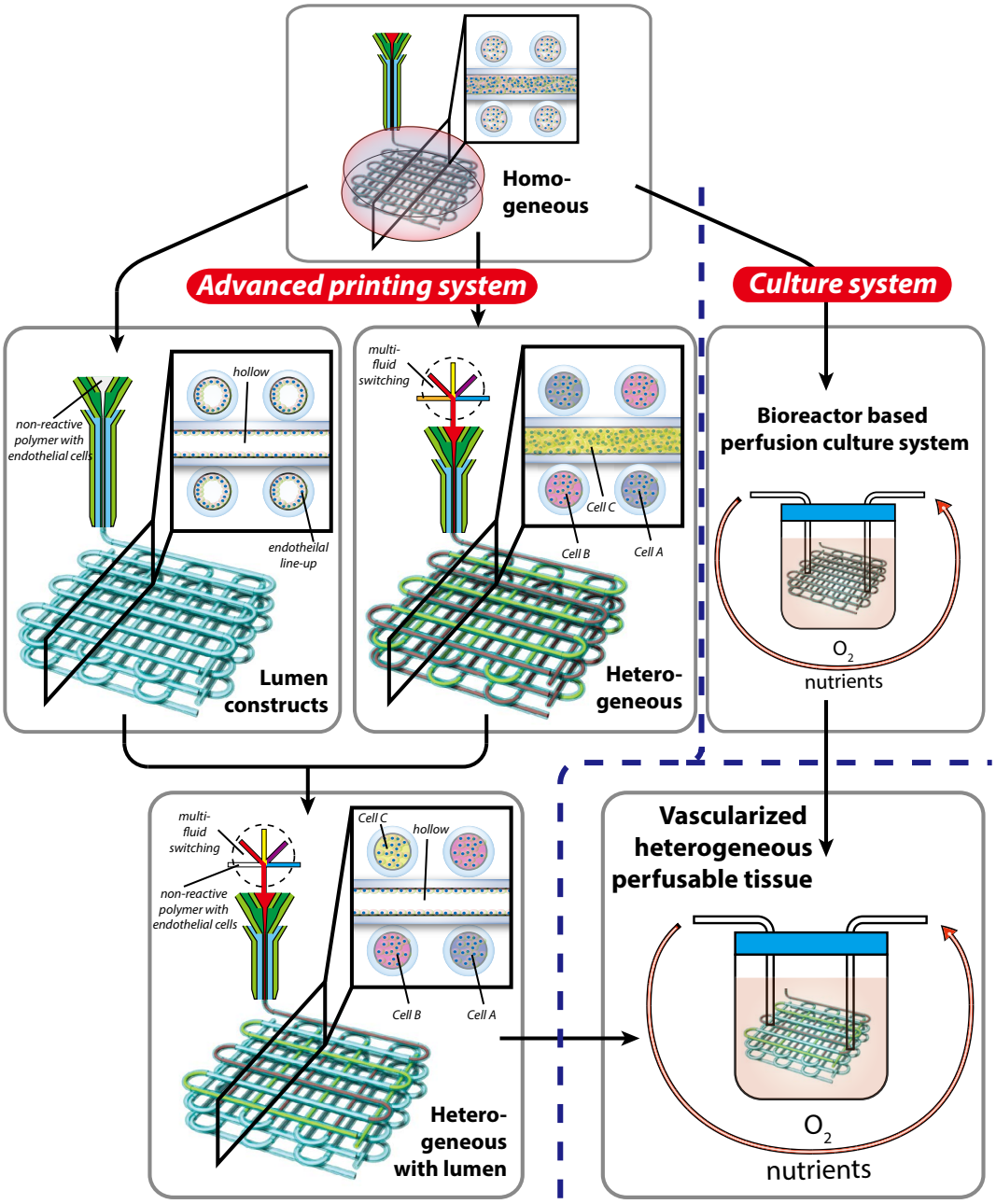

Fig. 1.10 Developement road map for the cell fiber based printing technology to achieve vascularized, heterogeneous and perfusable tissue. The efforts shall be devided into two sub-categories: (1) advanced printing system to integrate more functionalities to the printhead such as fluid switching; (2) culture system to develop bioreactors for active perfusion of the construct.

microfluidic fluid switching techniques could be integrated to enable the fabrication of heterogeneous cell fiber based construct with multiple types of cell fibers deposited with precise spatial control;

finally, the combination of these two technology is able to fabricate heterogeneous tissue constructs with capillary vessel networks. Alongside the development of printing system, the culture system development is also essentially important. Bioreactors with controlled oxygen delivery and the capability of perfusing the cell fiber based constructs will further increase the maturation speed of the cell fibers; in addition, the inletting and outletting system of the bioreactor actually mimics the major blood vessels which connect internal organs to circulation system, thus will facilitate the practical usages of the *in-vitro* reconstructed tissues such as for implantation purposes.

1.4.4 Towards clinically application of cell fiber based implantation graft

In this thesis, the proof-of-concept experiments of using the cell fiber based tissue construct as implantation graft is conducted. Based on the proof-of-concept work in this thesis, further developments towards real application of using the printed tissue constructs as implantation graft can be expected.

For practical application, several improvements on the technique is required.

First, the size of the printed construct should be able to scale up further to encapsulate more amount of cells, in order to be applied for larger animals comparing to mouse. While increasing the size of the construct, the mass transfer effect shall be taken into consideration to guide the shape optimization of the construct.

Second, other types of hepatocytes should be adopted to replace HepG2 cells which are used in this thesis; as a cancer derived cell, HepG2 cell exhibit abnormal liver functions comparing to normal hepatocytes, the encapsulation of normal hepatocyte is expected to create tissue constructs with more native liver functions. In addition, liver tissue is generally composed of both parenchymal (functional) and stromal (structural) cells in a mixed coexistent manner; such coexistence is essential for the function promotion of liver tissue. In future works, the parenchymal/stromal coexistence should be adopted for the cell fiber based constrcut by adpoting hepatocyte and stromal cells mixture as the cellular ink.

Third, foreign body react which will attack the implanted tissue graft shall be attenuated for longer survival of cells in the implanted graft. As shown in Fig. 1.11, the foreign body react will recruit immune

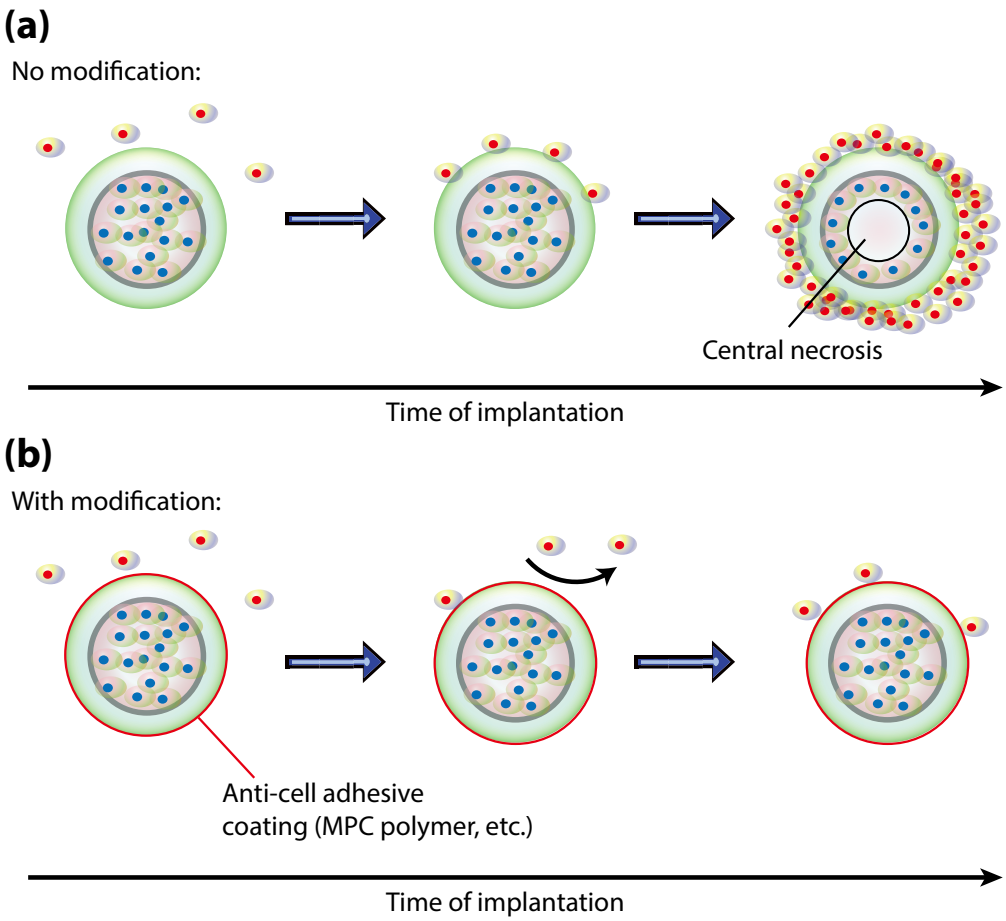

Fig. 1.11 The foreign body react can be attenuated by modifying surface chemistry of the alginate fibers. (a) without modification, immune cells will gradually adhesive onto the fibers and causes cells to die inside due to lack of mass transfer; (b) with modification, cell adhesion can be attenuated, thus enabling longer implantation time.

cells to adhesive on the surface of the alginate fiber based constructs, eventually causing the cells to die inside the central area of the fiber. Adjusting the surface chemistry of the alginate fiber which is used to encapsulate cells can be a possible method to attenuate the immune attack due to foreign body react. For the clinically application of the cell fiber based construct, methods for surface coating of anti- cell adhesive polymers (such as 2-Methacryloyloxyethyl phosphorylcholine (MPC) polymer, etc.) shall be developed.

1.5 Thesis outline

This thesis is composed of 5 chapters.

Chapter 1 describes the objective and significance of this research, introduces the background knowledges and previous works. The current challenge will be proposed upon analyzing previous works. Then, the proposed method in this work will be described.

Chapter 2 describes the construction of the bioprinter. The theory, design, fabrication and bench test of each key component of the bioprinter will be covered in details.

Chapter 3 describes the printing process, as well as the results of bioprinting w/o and w/ cells. Post-print culture of the cell-laden fiber based constructs will be further described.

Chapter 4 describes the application of the cell fiber based constructs.

Chapter 5 summarizes this thesis and provides future outlooks.

Chapter 2
The construction of the bioprinter for cell fiber printing

This chapter describes the theoretical consideration, the actual design and the implementation of the bioprinter. First, the system composition of the bioprinter will be introduced, followed by detailed description on each components of the bioprinter. Then, the actual design and fabrication of each component will be described in details, with results and analysis of the bench tests for each component.

2.1 System composition of the bioprinter

As shown in Fig. 2.1, the bioprinter is composed of (1) microfluidic printhead, (2) vacuum substrate, (3) 3-axis linear motor stage, (4) multi-syringe pump and the relative mechanical clamping (such as printhead fixation board, manual rotational stage) and fluidic tubing systems. The microfluidic printhead is capable of generating microfibers with core/shell configuration on-a-fly. The vacuum substrate is the key for smooth and feasible deposition of the microfibers generated by the microfluidic printhead. The 3-axis linear motor, onto which the microfluidic printhead is fixed, is used to automatically move the microfluidic printhead in three dimensions under computer programmed control. The multi-syringe

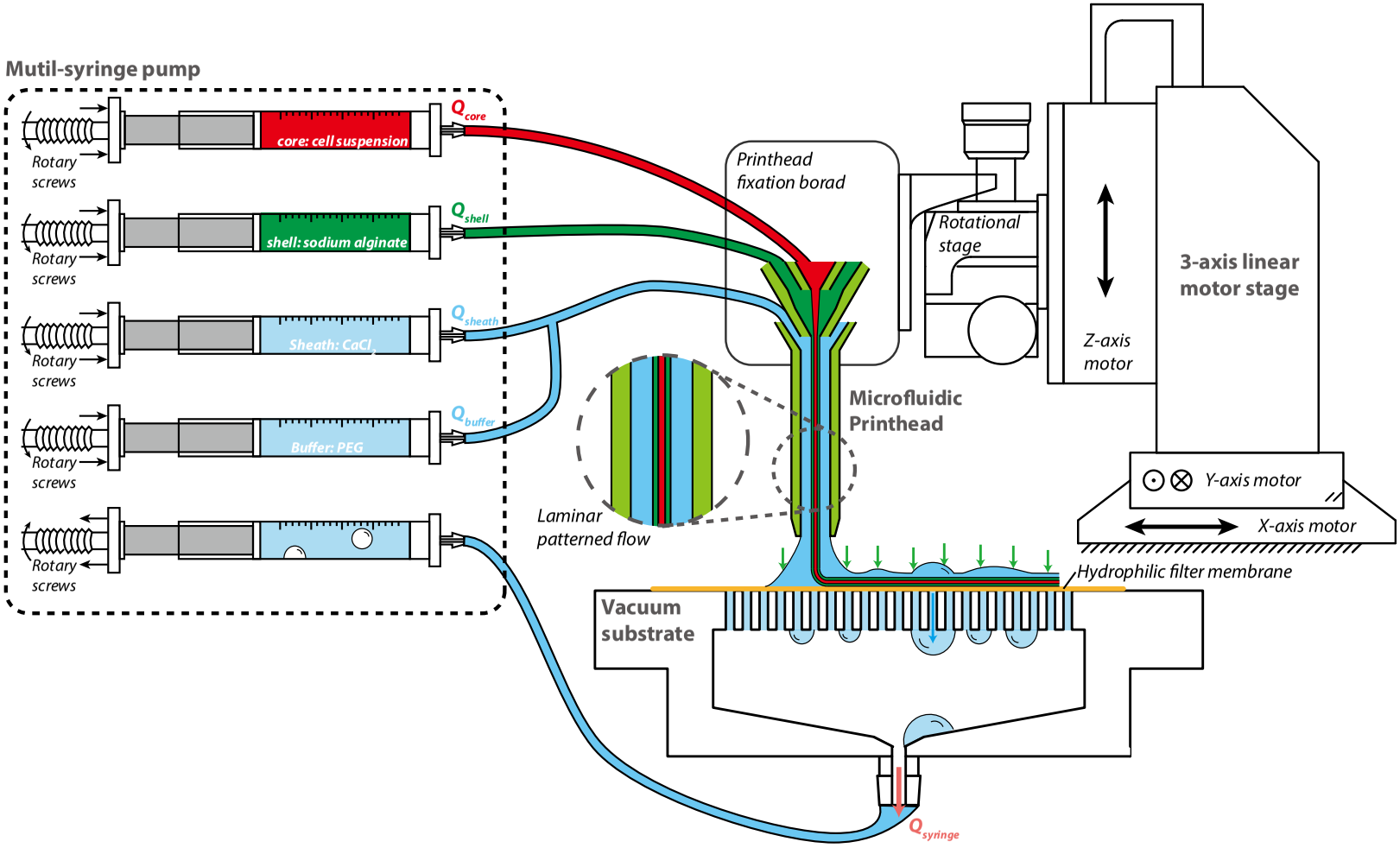

Fig. 2.1 Systematic scheme of the bioprinter including: (1) microfluidic printhead, (2) vacuum substrate, (3) 3-axis linear motor stage, (4) multi-syringe pump and the relative mechanical clamping (such as printhead fixation board, manual rotational stage) and fluidic tubing systems.

pump generates injection flows into the microfluidic printhead, as well as the ejection flow that generates vacuum for the vacuum substrate. During the printing process, all components cooperate automatically under computer control, in order to provide precise deposition of microfibers into complex patterns.

2.2 Microfluidic printhead

The microfluidic printhead is a kind of microfluidic flow focusing device, which is capable of forming co-axial flow patterns for the generation of threads. Here in this section, a brief review on the working principle and fabrication of the flow focusing device used for hydrogel microfiber formation will be given. The specifically requirements for using the microfluidic device as the printhead of the bioprinter will be discussed. Based on the comparison between each device fabrication methods, stereolithography based method is chosen to create the microfluidic printhead for the bioprinter proposed in this thesis. Detailed design and fabrication will be described in this section. Then, evaluation tests of the microfluidic printhead will be performed with a focus on the fiber spinning stability, fiber diameter control, core/shell mixing and fiber spinning velocity.

2.2.1 Microfluidic flow focusing for hydrogel microfiber spinning

Just as mentioned before, the microfluidic printhead is a kind of microfluidic flow focusing device. Flow focusing (a.k.a. hydrodynamic focusing) is a technique used for creating jets at extremely small scales[75]. In flow focusing, a central fluid stream is generated by confining it using a surrounding fluid stream. Amongst the many application of flow focusing technique, microfluidic flow focusing uses microfabrication tools to create microscale flow focusing.

When working with microfluidic flow focusing device, two or more fluids are introduced and combined inside the device. The part of the microfluidic channel at where different stream combines is called junction channel.The key to generate flow focusing in microfluidics is to have proper junction channel geometry. T-shaped or co-axial cylindrical shaped channel geometries are the major types for generating flow focusing. T-shaped channels are consisted of a central channels with two symmetrically

arranged sheath channels on its sides; co-axial cylindrical channels are consisted of two cylindrical channels with their axis aligned on the same position.

With microfluidic flow focusing, micro droplets/emulsions can be generated with high size-uniformity[76]; in addition, chemical reaction mechanisms can be combined with microfluidic flow focusing to enable microfiber synthesis[77]–[81]. Amongst the many materials used for microfiber synthesis, hydrogel attracted many research attentions due to its high potential for biomedical applications[23], [82].

2.2.2 Requirements on the microfluidic device for printing purpose

In the previous section, the basic working principle and application of the microfluidic flow focusing device is introduced. However, most of the current microfluidic devices are used for the purpose of spinning fibers either in a liquid bath or being collected on a spool, none has been used for printing purposes. Special considerations should be given for using the microfluidic flow focusing devices as printhead for the bioprinter. Table 2.1 summarized the two major technical requirements for the microfluidic flow focusing devices to be used as microfluidic printhead, detailed discussions are as follow.

First, since the time duration of the printing task is generally long, the continuous stable flow formation during the printing process is highly required. To satisfy such requirement, fluid channels with circular geometry and three dimensional configuration is necessary; it has been shown in previous reports that circular channel shows higher flow pattern stability and less clogging[83].

Requirements	Design features
Stable laminar flow formation	3D fluidic channel geometry
Precise gelation control	Precise outlet length (L_{out}) control

Table 2.1 Technical requirements for the microfluidic printhead and the relative design features to satisfy the requirements.

本図は雑誌掲載の形での刊行 (5 年以内に出版予定) が予定されるため、非公開とする

Fig. 2.2 The schematic of precise gelation contorl in the microfluidic printhead using outlet length L_{out} and its impact on the actual printing scenarios. (a) schematic illustration of the printhead during printing, the dashed box highlighted the part of fluidic channel where gelation of alginate fibers happens. (b) Gelation completeness of the fiber at the printhead outlet increase with increased L_{out}, due to the increased travelling time of fibers in the printhead. (c) Impacts of various fiber gelation completeness at outlet: low gelation completeness results in soft fibers which will be easily squeezed thin due to vacuum down force; proper gelation completeness results in printable fibers; high gelation completeness results in stiff fibers which easily stick to printhead inner walls and cause clogging. (d) and (e) Schematically illustration showing the shifting of printable zone with the varying printhead outlet length.

Second, the gelation control of the microfluidic device needs to be very precise. Considering the printing scenarios as shown in Fig. 2.2, the chemical crosslinking of the hydrogel is triggered at the junction channel inside the microfluidic printhead. As the flow travels inside microfluidic device from the junction channel to the outlet, the completeness of gelation gradually increases. The completeness of gelation at the outlet is affected by several parameters such as the concentration of hydrogel precursor and crosslinkers, as well as the crosslinking time. The crosslinking time is further decided by the flowrates of the fluids and the outlet length L_{out} (defined as the length from the junction point to the outlet). To achieve the proper completeness of gelation for optimized printing performance, all the parameters have to be well-tuned. Amongst all the parameters that affect the completeness of gelation, the concentration of fluids and flowrates can be flexibly tuned; yet the crosslinking time is difficult to tune since the changing of outlet length L_{out} requires changing of the microfluidic device. Moreover, since there are risks that the printhead will be broken due to occasionally wrong printhead movements during printing, the replacing printhead is better to be exactly the same comparing to the original one; if the L_{out} of the replacing printhead varies a lot comparing to the original ones, all parameters relating to the completeness of gelation have to be tuned again, which is extremely time-consuming. In addition, the printable zone (regarding alginate and calcium ion concentration) can be shifted by changing outlet length. Due to the above reasons, the precise control on L_{out} of the printhead during printhead fabrication

is highly required.

Currently, the approaches for fabricating the microfluidic flow focusing devices can be categorized as photolithography based[76], [84], [85], glass capillary based[20], [86] and stereolithography based[78], [87]. Photolithography based approach leverages the power of lithography techniques used for microelectronics fabrication to create quasi-planar patterns with given thickness, which is suitable for the fabrication of T-shaped junction channels. Glass capillary based approach utilized the assembly of pre-extruded micro glass pipettes/capillaries to create co-axial cylindrical channels. As described before, due to the improved stability of laminar flow pattern in the co-axial cylindrical channels comparing to it in the T-shaped channels, the glass capillary based approach is more favorable for microfluidic hydrogel fiber synthesis. However, the glass capillary based approach relies on manual assembly of glass capillaries, which might results in bad axial alignments. Moreover, the manual insertion of the glass capillaries into each other makes it impossible to control outlet length L_{out} , which is the important parameter for the purpose of microfiber printing.

Comparing to photolithography and glass capillary based approaches, the stereolithography technology provides new opportunities for flow focusing device fabrication. The stereolithography based fabrication approach fabricates three dimensional geometry pattern in a layer-by-layer fashion, as shown in Fig. 2.3. It can fabricate three dimensional co-axial cylindrical channels in a one-step manner with precise geometry control; in addition, multiple production of devices in one batch is also possible. Previously, stereolithography based methods have been used to fabricate flow focusing device for droplet generation/synthesis[78], [87].

To briefly summarize this section, it can be concluded that microfluidic printhead should: (1) be able to generate stable laminar flow with minimum clogging; (2) have precise control over its outlet length (L_{out}). As shown in Fig. 2.3, device fabrication technologies such as photolithography-based methods and glass capillary based methods failed to fulfill such requirements; in comparison, the stereolithography based methods is a more suitable choice. Therefore, in this thesis, the stereolithography based method is adopted to fabricate the flow focusing device for generating microfibers. The device is then integrated

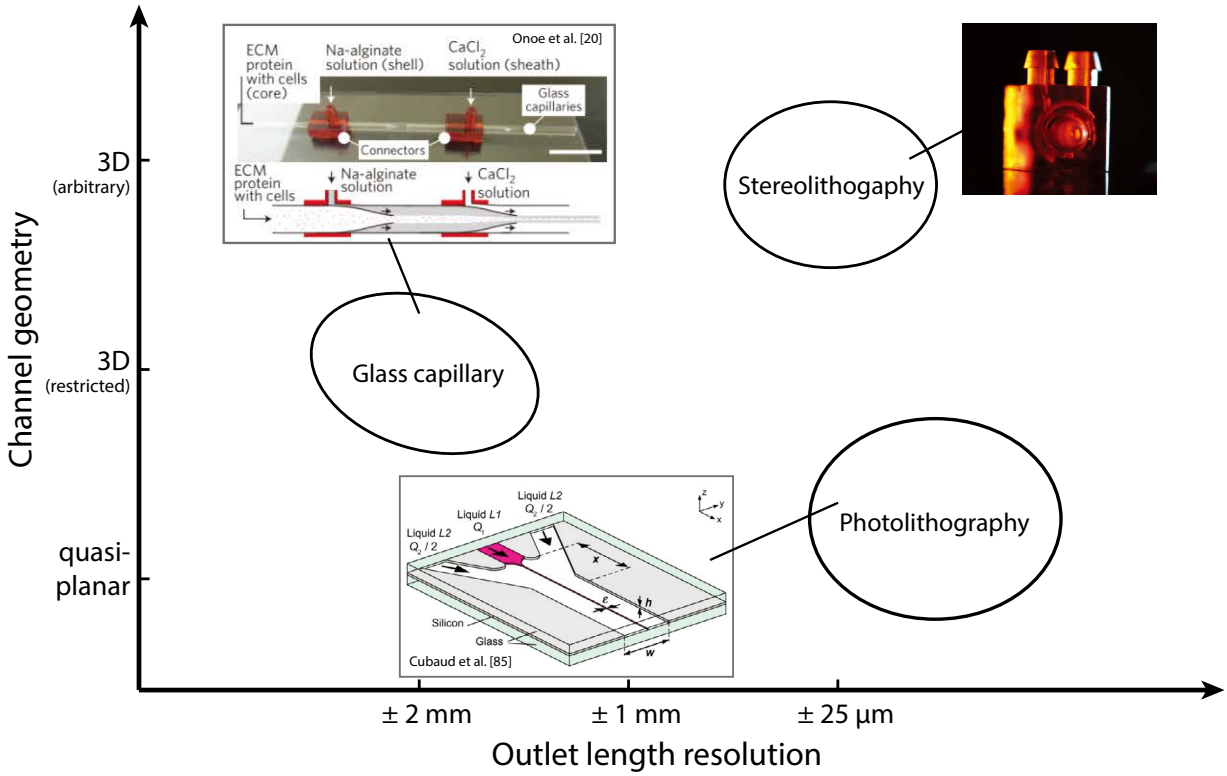

Fig. 2.3 Comparison of current availabe techniques for microfluidic printhead fabrication in terms of channel geometry and outlet length resolution.

into the bioprinter as its printhead.

2.2.3 Stereolithography-based printhead: design and fabrication

A commercial stereolithography prototyping machine (Perfactory, EnvisionTec, Germany) is used in creating the printhead. The workflow of the prototyping starts from 3-D modeling of the printhead using commercial computer aided design (CAD) software (Rhinoceros, McNeel); the 3-D model is exported into .stl format and post-processed to get rid of bad vertex and edges (Magics, EnvisionTec, Germany); the post-processed file is then transformed into .job file, which contains the layers of photo masks for photo-crosslinking the resin with their height settings; the .job file is then transferred to the stereolithography machine to perform the fabrication.

The design of the printhead is as shown in Fig. 2.5. As shown in the schematic on the top-left, schematically, the printhead is composed of three cone-shaped nozzles arranged in a co-axial fashion. The outlet of the first nozzle is inserted into the second nozzle, which enables the 1st level flow focusing to generate core/shell flow pattern of core and shell fluids. The outlet of the second nozzle is then inserted into the final nozzle, which enables the 2nd level flow focusing at where chemical crosslinking of sodium alginate in the shell fluid is triggered upon mixing with calcium ions in the sheath fluids; the length of the final nozzle controls the time of crosslinking, which decide the crosslinking completeness of the shell fluid at the outlet of the printhead. As indicated by the arrows in the front view and right view, the cone-shaped nozzles are designed just like in the schematics, the first and the second nozzle diameter is designed to be 0.3 mm, the wall thickness of the nozzle is designed to be 0.1 mm, which is close to the smallest feature the machine could fabricate; the outlet diameter of the final nozzle is designed into multiple versions with size ranges of 0.6 ~ 1 mm and 1.65 ~ 20 mm. As indicated in the top-down view, quadro symmetric fluid delivery design is adopted, the fluid (shell fluid, in this sectional view) is introduced from the single barbed style inlet, and separated into two major branches and finally to the four minor branches; such design will facilitate the fast and symmetric formation of the focusing

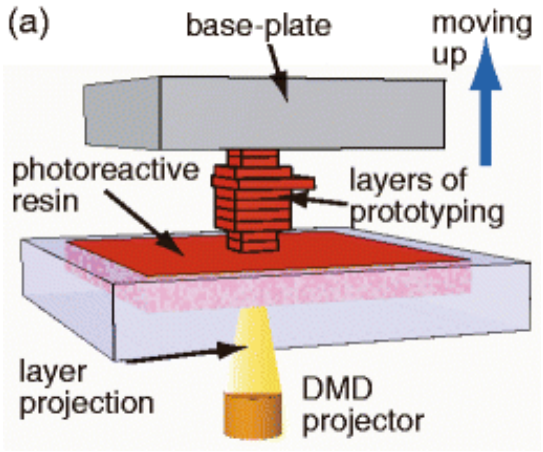

Fig. 2.4 Working principle of stereolithography[87]. A digital-mirror-device (DMD) projector generate patterned exposure to photoreactive resin, thereby solidfying thin patterned layers additively © Copyright 2011 IOP Publishing.

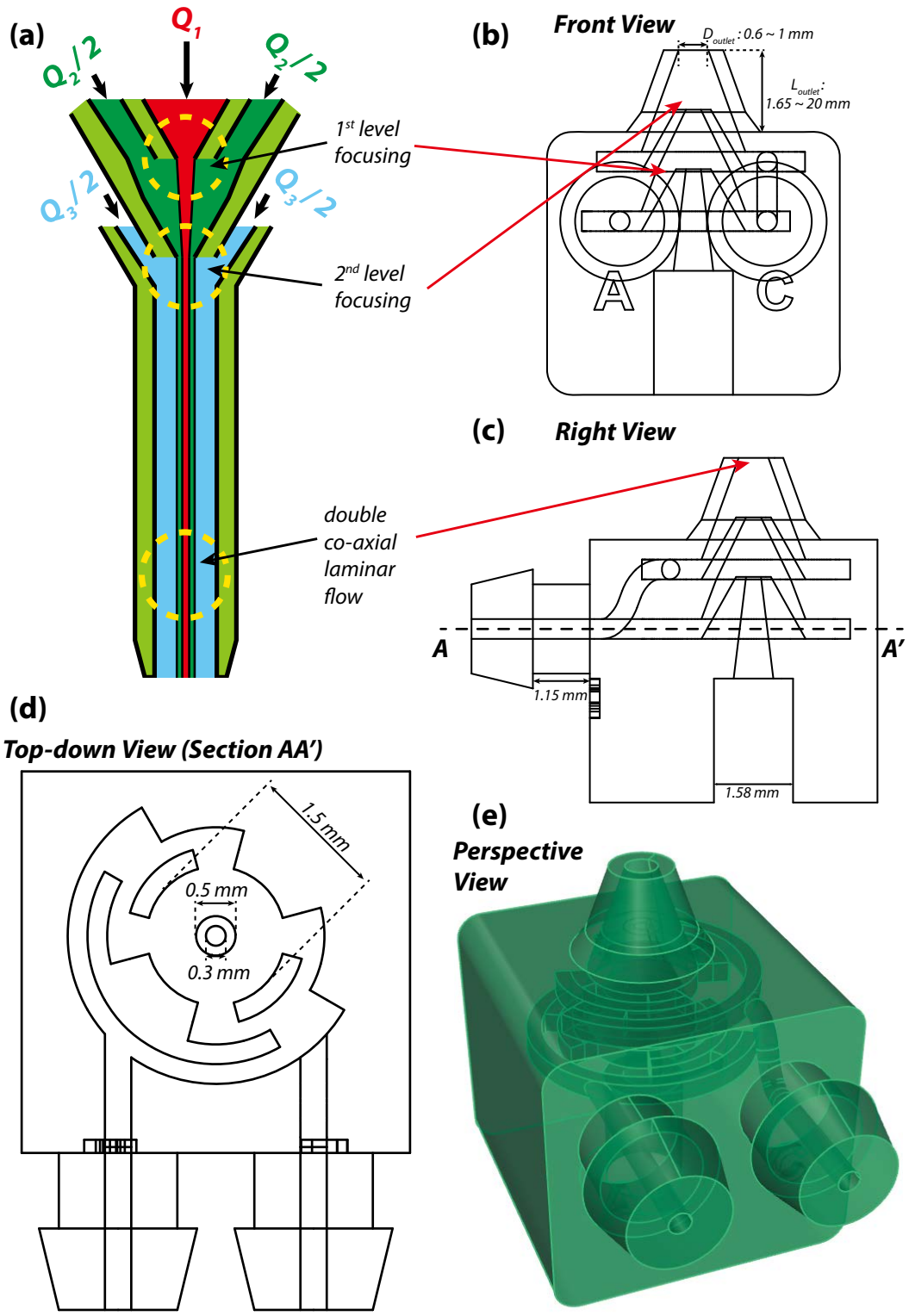

Fig. 2.5 The design model of the stereolithography based microfluidic printhead. (a) cross-section scheme of the fluidic channels; (b-e) front, right, top-down and perspective view of the printhead model.

fluid, shortening the distance needed for flow pattern stabilization. As indicated in the right view, the two inlets for shell and sheath fluids are designed in barbed style to facilitate easy connection with silicone tubes, the inlet for the core fluid is designed as a cylindrical hole with its axis aligned on the axial line of co-axial nozzles; due to limitation of stereolithography machine, barbed style is not adopted for core inlet, tubing of the core fluid will be accomplished by gluing teflon tubes to the inlet hole using adhesives.

Two different kinds of photo curable resin, R11 and HTM (EnvisionTec, Germany) are available for the stereolithography machine. Upon exposure to light, R11 resin cures into translucent red solids, HTM resin cures into nearly opaque green solids. Due to its optical feature, R11 resin is chosen to fabricate printhead for easy visualization of the fluid channels inside the printhead. However, the fabrication time it takes for R11 resin is much longer for HTM resin, hence HTM resin is used for fast prototyping of different printhead designs when the visualization of the fluid channels inside the printhead is not a necessity. The device right after stereolithography prototyping is as shown in Fig. 2.6 and Fig. 2.7; the array of printheads in the figures are attached to the base-plate. After detaching the printheads using knife and tweezer,the remnant resins are subsequently washed out using isopropyl alcohol (IPA) under gentle sonication. To check out the status of the microchannels inside and to avoid remnant resin which might cause clogs, IPA is then infused through the two barbed style inlets; the fabrication yield of the device is about 60 ~ 70%, most of the failure occurs due to clogging of channels, which is supposed to be caused by strong light exposures. After the IPA infusion, 100% ethanol is subsequently infused through the two barbed style inlets. Then, the devices are soaked inside 100% ethanol under gentle sonication. Finally, the printhead is collected in petri dishes and allowed to dry up overnight. On the next day, the printheads are coated with Parylene C to increase the hydrophobicity of the printhead surface and restrain potential leakage of toxic materials into fluids when performing bioprinting[88]. The zoomed-in photo of a printhead with parylene C coating with 0.6 mm outlet diameter and 1.65 mm outlet length is as shown in Fig. 2.8; with proper illumination, the microchannels inside is clearly visible.

2.2.4 Printhead bench tests: core/shell fiber spinning in water bath

Fig. 2.6 The microfluidic printhead with short printhead fabricated in an array using R11 resin.

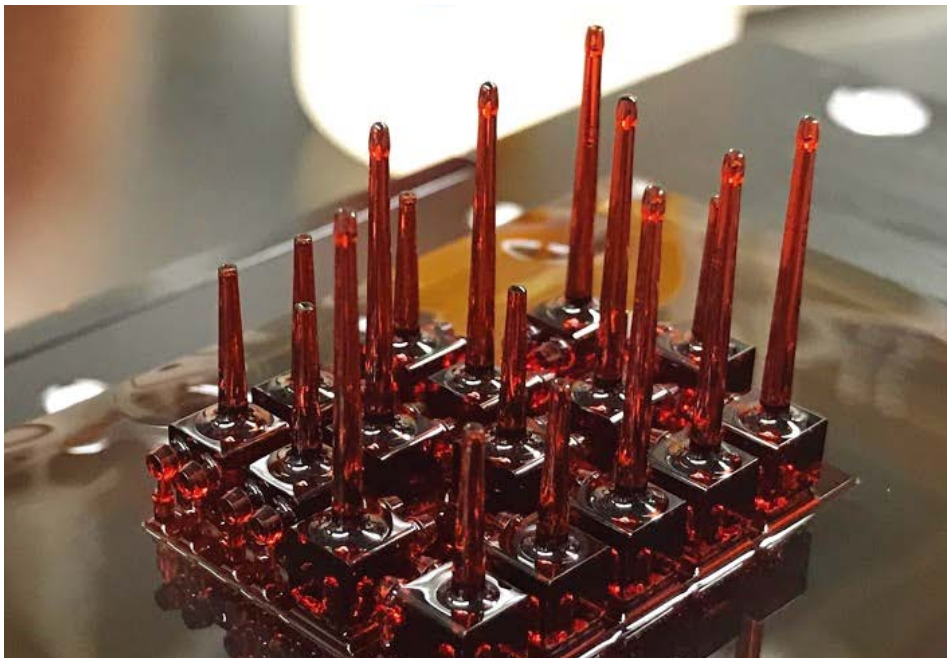

Fig. 2.7 The microlfuici printhead with various outlet length fabricated using R11 resin.

Before using the printhead for bioprinting, several bench test are essential to evaluate the performance of the microfluidic printhead. The questions remained to be answered are:

(1) Is the stereolithography-based printhead capable of spinning microfiber just like the soft-lithography based and capillary based device?

(2) How is the stability of the core/shell fluid pattern during the fiber spinning?

(3) Is it able to control the geometry features of the fluid patterns?

(4) How much does the core/shell fluids mix during the spinning process?

(5) Is it able to control the spinning velocity of the core/shell microfibers?

To find out the answers, an experimental setup, which is able to perform high-speed imaging of the fiber generation process, is conceived and realized for the bench tests, as shown in Fig. 2.9. The printhead is fixed with its nozzle arranged vertically downward onto a manually 3-axis stage (Narishige Group, Japan). The outlet of the printhead is either dipped into water bath or exposed in air. All fluids are infused into the device using a multi-syringe pump (Precision Shibasaki Co., Ltd, Japan) or pressure controller (MFCS, Fluigent, France) in a programmable fashion. The key of the experimental setup is the imaging setup, as shown in details in Fig. 2.10. Since the fiber spinning rate is fast, high-speed microscopic imaging system is adopted; the vertically downward arrangement of the printhead needs the optical setup to be setup in a horizontal fashion, back-light illumination using halogen light is necessary to capture clear images; an additional diffuser paper (Roscolux 1/4 Tough White Diffusion, Rosco, USA) is set up in between the backlight and the printhead to enlarge the illumination area; water bath are filled inside a customized square glass container to provide transparency and minimized light diffraction. Both the lighting and lens camera are controlled by one-unit PC based high-speed imaging system (VW-9000, Keyence, Japan).

本図は雑誌掲載の形での刊行 (5 年以内に出版予定) が予定されるため、非公開とする

Fig. 2.8　The closed up photos of the fabricated printhead with short outlet nozzle; two materials (R11 and HTM) are both available.

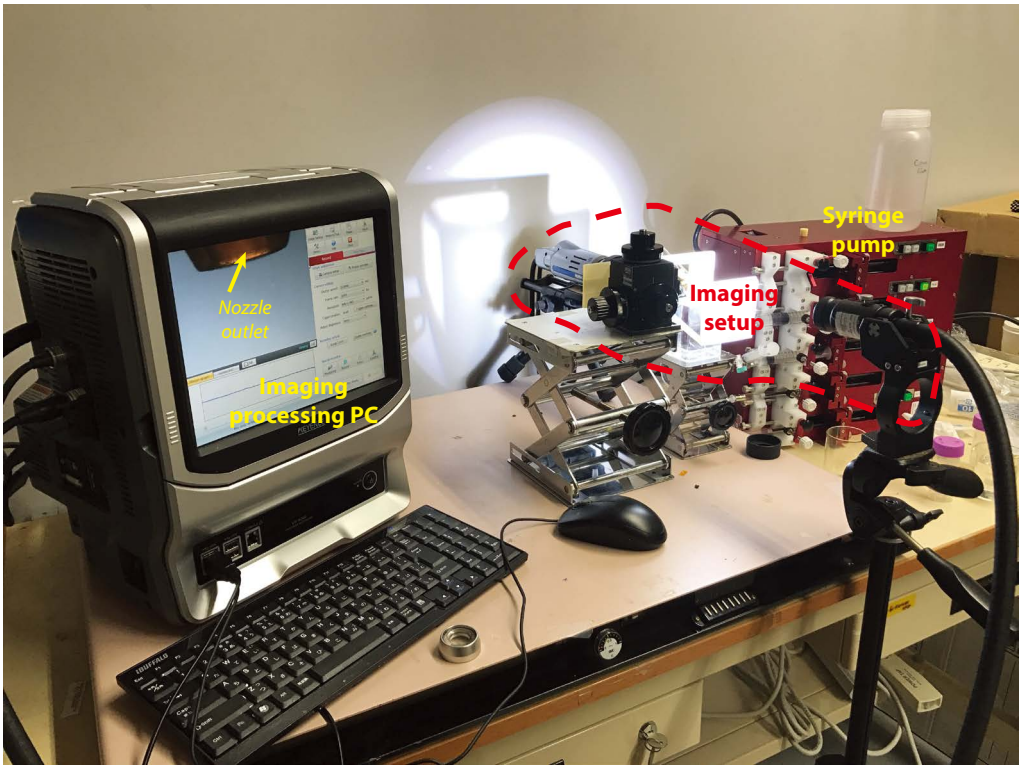

Fig. 2.9 The overview of the fiber-spinning imaging setup including imaging setup, imaging processing PC and syringe pump.

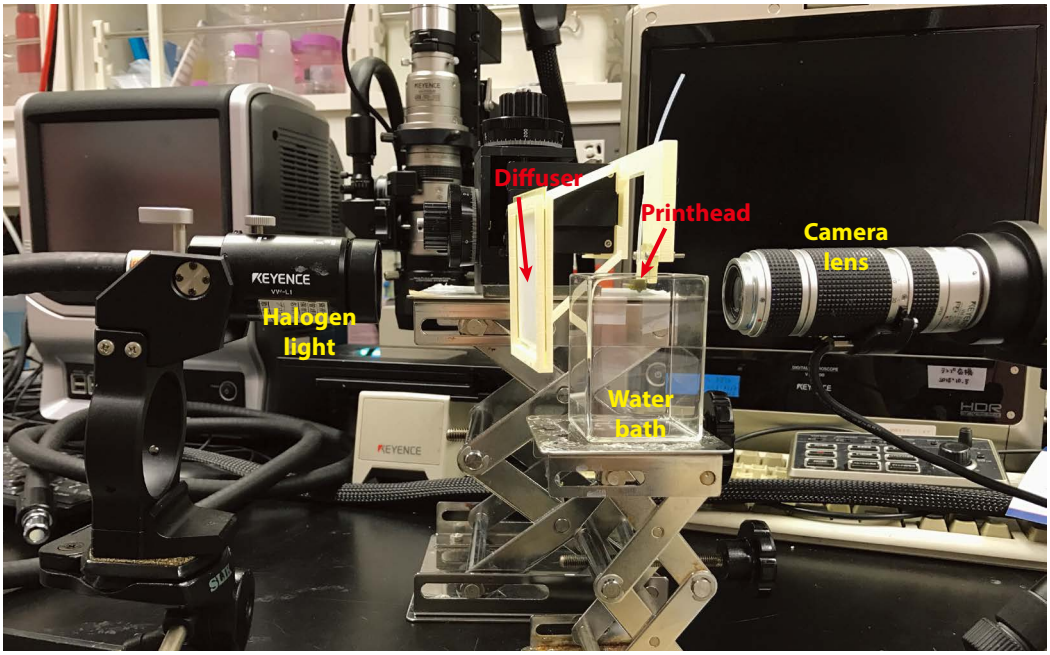

Fig. 2.10 The detailed arragement of the lighting, device (with water bath) and microscopic camera lens.

High-G content sodium alginate (IL-6G, KIMICA, Japan) is used as shell materials during all experiments in this section. Core fluids are chosen as polyethylene glycol (PEG)(Mw ~35k, Sigma-Aldrich, Japan) with optional mixing of red food dyes, blue/green inks, fluorescent nanoparticles or 3T3 cells for different purposes. The sheath solution are chosen as 90 mM calcium chloride aqueous solutions. To clearly imaging the fiber generation near the outlet of the printhead, the printhead fabricated using R11 resin with 0.6 mm outlet diameter and 1.65 mm outlet length is chosen for all experiments in this section.

The ability of spinning microfibers using the microfluidic printhead is first tested. As shown on the left of Fig. 2.11, microfibers (visualized by mixing red fluorescent beads in the core fluid) is being smoothly generated in the water bath; on the right of Fig. 2.11, microfibers (visualized by mixing green ink in the core fluid) is being generated in the hanging droplet with printhead outlet exposed in air.

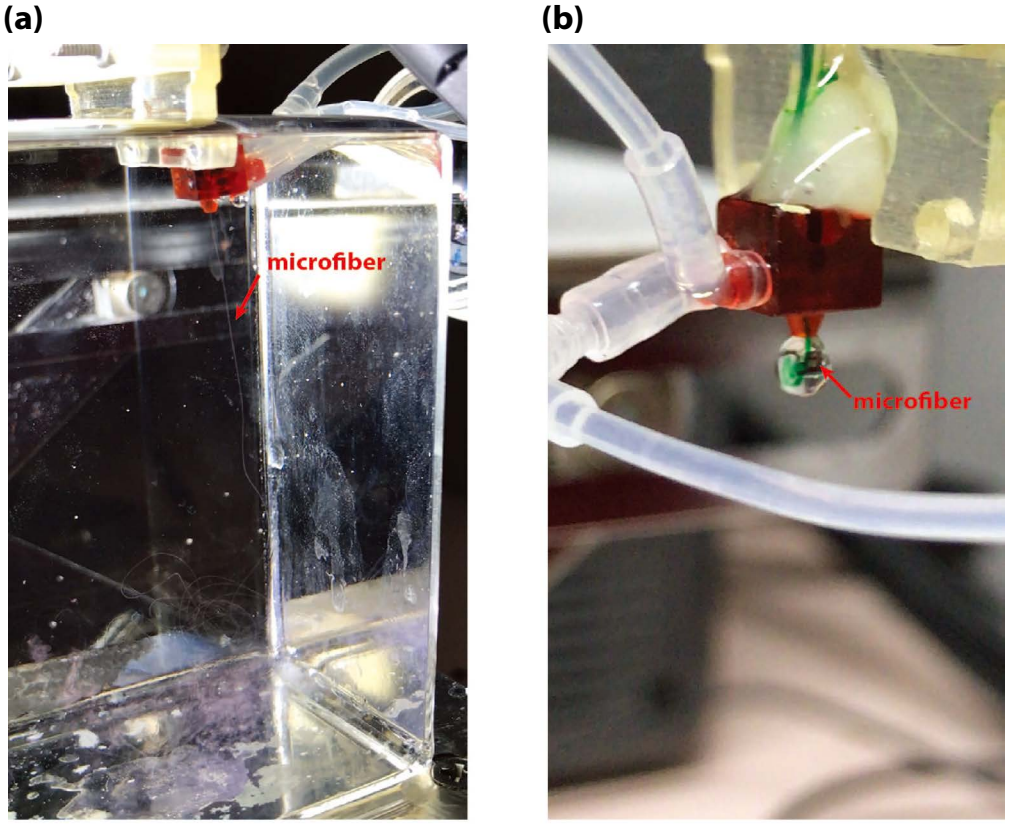

Fig. 2.11 Fiber-spinning in (a) water bath and (b) hanging droplet.

To check out the stability of the fiber spinning, two experiments are performed. In the first experiment, the infusion of core fluid is turned off at the beginning to allow stable formation of alginate microfibers, then the core fluid (with a flow rate equal to 1/2 of shell fluid) is switched on. As shown in the time lapse image serie in Fig. 2.12, upon switching-on the core fluid, the core region starts to build up with two separated flow fronts; as time going on, the core fluid pattern further develops and gets stabilized finally. In the second experiment, stable core/shell fiber spinning is achieved in the beginning; then, by manually twisting gears of the manual 3-axis stage (onto which the printhead is being fixed), shaking of the printhead on both horizontal and vertical direction is performed separately. As shown in the Fig. 2.13, the core/shell pattern of the fiber is stable under either direction of shaking.

To demonstrate the control on the diameters of the core and shell part of the fiber, core fluids (visualized using red food dyes) are injected using pressure controller under different pressures while

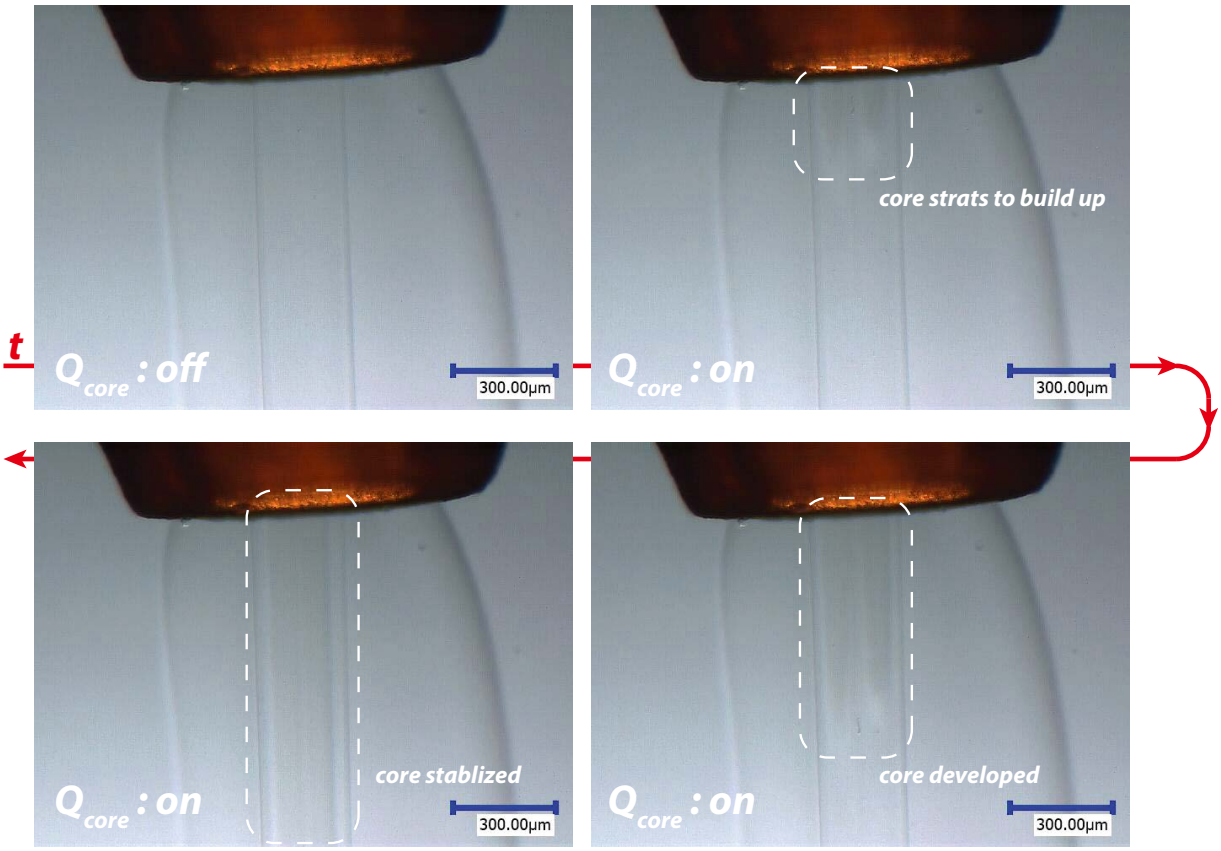

Fig. 2.12 Switch-on test of the core fluid to probe the stability of fiber spinning. Photos arranged along time axis (denoted in red color).

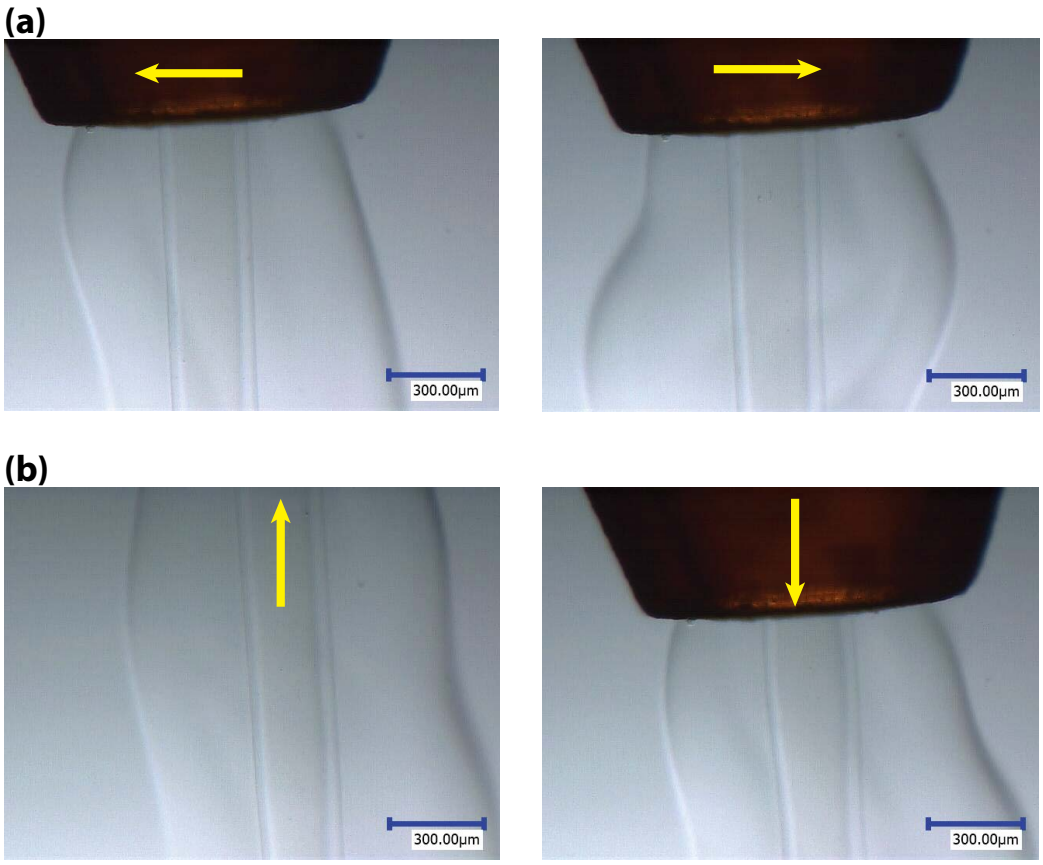

Fig. 2.13 Manual shaking of the printhead (a) horizontally and (b) vertically during fiber spinning to probe the stability of fiber spinning.

keeping the injection rates of other fluids constant. As shown in Fig. 2.14, by increasing the infusing pressure of core fluids, the diameter of both core and shell part of the fiber increases.

To check out how much the core and shell fluids mix up after fiber spinning, fluorescent nanoparticles are mixed into PEG solution based core fluid. Since the dispersed fluorescent beads will be immobilized if it is mixed up with sodium alginate, the thickness of the mixing layer of core and shell fluids could be investigated using fluorescent microscopy. On top-left of Fig. 2.15 is the optical image of the fabricated core/shell microfibers, a thin shell layer is clearly visible. The fluorescent image on the top-right indicates both the existence of both shell layer and the mixing layer of core and shell fluids. By analyzing the gray value profile along the section, the thickness of the mixing layer is about 20 μm.

The fiber spinning rate is also tested by varying the injection flow rates while keeping the ratio of them constant. The velocity of fiber spinning is analyzed using motion tracking software

(MotionAnalyzer, Keyence, Japan). From the data graph Fig. 2.16, the spinning velocity can be adjusted from ca. 5 mm/s to 50 mm/s by changing the flow rates.

In addition, the ability of encapsulating cells inside the core region of the microfibers is also briefly tested. In the experiments, NIH-3T3 cells mixed with PEG solution is used as core solution. As shown in Fig. 2.17, both the microscopic image during the spinning and the phase construct image show that it is capable of encapsulate cells using the microfluidic printhead. Interestingly, the fibers during spinning remains in sparse and uniform suspension status; while the cells soon aggregates into multicellular aggregates soon after fabrication. The reason is supposed to be the deceleration of fibers when it hits the bottom of the water bath reservoir, causing an inertia-induced aggregates of the cells.

2.3 Syringe-vacuum substrate

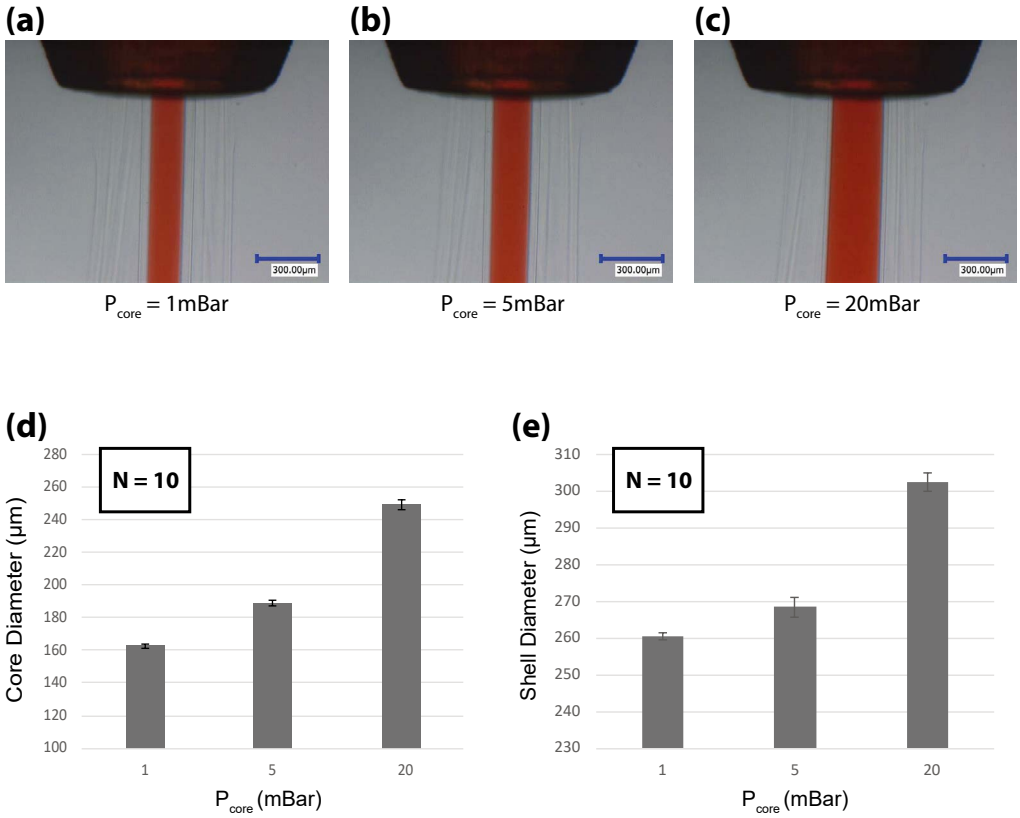

Fig. 2.14 The change of core/shell diameter with various core fluid injection pressures. (a-c) microscopic images of core/shell fiber generated at printhead outlet with various core pressures. (d-e) measured core and shell diameters. (mean ±s.d., n =10)

本図は雑誌掲載の形での刊行 (5 年以内に出版予定) が予定されるため、非公開とする

Fig. 2.15 The hollowed alginate microfiber fabricated with red fluorescent beads added to the core solution to probe the diffusion between core and shell fluids. (a) phase constrast and (b) fluorescent microscopic image of the hollow fibers. (c) high-magnification fluorescent image of the hollow fiber. (d) profile plot of gray scale value along the AA' dissection in (c).

Here in this section, the requirement for suitable substrate design for the printing purpose will be discussed, followed by the comparison of possible technical candidates for the creation of the printing substrate; upon comparison, pneumatic type mechanism is chosen to facilitate the depositing of fibers. As the implementation of the pneumatic mechanism, the syringe-vacuum (i.e. vacuum generated using syringe) substrate is proposed, followed with the description on its working principle and fabrication. Then, the results of bench tests of the substrate will be discussed to evaluate and optimize its performance.

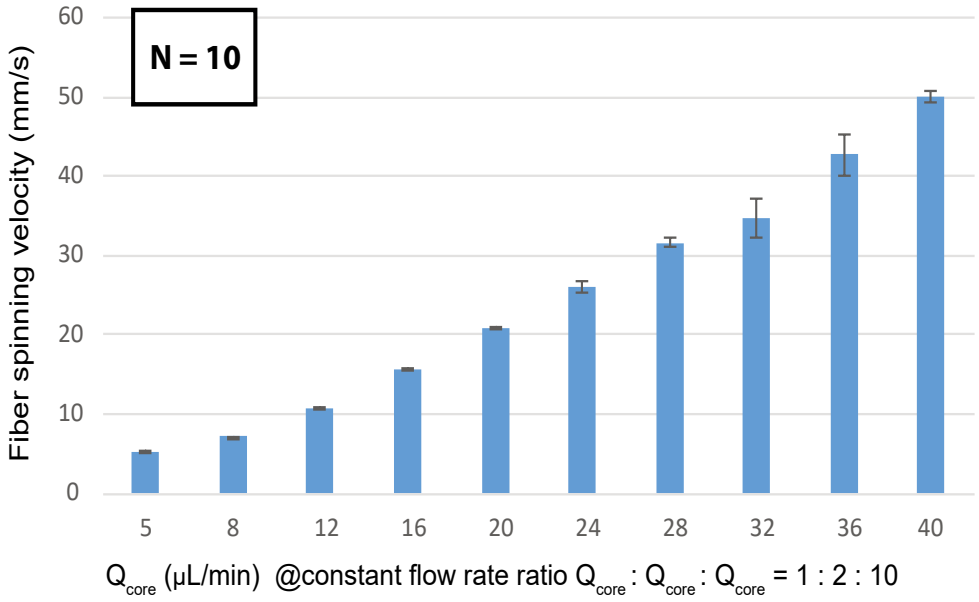

Fig. 2.16 Fiber spinning velocities under different flow rates. (mean ±s.d., n =10)

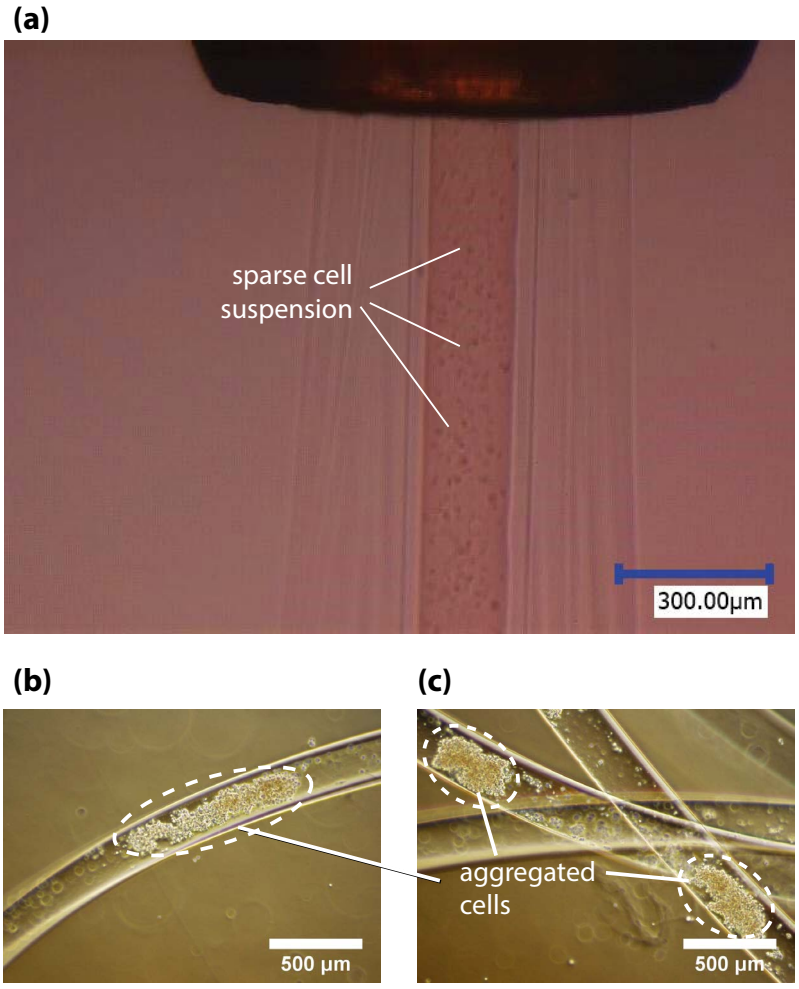

Fig. 2.17 Spinning of cell-laden microfibers using the stereolithography-based printhead. (a) microscopic images of fibers spinning at the printhead outlet, cell suspensions are sparse; (b-c) cell-laden microfibers collected immediately after spinning, cell aggeragats was inspected in the microfibers.

2.3.1 Requirements on substrate designs

Since the microfibers are made of hydrogel and cells which have very high water contents, the density of the hydrogel microfiber is close to the density of water. As a consequence, simply dispensing fibers in an aqueous environment will result in floating of fibers, making it impossible to accomplish the printing task, as shown in Fig. 2.18. To enable the printing of hydrogel microfibers, mechanisms for fixing fibers during its dispensing process are required. Possible mechanisms for fixing the fibers during dispensing can be categorized as magnetic, electrostatic and pneumatic types, as shown both in Fig. 2.19 and Table 2.2.

For the magnetic type mechanism, aqueous dispersion of magnetic particles can be mixed with the

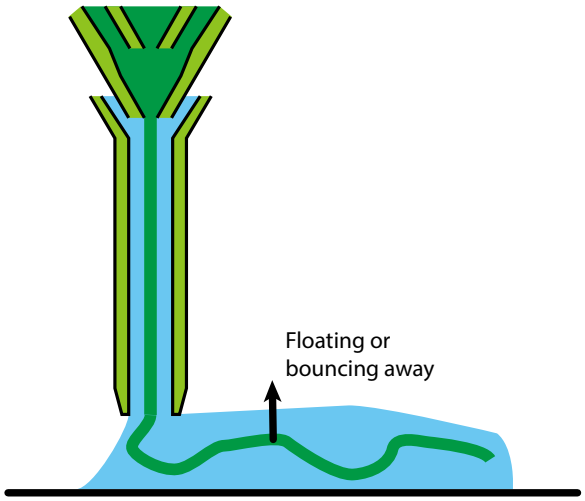

Fig. 2.18 The fibers float due to buoyancy or elastic bouncing without proper fixation mechanism.

hydrogel precursors; during fiber dispensing, a magnetic field can be introduced beneath the substrate; with the downforce generated by the magnetic interaction between the magnetic particles in the hydrogel

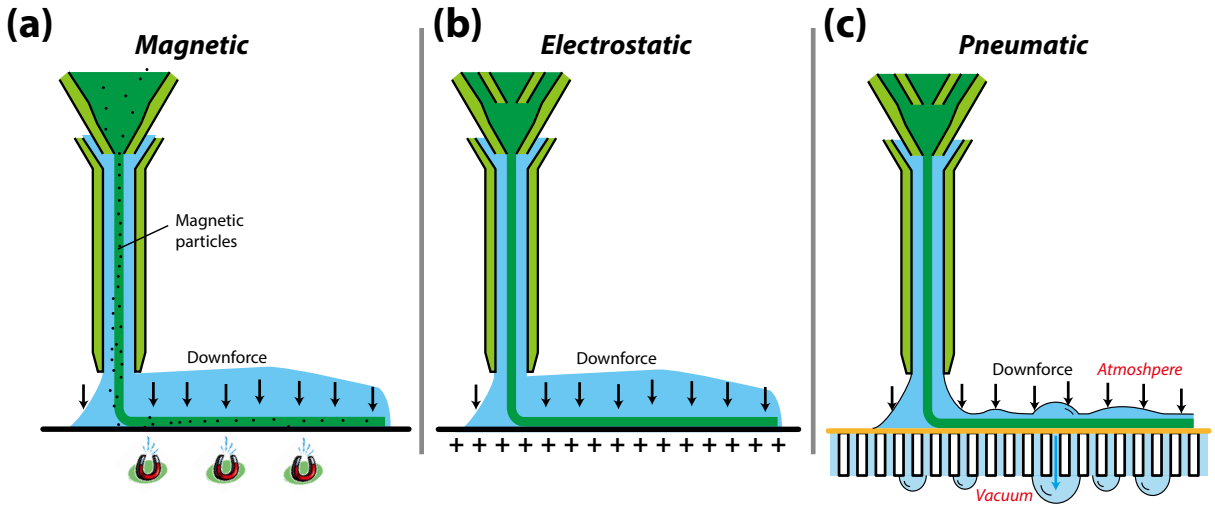

Fig. 2.19 Schemaitc illustration of the three possible mechanisms for fiber fixation: (a) magnetic, (b) electrostatic and (c) pneumatic.

Force type	Requirements	Cell compatibility
Magnetic	Mixing magnetic particles in fiber	Poor (mostly toxic)
Electrostatic	Electrostatic charge source	Might be damaging to cells (membranes)
Pneumatic	Vacuum filtration system	Potentially mild to cells

Table 2.2 Comparison of the three possible mechanisms for fiber fixation.

and the magnetic field beneath, the floating of fibers during dispension can be avoided[89]. The major problem of the magnetic method is that the magnetic particles are difficult to remove after fabrication, which is potentially toxic to cells.

For the electrostatic type mechanism, the fixation of the fibers relies on the electrostatic interactions between charges. Some hydrogels (such as alginate, chitosan, etc.) exhibit electrostatic properties; by creating a substrate with charges which is opposite to the charges of the hydrogels, the hydrogel

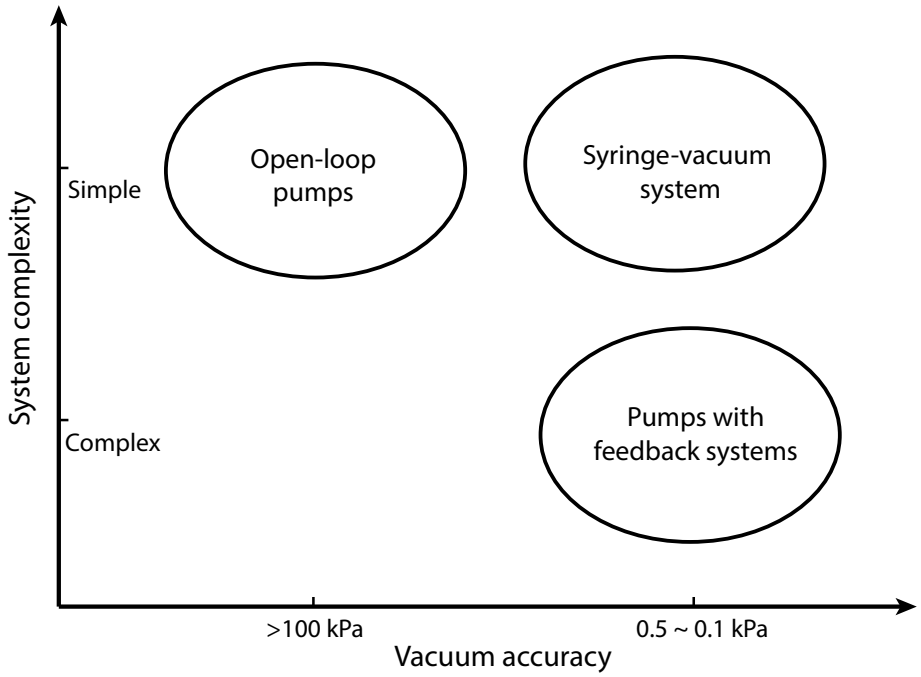

Fig. 2.20 Comparison of the vacuum generation techniques in terms of acurracy and system complexity.

本図は雑誌掲載の形での刊行 (5 年以内に出版予定) が予定されるため、非公開とする

Fig. 2.21 Schemaitc illustration of the syringe based vacuum substrate. The open/close state of the filter membrane depends on its wetting condition; the membranes are open when un-wetted and close when wetted unifromly.

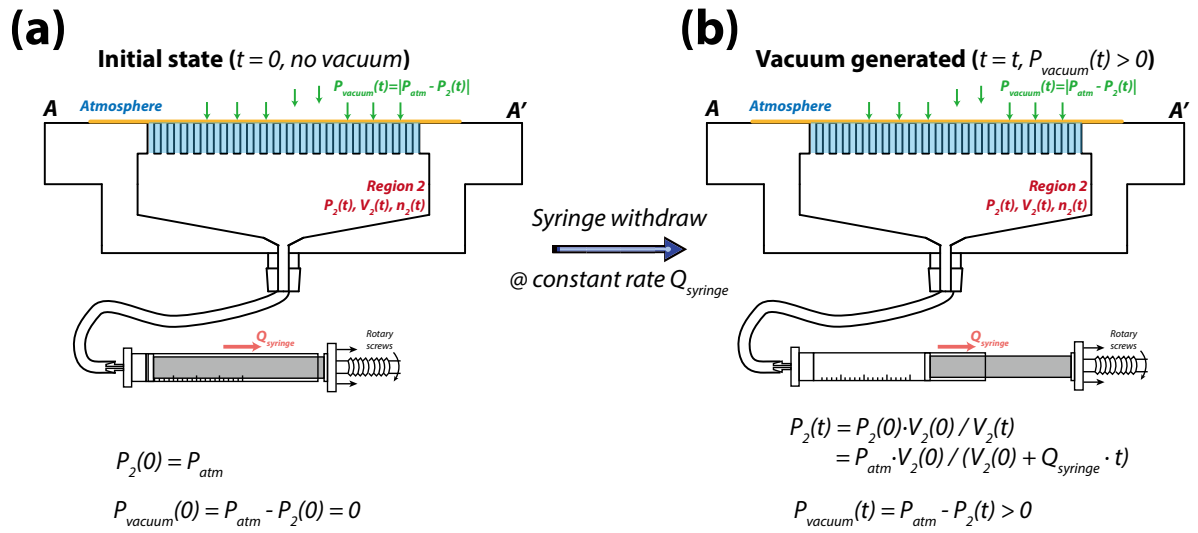

Fig. 2.22 Schematic illustration of the vacuum generation. (a) the initial state with filter membrane wetted. (b) upon sucking of syringe, the volume of enclosed chamber increases to generate the vacuum.

microfibers can be fixed due to the downforce generated by electrostatic interactions. However, since electrostatic force decreases as the distance of the fibers to the substrate increases during layer-by-layer deposition, the ability of depositing fibers into multiple-layered thick structure might be hindered.

For the pneumatic type mechanism, the fixation of the fibers relies on the vacuum downforce generated by the pressure difference between the upper side and downer side of the substrate. Comparing to the magnetic type and electrostatic type mechanisms, the pneumatic type is potentially gentle to cells(if the vacuum can be generated with controlled strength) and works on a long distance along the thickness direction of printed fiber based structures. With the reasons described above, pneumatic type mechanism is adopted in this work.

本図は雑誌掲載の形での刊行 (5 年以内に出版予定) が予定されるため、非公開とする

Fig. 2.23 Concept illustration of the bubble porint pressure of the filter membrane. (a) when applied prssure is lower than the bubble-point pressure, surface tension dominates so that the filter membrane is closed (with ignorable diffusion) ; (b) when applied pressure is higher than the bubble-point pressure, surface tension can not hold water in the membrane anymore, leading to gas leakage.

2.3.2 Design, working principle and fabrication of the syringe-vacuum substrate

As described in the previous section, pneumatic type mechanism is adopted in this work for the fixation of fibers during printing. To implement the pneumatic mechanism, the syringe-vacuum substrate is designed, fabricated and tested. In this section, detailed design and working principle of the syringe-vacuum substrate will be discussed, followed by the tests to evaluate and optimize its performance.

Terminology definitions

The word “vacuum” is broadly used under various definitions in many different areas such as physics[90], philosophy[91] and engineering[92]. To avoid ambiguity, several terms related to the word “vacuum” will be defined here. First, in engineering and applied physics, the word “vacuum” refers to any space in which the pressure is lower than atmospheric pressure[92]; this definition of vacuum is adopted the way it is throughout this thesis without any special declarations. “Vacuum pressure” refers to the absolute value of the pressure difference between the vacuum space/area and the atmosphere. “Syringe-vacuum” refers to the vacuum generated using syringes; such term is also used to describe the substrate which is featured with a vacuum generated using syringes. “Vacuum down force” is the pneumatic downforce generated by the pressure difference between the upper side and down side of the substrate, which facilitates steady deposition of the printed fibers and evacuates the being dispensed sheath fluids to avoid its pooling.

本図は雑誌掲載の形での刊行 (5 年以内に出版予定) が予定されるため、非公開とする

Fig. 2.24 Vacuum pressure's change over time during bench test; sucking of syringe at a constant rate is turned-on at the beginning of the test and turned-off until a peak vacuum pressure is reached.

Vacuum generation techniques comparison

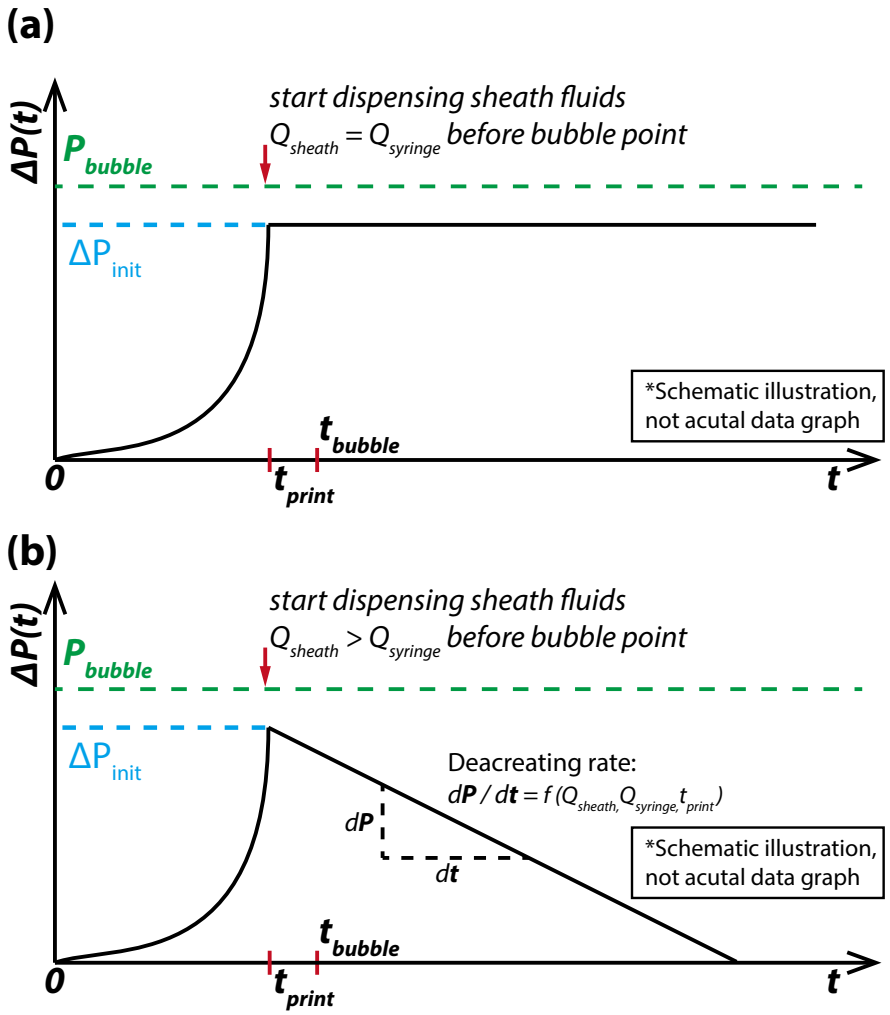

Fig. 2.25 The working principle of the syringe-vacuum substrate. (a) for the case when the rate of dispensing sheath fluids is same with syringe sucking rate, the vacuum pressure will be constant during the printing; (b) for the case when the rate of dispensing sheath fluids is larger than syringe sucking rate, the vacuum pressure will decrease to zero during printing.

本図は雑誌掲載の形での刊行 (5 年以内に出版予定) が予定されるため、非公開とする

Fig. 2.26 The perforated chamber fabricated using commericial 3-D printer. (a) schematic illustration of the perforated chamber; (b) photograph of the fabricated chamber.

For the purpose of fixing hydrogel microfibers with less damage to cells, the absolute value of vacuum pressure should be small (5~10 kPa). Currently, there are majorly two types of vacuum generation system which is commercially available: open-loop pumps and pumps with feedback systems. The open-loop system can be simply built up by assembling commercially available vacuum pumps and connect them to closed chambers in which the vacuum will be created; such system is easy to built, but the pressure accuracy is generally low (>100 kPa)[93]. On the contrary, pumps with feedback system utilize commercialized pressure controller in combination with vacuum pumps, which can achieve vacuum pressure with high accuracy (0.1 kPa ~ 0.5 kPa), yet the system is quite complex with high costs[94]; moreover, it cannot be directly integrated with syringe pump systems (which is already chosen for fluid injection purposes). It is under this context, the syringe-vacuum methods is proposed. As shown in Fig. 2.20, the syringe-vacuum system is a facile method to generate gentle vacuum with high accuracy; in addition, the syringe-vacuum can directly utilize the syringe pumps, making the whole system simple. Detailed description of the syringe vacuum system can be found as follow.

Design and working principles

The syringe-vacuum substrate is consisted of filter membrane, perforated chamber and syringe (mounted on a syringe pump). As shown in Fig. 2.21, the filter membrane (hydrophilic) is set on top of the lid of the perforated chamber; the lid is perforated to allow liquids to pass through while providing mechanical support to the filter membrane at the same time. The cavity beneath the lid is connected to the syringe through the barbed style connector using silicone tubings. The filter membrane is wetted with water. Once wetted, gas does not penetrate through the hydrophilic filter membrane in a bulky way, hence the whole system could be separated into the atmosphere on the upper side of the membrane and a closed system *Region 2* which is consisted of the space in the perforated chamber, the tubing and the syringe.

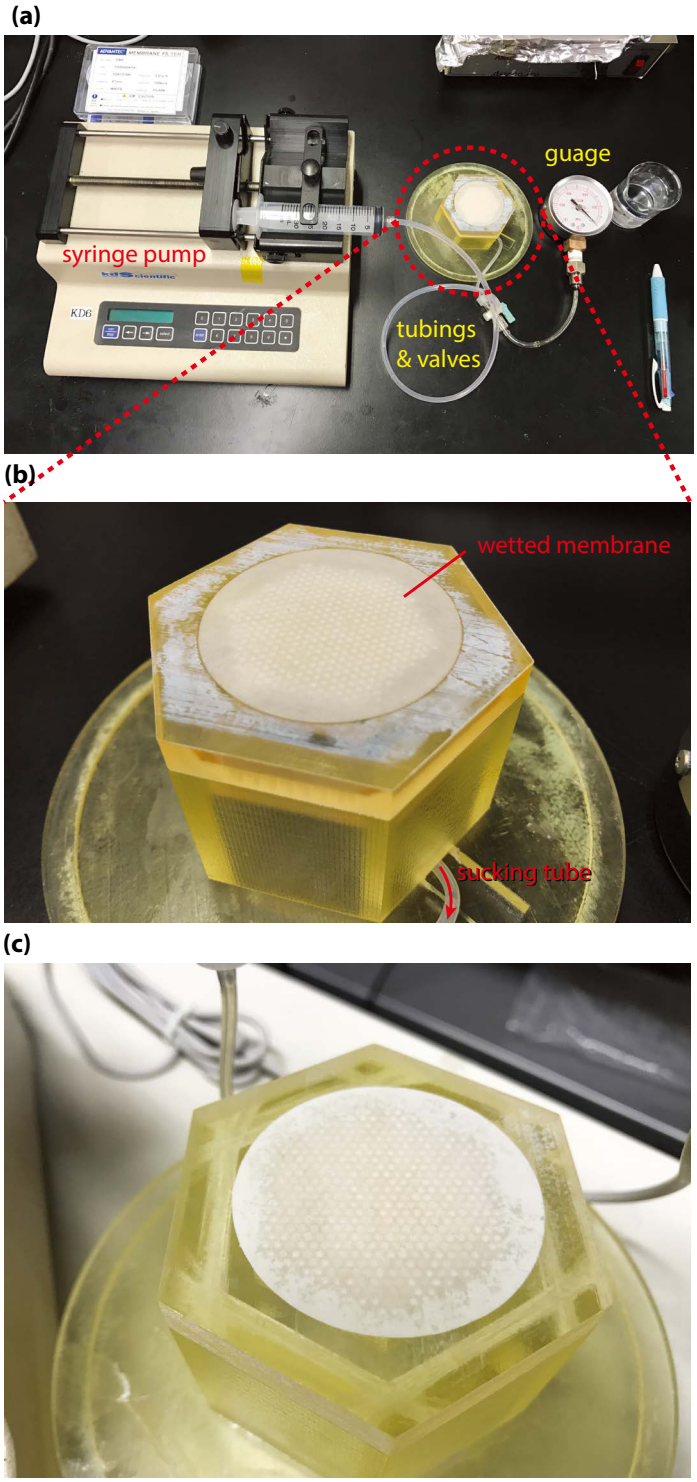

Fig. 2.27 Bubble point test setup. (a) a vacuum gauge is incorporated into the syringe-vacuum substrate system. (b) filter membrane with initial wetting; (c)filter membrane with vacuum beneath, dehydration cuases the membrane to be less transparent comparing to the initial state.

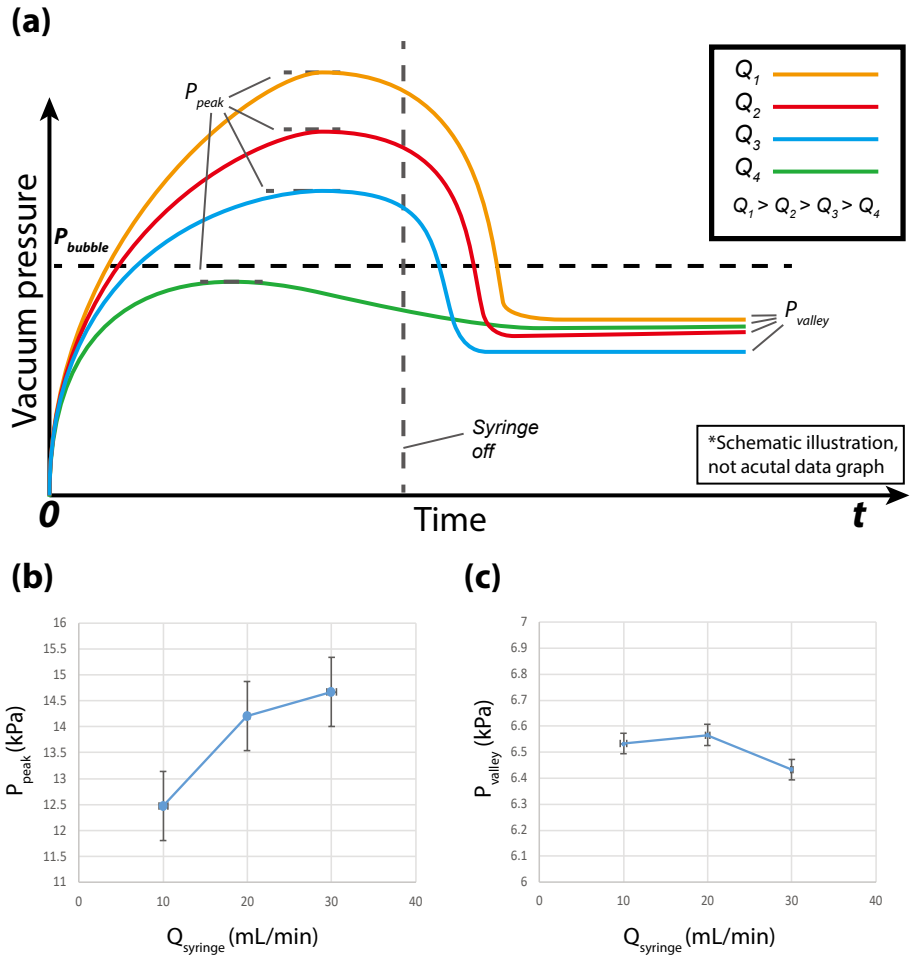

Fig. 2.28 The relationship between pressure and time under different syringe withdrawing rates: (a) representaive diagram; (b-c) test results of the peak pressures and valley pressures. (mean ±s.d., n =3)

As shown in Fig. 2.22, suppose the syringe (with zero initial volume) is operated on withdraw mode at a certain flow rate $Q_{syringe}$ for a certain time duration. The region on the upper side of the filter membrane is atmosphere with constant atmospheric pressure P_{atm}. For the *Region 2* beneath the filter membrane, suppose that the chamber volume (including the tubing volume and syringe volume) is $V_2(t)$, the pressure $P_2(t)$ could be calculated using ideal gas law. At the initial status when $t=0$, the vacuum pressure is 0 since $P_2(t)$ is equal to P_{atm}. Upon constant withdrawing of the syringe at rate $Q_{syringe}$, the pressure of *Region 2* can be calculated using the idea gas law, the vacuum pressure increases when $P_2(t)$ decreases due to the increasing $V_2(t)$.

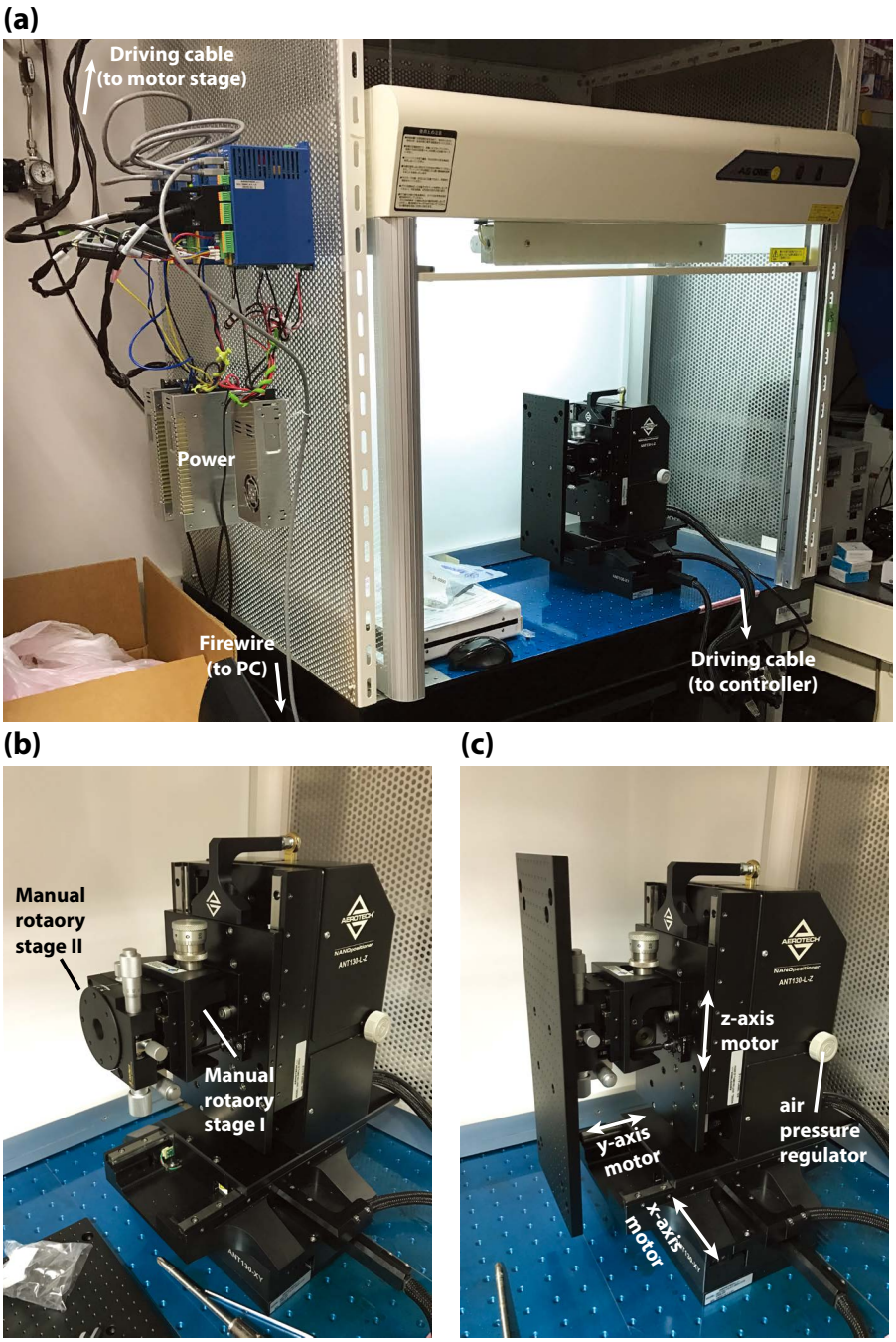

Fig. 2.29 The photo of the 3-axis automatic motion control system. (a) overall setup with power supply, controller, clean hood and motor stage; (b-c) detailed installation of motor stage.

Theoretically, according to the deduction given above, the vacuum pressure of the substrate can keep on increasing as long as the syringe does not reach its maximum volume. However, in fact there is another parameter which limits the maximum vacuum pressure. The parameter is the bubble-point pressure of the filter membrane. Wetted membrane filter of very small pore size will hold liquid in the pores by surface tension and capillary force. With proper wetting, bulky flow of gas is restricted due to the surface tension (gas does also penetrate through due to diffusion, but for small area filtration membrane, the gas penetration rate caused by diffusion is ignorable[95]). The pressure of a gas required to force the entrapped liquid through and out of the fully wetted pore capillary is called the “bubble point pressure” (P_{bubble}). As shown in Fig. 2.23, bubble-point pressure is a threshold pressure; if the pressure applied to the wetted filter membrane is lower than the bubble-point pressure, gas will not pass through the filter membrane in a bulky way; if the pressure applied is higher than the bubble-point pressure, the filter membrane will be dewetted (i.e. the liquid is forced out from the pores of the filter membrane) and gas will pass through in a bulky way. The bubble point pressure is related to the pore size of the membrane, pore shape of the membrane, liquid-solid contact angle and surface tension of the liquids; qualitatively, the larger the pore size, the smaller the bubble point pressure[95].

The scenario for testing bubble point with the syringe-vacuum chamber is depicted as follow. First, with small amount of water wetting the filter membrane (no further water supply with be added during the test) under a constant syringe withdrawing rate, the time course of vacuum pressure change in the syringe-vacuum substrate can be depicted as shown in Fig. 2.24. During this peroid, the vacuum pressure is smaller than the membrane filter’s bubble-point pressure, the vacuum pressure will increase with the withdrawing of the syringe. Then, once the vacuum pressure reaches the bubble-point pressure (P_{bubble}) , the filter membrane is forced open, at this time, the gas leaking rate will increase untill a balance between gas leaking and syringe sucking is reached, which is indicated by the appearance of a peak value of the curve depicted in the illustration. When the peak value (P_{peak})is reached, syringe sucking will be turned off, a pressure drop will be oberved until the remnant water in the membrane redistribute to re-wet the opened pores; upon re-wetting of the pores, gas leakage is prevented again to thus a stable

vacuum pressure inside the chamber, which is indicated by the appearance of a valley value (P_{valley}) of the test curve. Further test results of peak and valley pressures will be discussed in Section 2.3.3.

Since the constant withdrawing of the syringe might cause the pressure to fluctuate or eventually leads to the failure of vacuum generation, the actual operation strategy of the syringe-vacuum substrate during printing should strive to control the vacuum pressure actively, so that it does not reach the bubble point pressure during the whole printing process. In fact, considering that the printing nozzle is constantly dispensing sheath fluids during the printing process, the dispensed sheath fluids can be utilized to compensate the volume change caused by syringe withdrawing. If the dispensing rate of the sheath fluid is no less than the withdrawing rate of the syringe-vacuum substrate, the vacuum pressure will not increase once the dispensing process is triggered, since the volume increase caused by syringe withdrawing is no faster than the volume decrease caused by sheath fluid intake. With the above considerations, the operation mode for the syringe-vacuum substrate during printing is proposed as follow: (1) wet the filter membrane with small amount of water; (2) withdraw the syringe to a certain volume while monitoring the vacuum pressure so that it does not go over the bubble-point pressure; (3) start printing procedure with the dispensing of sheath fluids, at the same time, tune the syringe to a constant sucking rate equal to or smaller than the sheath flow dispensing rate. Assuming that sheath fluid evacuation rate is much faster than its dispensing rate, a dynamically constant vacuum pressure (when the sheath dispensing rate is equal to syringe withdrawing rate) or gradually decreased vacuum pressure (when the sheath dispensing rate is larger than syringe withdrawing rate) will be maintained during the whole dispensing process, as shown in Fig. 2.25.

Fabrication of the syringe-vacuum substrate

To implement the syringe-vacuum substrate, the perforated chamber, as well as chamber supporter is designed using CAD software (Rhinoceros, McNeel) and fabricated using a commercial 3D printer (KEYENCE, Agilista-3200). Hexagonal honeycomb pattern was adopted for perforation due to its excellent mechanical strength both in axial and out-of-plane direction[96], [97]. The hexagonal radius of

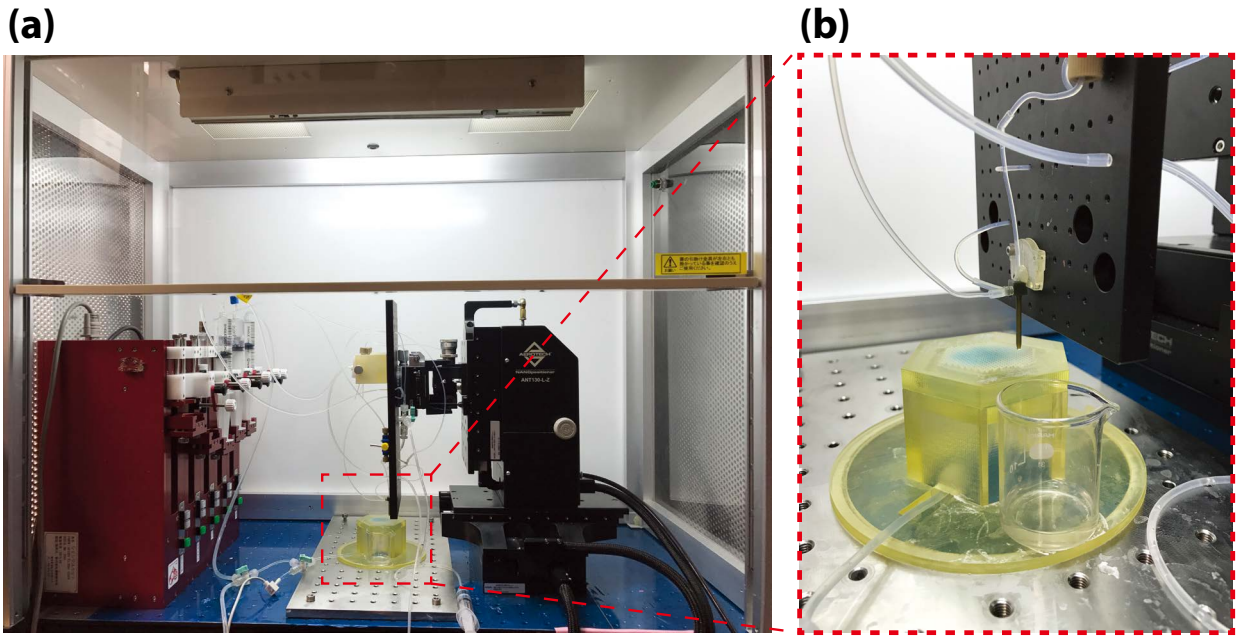

Fig. 2.30 The photo of the assembled bioptrinter. (a) overall setup of the printing system; (b) zoomed in photo of the printhead and syringe-vacuum substrate.

perforated holes is 0.5 mm, all holes are arranged at centres of hexagonal cell array generated with 1 mm cell radius. Thickness of the perforated lid is 4 mm. The cavity beneath is designed with > 8 mm depth so that water does not accumulate at the cavity's peripheral due to surface tension. The volume of the cavity is designed to be 11.522 mL, ignoring the volume of the tubing and the bubble-point effect of the filter membrane, a vacuum pressure of 302.62 kPa can be achieved after 1 min of syringe withdrawing at 5 mL/min. The bottom of the cavity is designed in a barbed style for easy connection to syringe using silicone tubes. The design model and fabricated perforated chamber is as shown in Fig. 2.26. Filter membrane (hydrophilic, polyester coated with cellulose, Y100A047A/Y020A047A, ADVANTEC, Japan) was purchased from Toyo Roshi Kaisha, Ltd. The pore size of the filter membrane is 10 μm, with a bubble-point pressure of 17 kPa.

2.3.3 Bench tests of the syringe-vacuum substrate

The system is subjected to a bench test before using for actual printing. The goal of the bench test is to

find the pressure range under which vacuum pressure could be almostly maintained constant (ignoring the slow evaporation of liquids). Though the bubble-point data could be found on the data sheet provided by the filter membrane manufacturers[95], the actual working condition is different from standard bubble-point test condition; in the actual working condition of the syringe-vacuum substrate, both side of the membrane is exposed to air so that it could not be maintained under constant wetting condition as it is in standard bubble point test; in addition, the volume increasing rate of the syringe is small comparing to the case using valve-pumps. Therefore, the actual bubble-point should be tested using a setup mimicking the actual working condition during printing. With the test, an optimized vacuum range could be decided. On one hand, the vacuum should not be too small, otherwise water could not be evacuated promptly, which will cause fibers to float during the bioprinting process; on the other hand, the vacuum value should also be as gentle as possible, otherwise the fibers will be squeezed flat onto the substrate, causing deteriorated geometry fidelity and bad cell viability.

The actual setup of the test is as shown in Fig. 2.27. An analog vacuum gauge is integrated into the system to monitor the vacuum pressure inside the cavity. During the test, the filter membrane (pore size: 10 μm) is first set on top of the perforated chamber, and wetted with 0.5 mL of Milli-Q water. Until the water wetted the whole area of the filter membrane, withdrawing of the syringe by syringe pump is switched on with a constant withdrawing rate; the withdrawing will be turned off if the vacuum pressure stops to increase. The readout of the vacuum gauge is recorded after the withdrawing begins. With the vacuum beneath, the filter membrane get partially dehydrated as shown in Fig. 2.27 (c). The results of the tests is summarized in Fig. 2.28. It is interesting to see that, the behaviour of the filter membrane differs a lot in comparison with the standard setup for bubble-point test performed by membrane manufacturers [95]: first, the maximum value of vacuum pressure (V_{peak}) is related to the withdrawing rates, as shown in the representative diagram in Fig. 2.28 (c); second, when the withdrawing is turned off, the vacuum pressure quickly drops down to a stable value (V_{valley}), which is ca. 6.5 kPa regardless of different syringe sucking rates.

In conclusion, to use the syringe-vacuum substrate, it is required that (1) the system is capable of

monitoring vacuum pressure during the whole process; (2) it is safe to operate the substrate with a vacuum pressure below ca. 6.5 kPa, according to the value of P_{valley} given shown in Fig. 2.28.

2.4 Motion control system

Motion control system provide precise motion control of the printhead, allowing the patterning of fibers into 3-D shapes. In combination with the motion control system, the clamping and tubing system provide stable fixation of the printhead and feasible fluid injection from the syringe pump the the microfluidic printhead. Smooth movement and pulseless fluid delivery guarantees the quality of the additive manufacturing.

The motion control system is composed of several parts as follow. First, a 3-axis linear motor stage (Aerotech KK, Japan) is the basis of the motion control system, as shown on top of Fig. 2.29. The motor stage is fixed onto a metal table, housed inside a clean bench. Driving signals and motion feedback signals are transferred in between motor stage and computer through separate motion controllers. Three seperate controllers are interconnected in a serial fashion and finally connected to PC, all using Firewire cable, .Then, on top of the motor stage, two manual rotary stages are further installed; one is capable of manually adjusting out-of-plane angles, another is capable of manually adjusting in-plane angles. Finally, a metal bread board with M-2 screw holes is installed on the manual rotary stages, onto which the printhead will be fixed upon.

Motion of the motor stage is programmed based on Aerobasic programming language (Aerotech KK, Japan). Aerobasic programming language is based on G-codes and M-codes (the industrial standard programming language for robotic control), with advanced functions for velocity blendings. The motion feedback of the motor stage is collected using the built-in sensors, and can be inspected using A3200 Digital Scope software (Aerotech KK, Japan).

2.5 System assembly

All the components designed and fabricated in this chapter is finally assembled into the bioprinter as shown in the photo (Fig. 2.30). The motor stage (with the manual stages and breadboard) is housed inside the clean bench.

The tubing system is configured as follow. For the injection of low viscous (< 30 cP) fluids to the microfluidic printhead, Teflon tubings with inner diameter of 0.5mm and outer diameter of 1/16" is adopted; the small inner diameter provides faster fluidic response due to decreased tubing volume, the stiffness of the tubing also contribute to stable fluid injection during printing. For the injection of viscous fluids such as sodium alginate aqueous solution (> 100cP), silicone tubes with inner diameter of 1 mm and outer diameter of 3 mm is adopted; the major reason is to reduce the fluidic pressure inside to tubing, thus reduce the risk of liquid leakages. All the fluidic tubings are connected from the syringe pump to the microfluidic printhead, with proper fixing by threading the tubes through the screw holes of the fixation breadboard; such configuration eliminate relative movements in between the printhead and the tubings. Since the inlets of the printhead are barbed type which needs to be connected with Teflon tubes using deformable silicone tubes as connectors, the relative movement in between the printhead and the tubings will cause deformation of the deformable silicone tubes, which will further cause fluid rate changes. For the connection of syringe-vacuum substrate, silicon tubes with inner diameter of 4 mm and outer diameter of 6 mm is adopted. In addition to the tubings, a digital vacuum gauge is also integrated into the syringe-vacuum substrate to provide real time measurement of the vacuum pressure inside the substrate.

2.6 Summary

In this chapter, the construction of the bioprinter is described in details. Following the description of the whole system, the design, fabrication and tests of each components are discussed. First, the microfluidic printhead is designed and fabricated using stereolithography-based approach; bench tests performed on the printhead shows that it is capable of generating core/shell hydrogel microfibers steadily, with

well-controlled fiber spinning velocity. Second, the syringe-vacuum substrate is then conceived and implemented, by combining a commercially available filter membrane with a perforated vacuum chamber designed and fabricated using a commercial 3-D printer. The working principle of the vacuum substrate is then proposed and analyzed, with corresponding bench test experiments to verify the proposed working principle. Finally, the motor stage system, tubing system and the system assembly is described at the end of this chapter.

Chapter 3
Evaluation and capability demonstration of the bioprinter

In the previous chapter, the construction of the bioprinter for cell fiber printing is described with details on the design, implementation and bench tests of each components, as well as the considerations and practices on assembling the components into the actual bioprinter. This chapter describes the evaluation and capability demonstration of the bioprinter. This chapter will start with a detailed description on the workflow to perform the printing of core/shell hydrogel microfibers. Then, an overview on all the tunable fabrication parameters will be given, followed by the description on the strategy to find out the suitable parameter values for printing; the actual printing process is performed and evaluated to decide the suitable printing parameters. Finally, with the suitable printing parameters, the printing of cell-laden core/shell hydrogel microfibers will be performed with post-print cell viability evaluation and discussions on the post-print maturation methods of the printed construct.

3.1 The workflow of the core/shell microfiber printing

This section introduces the basic workflow for the actual printing of alginate microfibers using the

本図は雑誌掲載の形での刊行 (5 年以内に出版予定) が予定されるため、非公開とする

Fig. 3.1　The basic workflow of the printing process.

bioprinter. As shown in the illustrations in Fig. 3.1, the printing process can be divided by several steps as follow. First, for the creation of vacuum, the syringe-vacuum substrate is set up by putting the filter membrane on top of the perforated chamber and wetting the membrane using small amount of Milli-Q water; the withdraw of the syringe pump is then turned on; upon the withdrawing of the syringe, the vacuum pressure will be gradually built-up, during this process, the printhead is set at the standby position with a beaker put beneath it for collection of waste fluids. Then, when the vacuum pressure reaches 3 ~ 6 kPa (empirical pressure value which is enough for fast evacuation of dispensed water), the injection of the bio- inks is started; with the injection started, the buffers (55 mM citrate, for the prevention of clogging before and after fiber spinning) will be gradually exchanged by the cation containing sheath fluids (calcium chloride solution), calcium alginate microfibers will start to form at the outlet of the microfluidic printhead when buffers are fully exchanged. Then, once the alginate fibers are formed, the printhead moves away from its stand-by position and starts to write programmed three dimensional patterns on top of the syringe-vacuum substrate. The first two layers of fibers are called the “rafting layers”. During the dispensing of the rafting layers, the syringe-vacuum substrate will operate at a high vacuum pressure, which is the key to ensure feasible deposition of the fibers, since the high vacuum pressure guarantees immediately evacuation of the sheath fluids so that the fibers have no chance to float. Since the rafting layers are subjected to high pneumatic downforce, it is potentially harmful to cells, hence during the printing of the rafting layers, the injection of core fluids (cotaining cells) is switched off. Then, after the deposition of the rafting layers, the vacuum pressure is controlled to gradually decrease to zero within 1~2 min, which will result in slightly pooling of the sheath fluids. The slightly pooling of sheath fluids will not affect the deposition of fibers in this status as long as the height of the pooling liquid is lower than the printed construct. After the motor stage finishes its programmed

path, the generation of the fibers is stopped immediately by exchanging the sheath fluids with buffers. Finally, the printhead gets back to its standby position; the printhead is thoroughly washed with buffers to be ready for the next print.

3.2 Tunable parameters and their influences on printing quality

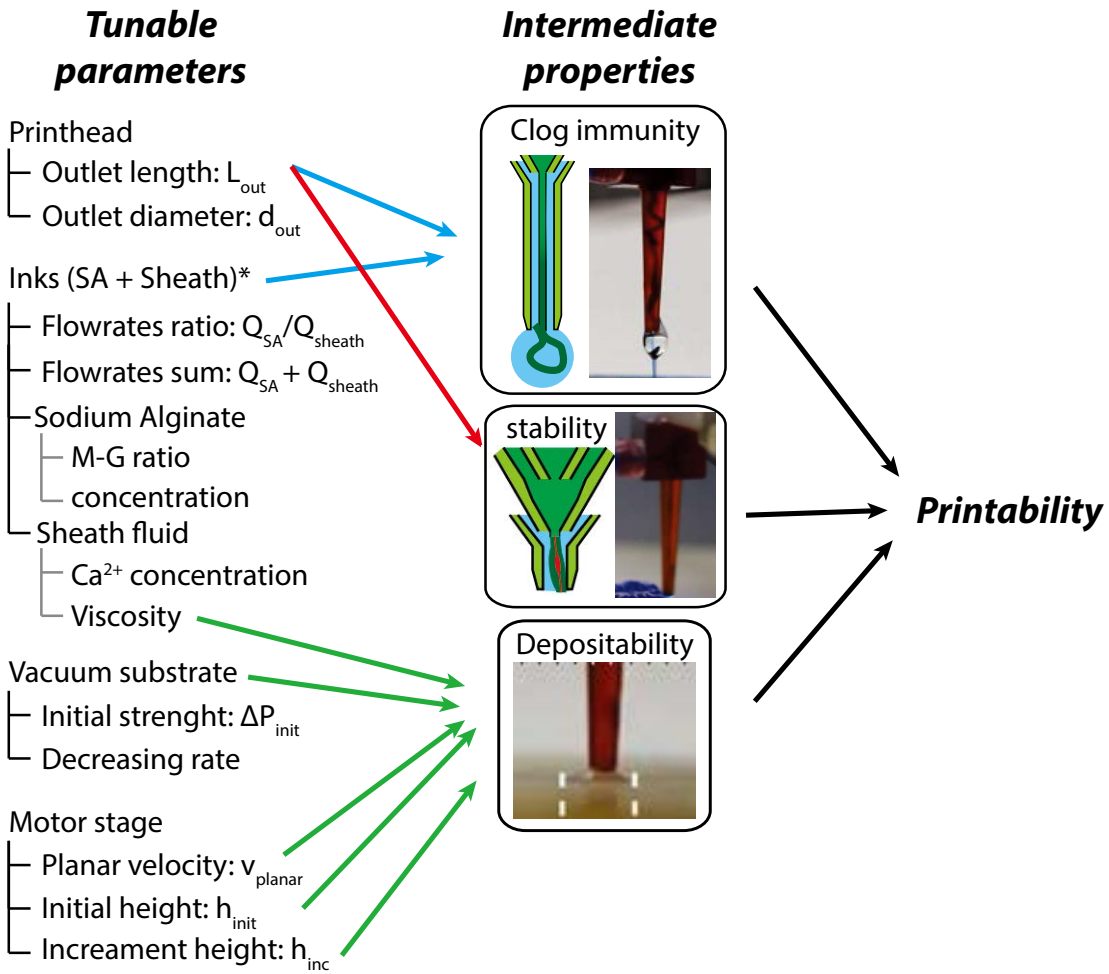

Fig. 3.2 The list of all the tunable parameters and their relationship with the intermideiate properties such as clog immunity, stability and depositability which finally decides the printability.

As a complex system with many tunable parameters, the bioprinter needs to be well-tuned prior to being used for the printing of cell fibers. In this section, all the tunable parameters that affects the quality of printing will be discussed. For the tuning of printing parameters, hydrogel microfibers without cells will be used, since cells do not drastically affect the rheological properties of the fluids. Because there are many interactions in-between these parameters, the whole process towards the stable protocol (i.e. the set

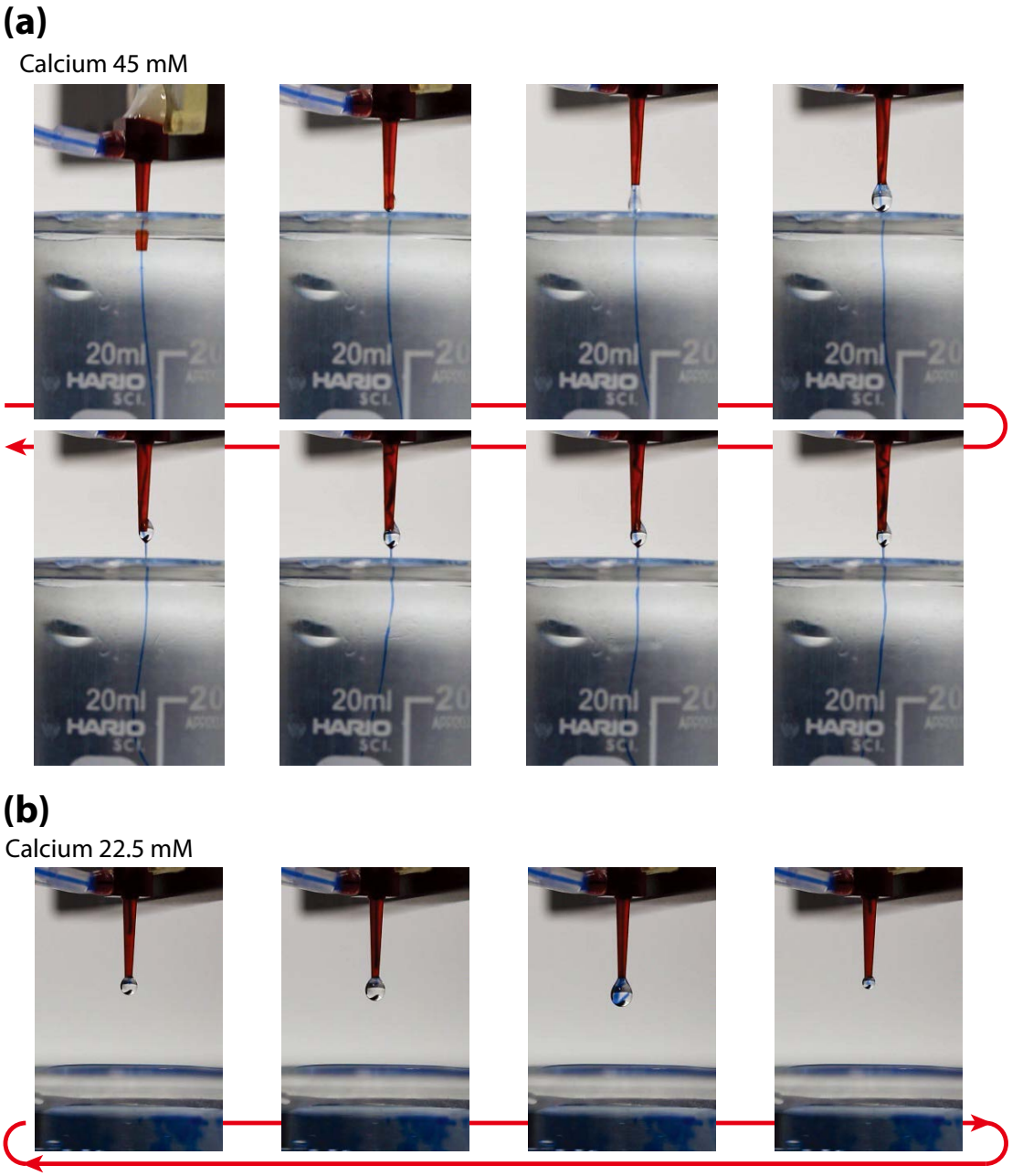

Fig. 3.3 Influence of instability at the tip under various calcium ion concentrations in sheath fluids. (a) 45 mM causes clogging when moving the printhead away from bath; (b) 22.5 mM exhibits no clogging within dripping drops.

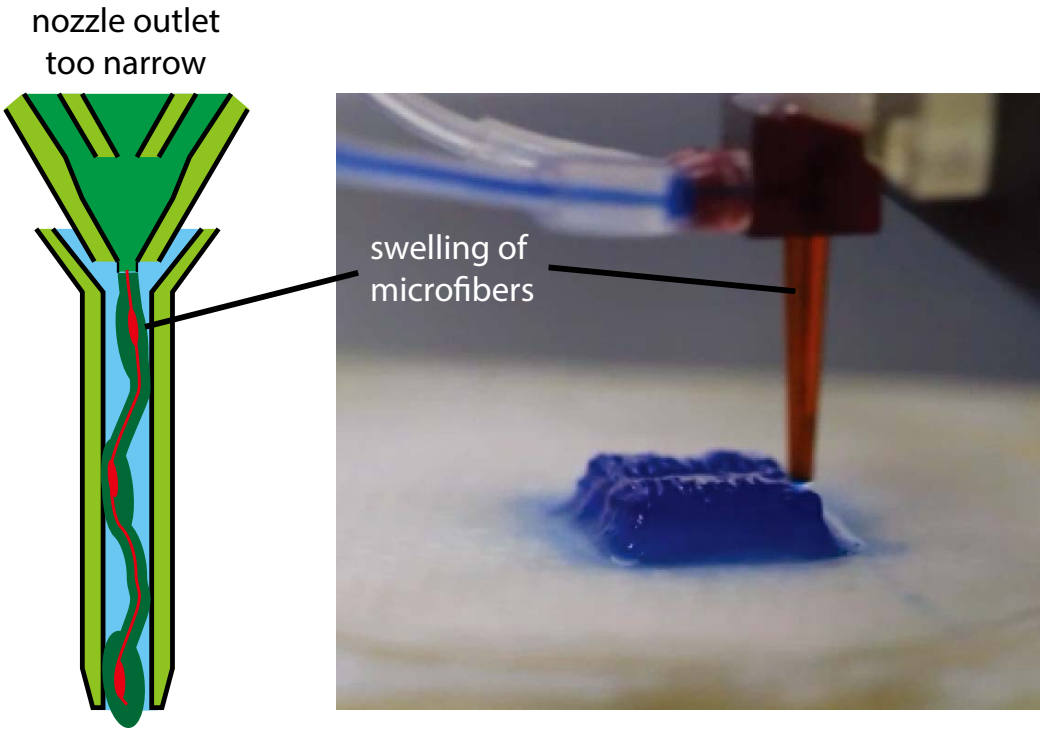

Fig. 3.4 Microfibers swelling due to the narrow nozzle outlet, which will deteriorate size uniformity of the printed fibers as well as cause clogging during printing.

of parameters that works stably) is a step-by-step process, in which the variable range of each parameters is narrowed down and finally converges to a suitable fabrication protocol. Such protocol will be used to proceed to the printing of cell-laden microfibers.

As described in the first chapter of this thesis, the bio- inks used for the bioprinters contain two aspects of properties: biocompatibility and mechanical integrity. Since the printing of cell fibers will guarantee the biocompatibility of the bio-ink in the core region of the microfibers, the mechanical integrity of the alginate becomes critical, since the mechanical integrity decides the printability and printing qualities such as structural fidelity, etc. The fundamental need for a feasible printing protocol is the ability to smoothly stack up layer-by-layer.

The fabrication parameters for the bioprinter could be categorized into 4 subcategories according to which system components they belong to, which are the fabrication parameters of (1) the printhead, (2)

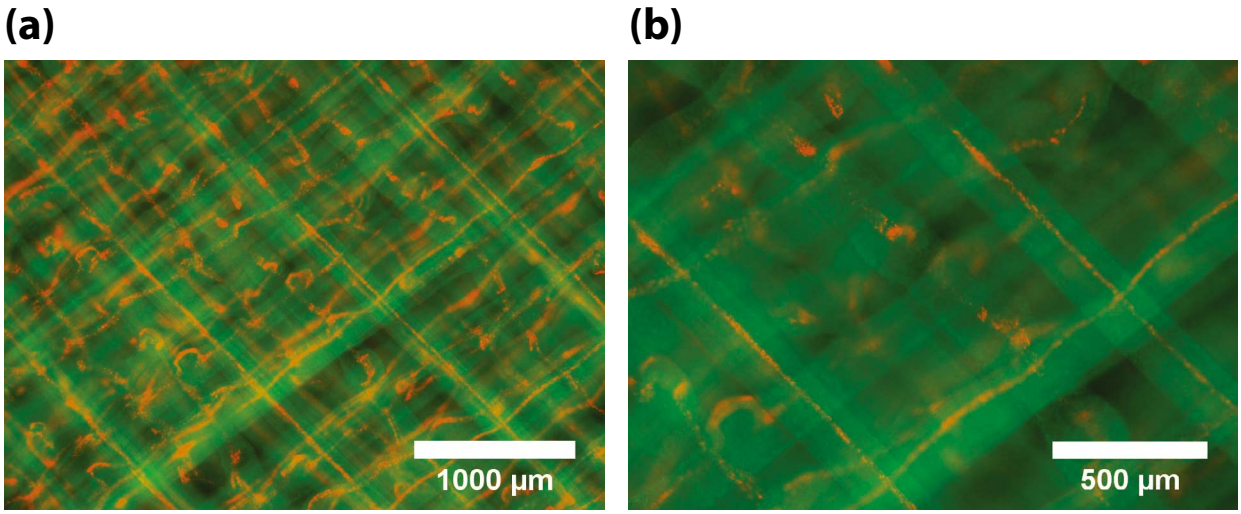

Fig. 3.5 Failed core/shell feature formation using the short printhead. (a) low and (b) high magnification microscopic images are shown respectively.

the inks, (3) the vacuum substrate and (4) the motor stage.

3.2.1 The predetermined parameters

Amongst the many parameters, several are relatively isolated with not so many interaction with others. They are generally constrained to certain ranges due to various practical reasons. Strategically, to narrow down the working range of all the parameters, these isolated parameters should be decided at first.

First, as the fluids are delivered upon the injection of the syringes, the response lag in between the start of syringe injection to the actual flow rate stabilization in the microfluidic printhead should be minimized. For this purpose, low viscosity sodium alginate (50~80 cP @1wt%, IL-6G, KIMICA, Japan) is adopted.

Second, though the fiber spinning velocity can be as fast as 40~50 mm/s according the results shown in Fig. 2.16, the printhead speed is limited by the performance of the motor stage; in practice, for printing speed > ca. 20 mm/s, a strong jerk will be introduced at the turning point of the zigzag motions, causing strong vibration of the fixation table of the motor stage. Hence the planar velocity of the motor stage is narrowed down to 10 ~ 20 mm/s. Because it is better that the fiber spinning velocity matches with the

planar speed of the motor stage, the flow rates of the core/shell/sheath fluids are fixed to 16/32/800 uL/min, which will generate fibers at a velocito of 15 mm/s according to Fig. 2.16.

Third, the viscosity of the sheath fluid is also predetermined to ~ 10 cP. Such level of viscosity will decrease the viscosity contrast of shell fluids (i.e. sodium alginate aqueous solution) which generally has viscosity higher than 100 cP. Several literature[98]–[100] have shown that if the viscosity contrast of

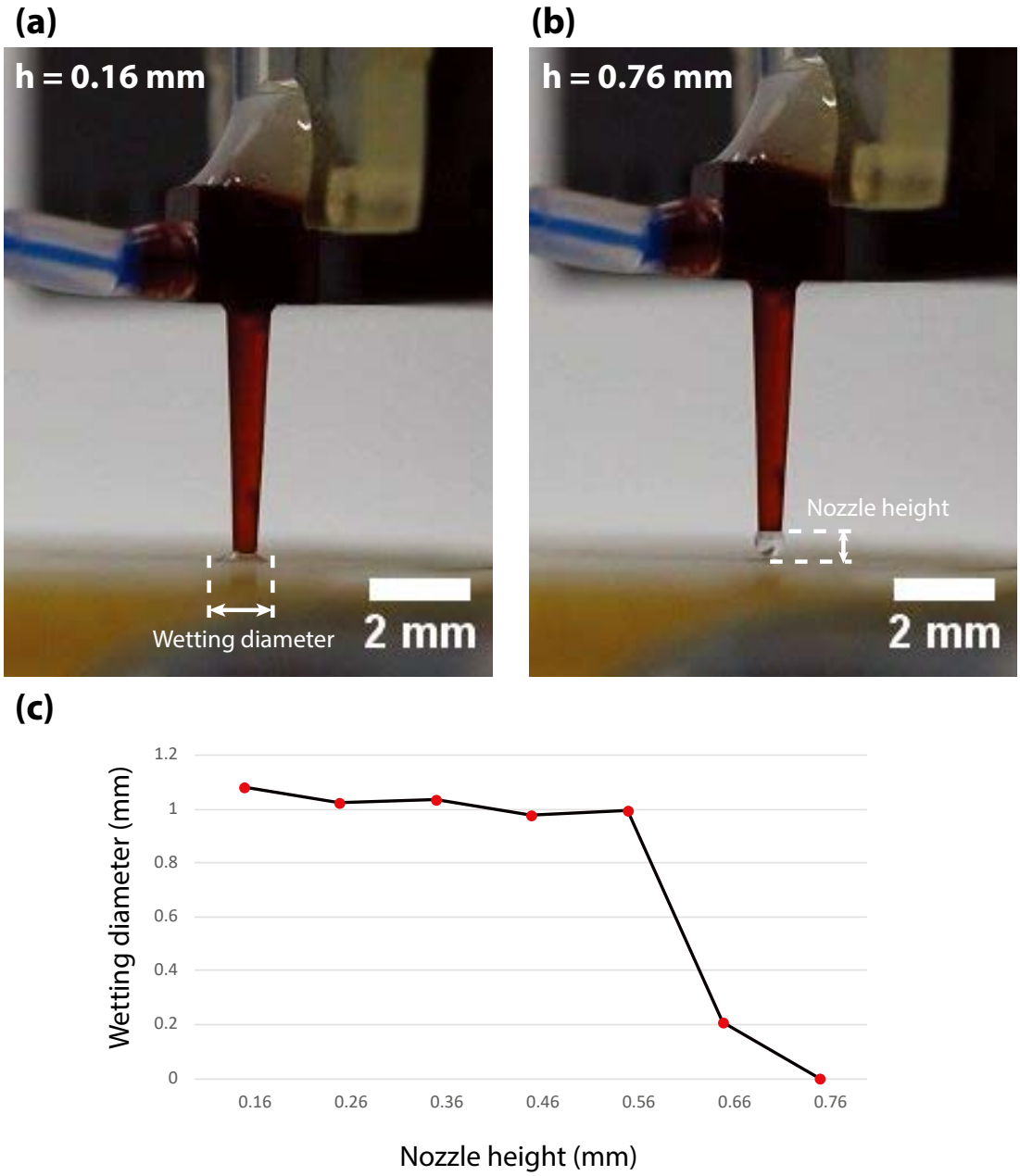

Fig. 3.6 The initial distance for printing and its effect on the surface wettability of the substrates. Representative images with height of (a) 0.16 mm and (b) 0.76 mm are shown respectively; (c) data graph on the relationship between wetting diameter and nozzle height.

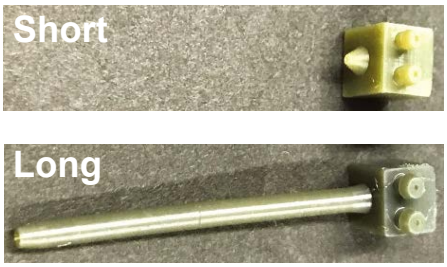

Fig. 3.7 The two types of printhead used for the printing of alginate fibers.

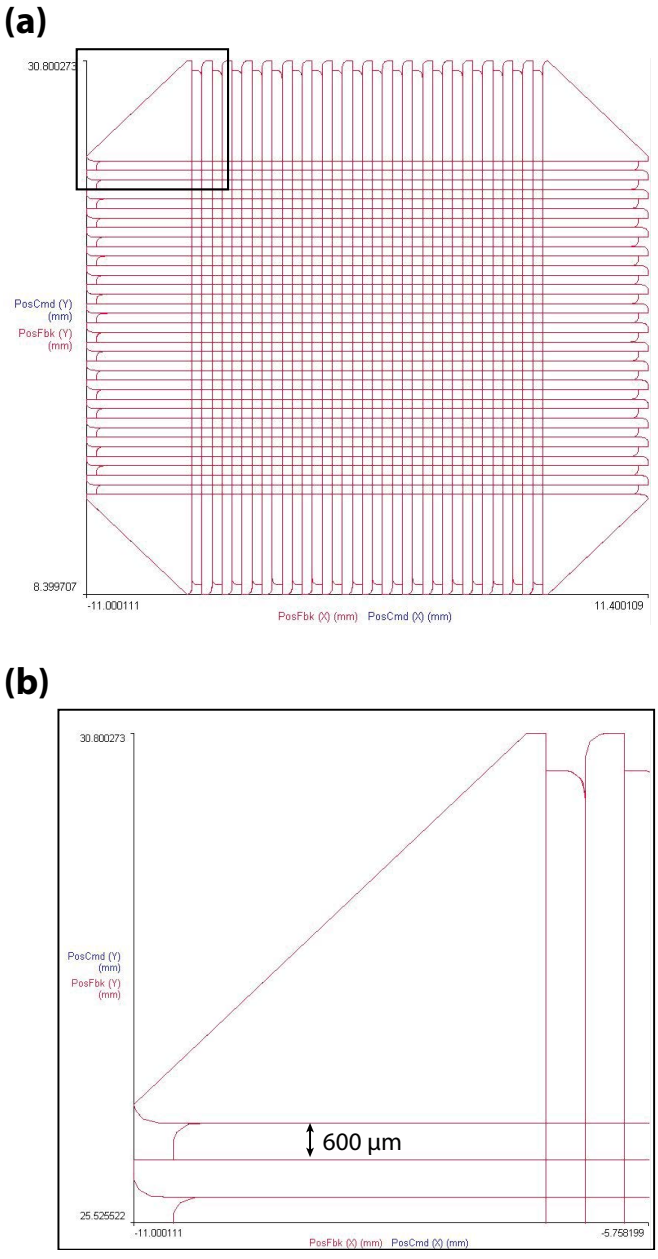

Fig. 3.8 Planar trace of the motion control programs for the printing of the mesh type structure. (a) x-y plot of the toolpath for the mesh construct; (b) zoomed in view showing detailed design geometries.

本図は雑誌掲載の形での刊行 (5 年以内に出版予定) が予定されるため、非公開とする

Fig. 3.9 The printing process of the bioprinter using long printhead. Sodium alginate is dyed with blue inks for visulization purpose only.

sodium alginate against its surrounding fluids is higher than 110, the alginate stream will starts to bend or coil periodically; to avoid such kind of bending/coiling, PEG (Mw 35k, Sigma-Aldrich, Japan) at 5 wt% is added to the sheath fluids. Another benefit of doing so is that higher viscosity can enhance the position stability of dispensed fibers against environmental vibrations during printing.

In this section, the parameters that are relatively independent are narrowed down. Other parameters which have relatively twisted interactions with each other will be described in the next section.

3.2.2 Intermediate properties

As described before, there are many interactions in-between many of the parameters. To clarify how these parameters affect the printing system, the relationship of each parameters and their effects is summarized in Fig. 3.2. Many of the tunable parameters affects a same intermediate properties at the same time. The intermediate properties are the bridge between the tunable fabrication parameters and the final printing quality. Such properties include :(1) clog immunity; (2) stability; (3) depositability. Detailed descriptions on each of the intermediate properties will be given as follow.

First, the clog immunity describes whether the printhead is able to generate fibers continuously without clogging during the whole printing process. This parameter is majorly affected by the parameters of the microfluidic printhead. Unlike spinning fibers in a water bath as described in the bench tests of the microfluidic printhead in chapter 2, the printing scenario requires the printhead to operate outside the water bath. When the printhead outlet is taken out of the water bath, droplet will be generated at the printhead outlet. Droplet formation will introduce periodic perturbation of flow rates at the outlet of the channel, under such perturbation, the clogging of fibers might happen. To enhance the clog

本図は雑誌掲載の形での刊行 (5 年以内に出版予定) が予定されるため、非公開とする

Fig. 3.10 Optimization on sodium alginate concentration and calcium cholride concentrations. (a) illustration of different printing conditions. (b) printability data for short and long nozzle.

本表は雑誌掲載の形での刊行 (5 年以内に出版予定) が予定されるため、非公開とする

Table 3.1 Optimized tunable parameter sets for the printing of cell fibers.

本図は雑誌掲載の形での刊行 (5 年以内に出版予定) が予定されるため、非公開とする

Fig. 3.11 Printed alginate fiber based construct. (a-b) photograph of the printed construct; (c) reltaive thickness measurements. (mean ±s.d., n =15)

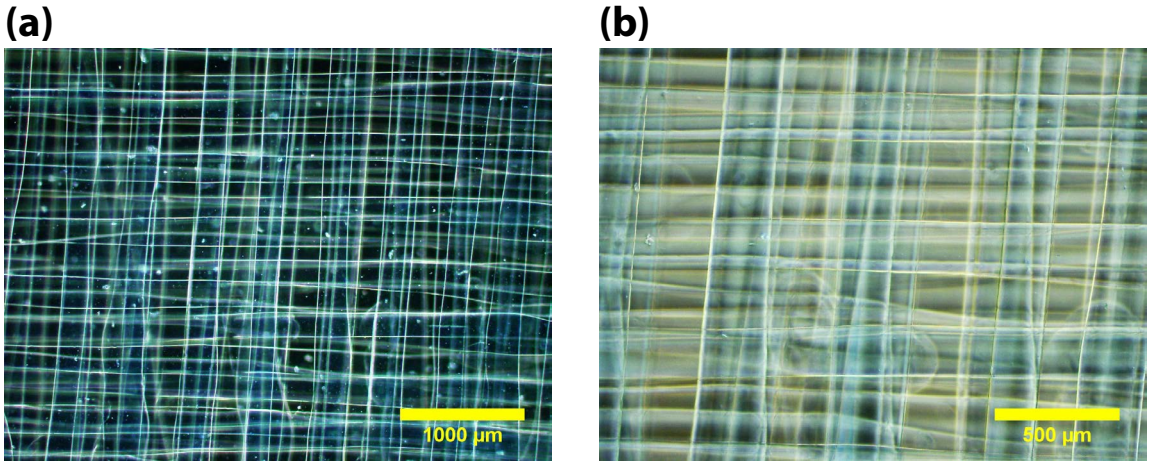

Fig. 3.12 Microscopic image of the printed construct with (a) low and (b) high magnification.

本図は雑誌掲載の形での刊行 (5 年以内に出版予定) が予定されるため、非公開とする

Fig. 3.13 The demonstration of printing arbitrary shaped constructs using "TLAB" as an example. (a-b) the toolpath for odd and even layers; (c) photograph of the printed pattern.

本図は雑誌掲載の形での刊行 (5 年以内に出版予定) が予定されるため、非公開とする

Fig. 3.14 The photograph of the construct based on core/shell alginate microfibers. (a) collected with membrane in 60 mm petri dish; (b) transferred onto slide glass.

本図は雑誌掲載の形での刊行 (5 年以内に出版予定) が予定されるため、非公開とする

Fig. 3.15 The microscopic images of the (a) center and (b) edge of the construct construct based on core/shell alginate microfibers.

immunity, the gelation completeness of the fiber at the printhead outlet should be well controlled, so that the fibers will not be too sticky to attach to the side wall of the printhead outlet. To demonstrate its effect, a set of preliminary experiments are performed. In the experiments, the gelation completeness is tuned by changing the concentration of calcium ions in the sheath fluid. During experiment, the fibers is first spinning inside a water bath, after the spinning of the fiber gets stable, the printhead is gradually withdrawn up. As a result demonstrated in Fig. 3.3, the case with 45 mM calcium ions in the sheath fluid results in immediately clogging once the nozzle leaves the water bath; on the contrary, the case with 22.5 mM calcium ions shows that no clogging happens even the fibers are generated directly in dripping droplets. The results of the experiments show that, in order to increase the clogging immunity, it is necessary to lower down the gelation completeness of the microfibers at the microfluidic printhead, otherwise the clogging will happen very frequently during printing.

Second, the stability describes the stableness of the laminar flow pattern when the printhead is

本図は雑誌掲載の形での刊行 (5 年以内に出版予定) が予定されるため、非公開とする

Fig. 3.16 Confocal microscopy analysis of the printed core/shell construct. (a) 3-D reconstructed image; (b) orthogonal image slices of the 3-D data.

subjected to high speed movements. In section, it has been proved that the fiber spinning in the water bath using the microfluidic printhead is stable against the on/off switching of core fluids as well as manually shaking of printhead. However, when using the printhead for printing purpose, the movement of the printhead causes fiber elongation (when printhead accelerates) as well as sudden deceleration (when printhead turns over to the opposite direction), since the printhead speed cannot be always the same all the time. Such elongation and sudden deceleration will introduce a strong instability to the laminar flow pattern generated in the microfluidic printhead. In experiment, it is found out that the diameter and length of outlet shall not be too small to guarantee stability. Fig. 3.4 shows the case of using printhead with long outlet length (20 mm) and small outlet diameter (0.6 mm). As a result, the fibers swell at the junction channel of the printhead, when the printhead turns over its moving direction. Next, the case of printing core/shell pattern using printhead with short outlet length (1.65 mm) and small outlet diameter (0.6 mm) is also tested. During the experiment, the core region is labeled with red fluorescent beads, while the shell is labeled with green fluorescent beads; the flow rate ratio of core against shell is 1:1, theoretically the core/shell diameter ratio of the fabricated fiber will be ca. 0.707. The experiment results shows the effect of bad stability that affects the core/shell pattern of the fabricated fibers, It can be seen from Fig. 3.5 that the the core/shell feature of the fibers printed using the short nozzle is not well established, the core of the fibers are too thin with crimped shapes; in addition, the shell is also not uniform in diameter, with frequent swelling. Such kind of poor definition of core/shell feature is due to: (1) lack of calcium penetration inside the sodium alginate solution due to short traveling time (<< 1s) in the microfluidic channels; (2) the outlet nozzle diameter of the printhead is small and short, making it vulnerable to the instability generated by swiping movement of printhead against the printing substrate.

Third, the depositability describes the ability for the fibers to be deposited onto the syringe-vacuum

本図は雑誌掲載の形での刊行 (5 年以内に出版予定) が予定されるため、非公開とする

Fig. 3.17 Manually peeling off the fibers: the printed construct actually can be deconstructed by peeling off the fibers.

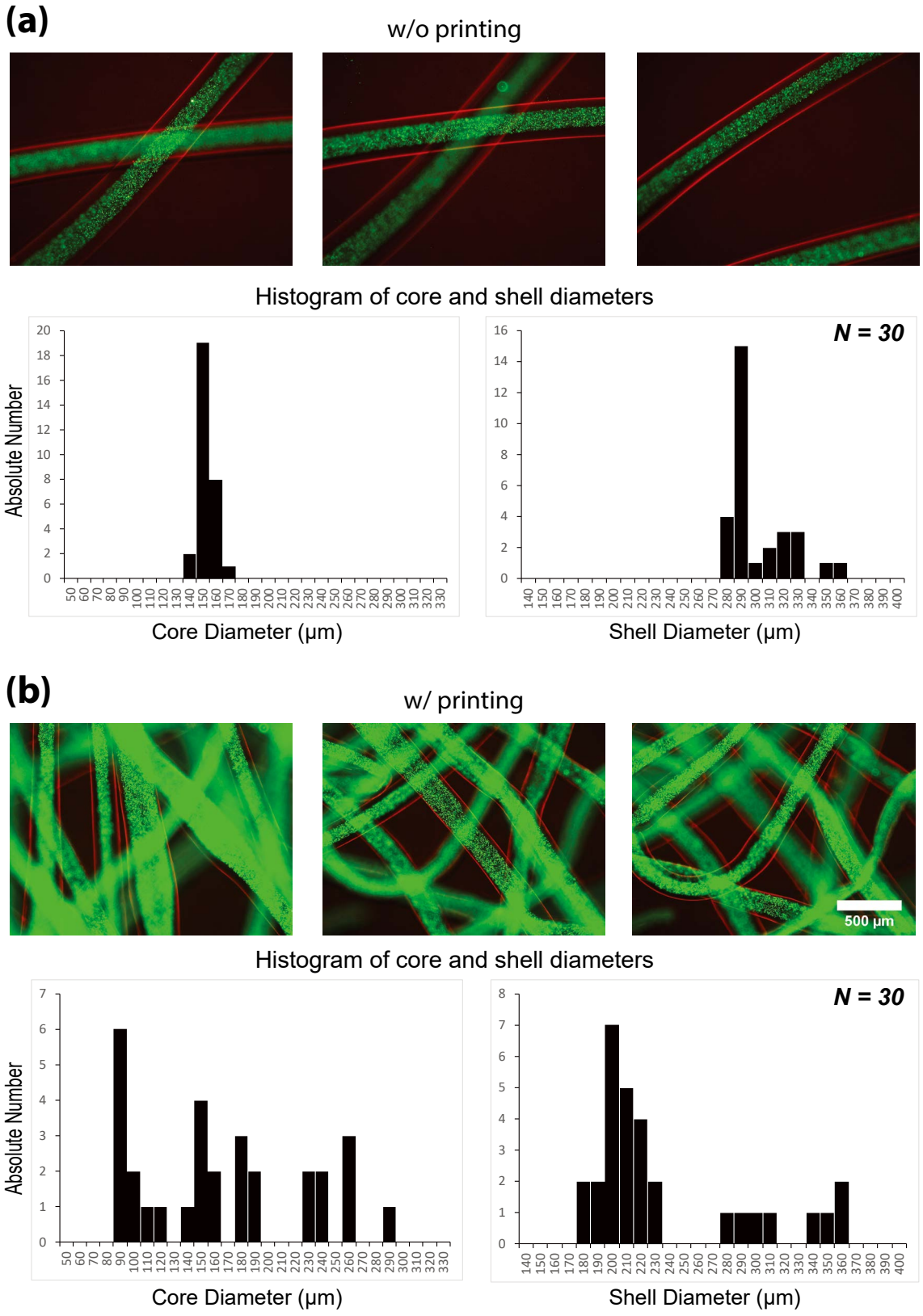

Fig. 3.18 The photograph of the fibers (a) without printing and (b) with printing, the fiber diameter distribution is less uniform when printed. (scale bar: 500 μm).

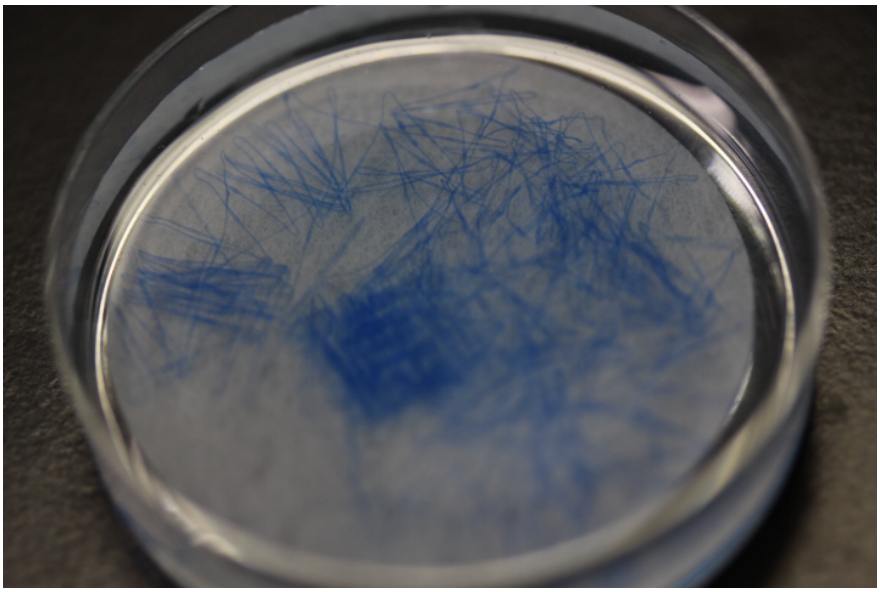

Fig. 3.20 Fully decomposited constructs into sparse fibers with strong shaking.

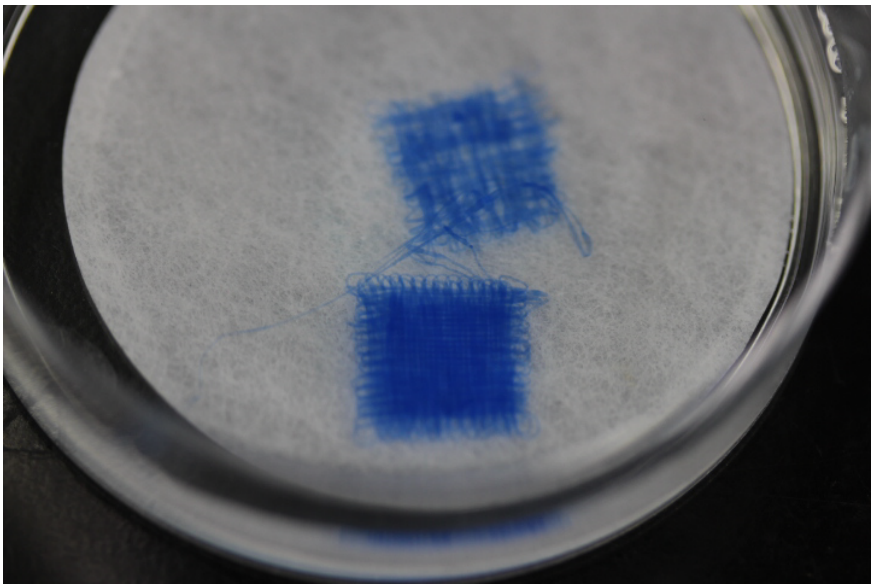

Fig. 3.19 Layering of the printed construct after gentle shaking.

substrate. Two key factors decides the deopsitability of the fibers: vacuum strength and the initial distance of the printhead to the substrate. First, the vacuum strength decides the evacuation rate of the dispensed sheath fluids; if the evacuation rate of the dispensed sheath fluids is too low, the sheath fluids

will starts to pool up and causes the deposited fiber to float. Second, the initial distance of the printhead to the substrate should be properly set up; on one hand, if the distance is too small, the fibers coming out from the printhead will find no space to escape, thus will cause clogging of the printhead; on the other hand, if the distance is too large, droplets will be formed on the outlet of the printhead, and the droplet will not be able to contact and wet the printing substrate, leading to failure on fiber deposition. The initial distance is decided by the following experiment. During the experiment, the printhead is positioned on top of the syringe-vacuum substrate. The vacuum (5 kPa) in the substrate is formed before the printhead gets close up. The sheath fluid dispensing rate of the printhead is then set to be the same as the syringe withdrawing rate of the substrate (the rate is 0.8 mL/min, specifically). Then, the height of printhead is adjusted to check out the wettability of the dispensed liquid on the substrate. From the results shown in Fig. 3.6, the printing surface is stable with constant wetting of the vacuum substrate at heights smaller than 0.56 mm.

Above all are the three important intermediate parameters that affects the quality of printing process. To show the effects of them, several preliminary experiments are conducted. However, the final optimization of these parameters cannot be decided at this stage; it shall be decided by performing the actual printing process and tuning the parameters according to the considerations given in this section.

3.3 The printing of alginate microfibers

With the strategy built-up in the previous section, experiments are performed to find out the stable protocol with which core/shell alginate microfibers can be printed. The trials are organized by the different printhead that is used for experiment, since the change of the tunable parameters related to the design of printhead is the most time-consuming part; it involves re-design of the printhead CAD models, re-fabrication using stereolithography, reinstallation and calibration of the printhead on the tip of the motor stage. As shown in Fig. 3.7, Two printhead, a “short printhead” (with outlet diameter and outlet length of 0.6 mm and 1.65 mm), and a “long printhead” (with outlet diameter and outlet length of 1 mm and 20 mm) are tested. The target structure to be printed is a mesh type structure with its planar geometry

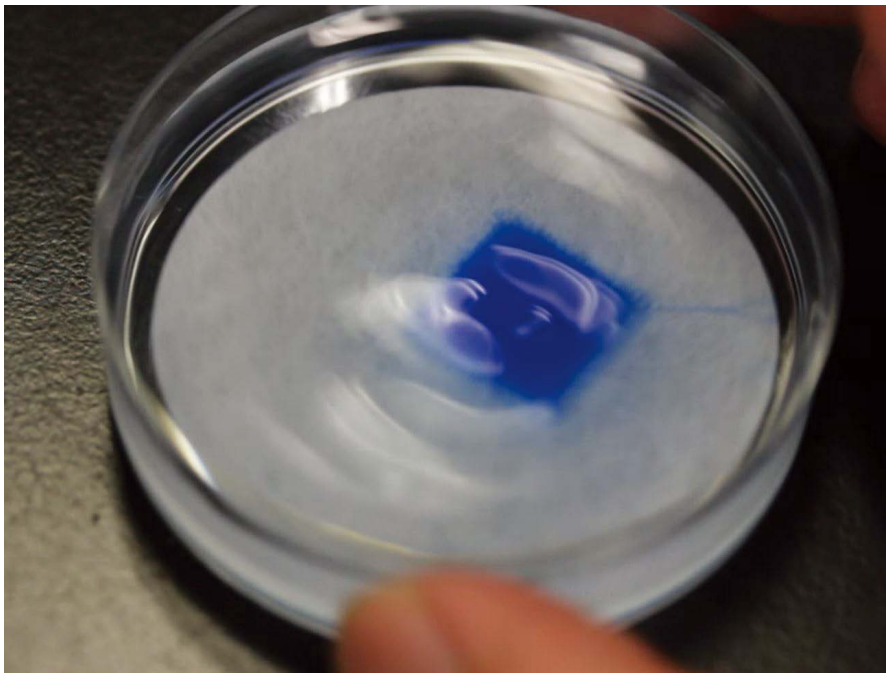

Fig. 3.21 Fibers stable with preserved microfeatures after the incubation process.

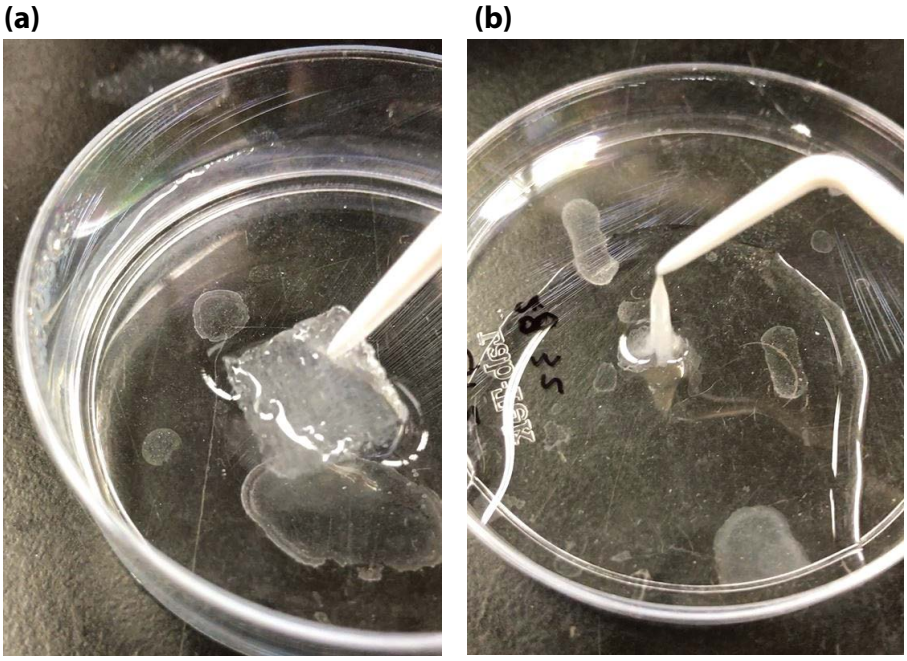

Fig. 3.22 Fiber based construct after cation particle treatment. (a) after applying cationic particles:handleable with tweezer; (b) the treated constrcut can not be fully dissolved after 55 mM citrate treatment (>10 min).

shown in Fig. 3.8. The planar pattern is composed of zigzag lines with a pitch distance of 600 μm. The automatic control program is written in Aerobasic programming language and compiled using A3200 Motion Composer (Aerotech KK, Japan). Fig. 3.8 contains not only the programmed traces of the motor, but also the sensor feedback which is recorded during the execution of the program, the programmed traces and recorded traces are colored using red and blue color; since the recorded traces are precisely matched up with the programmed traces, most of the blue curves are covered by the red curve on top of them.

3.3.1 Printing demonstration and protocol optimization

The printing process is demonstrated as shown in Fig. 3.9. Since the flow rates are predetermined as described in the previous section, the optimization of the printing parameters is focused on finding the proper sodium alginate concentration for the core fluid and the calcium concentration for the sheath fluids. During printing, to judge whether the fibers generated by the microfluidic printhead is able to stack up or not, the following inspectable features should be checked out. First, the geometrical size of the deposited fibers should be checked out, especially its relationship with the incremental height of the motor stage; if the height/thickness of the fibers deposited does not match up with the incremental height of the motor stage, the printhead will gradually get too close or too far away from the printed construct, leading to deteriorated stackability of the fibers. Second, the flexibility of the generated fibers at the outlet of the printhead should be checked out; if the fibers generated at the outlet are too stiff, the fibers can not bend and conform to the planar direction, which will cause the fibers to bounce up and misalign, making it difficult for the fibers to stack up. Third, if the fibers clogged at the outlet of the printhead, the printing process will need to be abandoned and restart again. Fourth, if the fibers are floating (i.e. not attached to each other), the printing will be not able to proceed on. If the printing process failed, one should inspect the above four inspectable features.

In experiment, various sodium alginate concentration of 0.5 wt%, 1 wt%, 1.5 wt% and 2 wt% and various calcium concentration of 10 mM, 20 mM, 50 mM, 100 mM and 200 mM are tested. Judging

from inspectable features during the printing process, the printing process is scored as “unable to stack up”, “printable” and “frequent clogging”. As shown in the Fig. 3.10, some of the tested conditions failed to stack up due to lack of mechanical integrity (alginate concentration too slow, gelation completeness not enough), resulting in too thin fibers deposited; some of the conditions failed due to frequent clogging during the printing process. The printable conditions for both short and long printhead are highlighted in the graph; for the short printhead, the printable conditions are alginate concentration of 1.5 ~ 2 wt% and calcium concentration of 100 mM; the printable conditions are alginate concentrations of 1.5 ~ 2 wt% and calcium concentration of 20-50 mM. It could be found out that the calcium concentration suitable for printing is quite different in between the short and long printhead. The reason is the long printhead has increased length for prolonged traveling time (ca. 1.33s) of microfibers in the printhead, thus to achieve the same extent of gelation completeness at the outlet, the required concentration is much lower.

Through the experiments, we conclude that the long printhead is the preferable printhead design since it requires lower calcium concentration in sheath fluids which is less cytotoxic. The optimized final printing protocol containing all the tunable parameters can be found in Table 3.1.

3.3.2 Characterization of the printed mesh construct

本小節は雑誌掲載の形での刊行 (5 年以内に出版予定) が予定されるため、非公開とする。

3.4 The printing of cell fibers

本節は雑誌掲載の形での刊行 (5 年以内に出版予定) が予定されるため、非公開とする。

3.5 Summary

In this chapter, the the actual operation of the bioprinter is tested. First, by analyzing the relationship in between the many tunable parameters, the stable protocols for printing alginate microfibers is probed by several printing trials. Then, cell-laden core/shell microfibers are printed using the stable protocols. After printing, different culture methods are tested for the maturation of cell fibers inside the printed constructs. As a result, we found out that the static culture method is unable to maturate the printed core/shell cell-laden fibers into cell fiber, while rotary culture method is capable of forming cell fibers upon culture.

Chapter 4
Applications of the cell fiber printing technology

This chapter describes the application of the tissue printing and culture technique developed in the previous chapters. The first and the most essential application of the bioprinting technique is the reconstruction of macro-sized in-vitro tissue models with tissue-like morphologies and functions. In addition, the tissue construct rebuilt in-vitro is proposed to be used as implantation graft for the treatment of acute liver failure, a disease which demands short-term replacement liver graft.

4.1 In-vitro tissue model reconstruction and evaluation

本節は雑誌掲載の形での刊行 (5 年以内に出版予定) が予定されるため、非公開とする。

4.2 Evaluations on the applicability of the tissue construct as implantation graft

本節は雑誌掲載の形での刊行 (5 年以内に出版予定) が予定されるため、非公開とする。

4.3 Summary

In this chapter, applicability of the cell fiber printing technique is tested.

First, the cell fiber printing technology is used to create thick tissue construct based on HepG2 cell fibers. The thickness of the reconstructed tissue is approximately 2/4 mm, consisting of 2 layers of rafting fibers and 10/22 layers of HepG2 cell fibers. H&E staining is performed for the histological analysis of the thick tissue construct. As a result, the cells were densely packed and highly viable, which shows that the printing technique is applicable for replicating in-vivo tissue like morphology. In addition, the reconstructed HepG2 cell fiber based tissue is able to secreat human albumin *in-vitro*. ELISA test results show that the cells in the printed construct has enhanced albumin secretion function, comparing to the cells in traditional 2D cell culture.

Then, the applicability of the HepG2 cell fiber based construct to be used as implantation graft is also tested. During the implantation and retrieval procedures, the good mechanical integrity of the construct make it easier to handle. After 3 days of implantation, human albumin was detected in mouse blood samples, showing the cell fiber based construct a potentially useful short term replacement tissue graft for the treatment of acute liver failures. Further experiments show that the increased thickness (from 5 layers to 12 layers) does not significantly increase albumin productivity *in-vivo*, which is supposed to be caused by decreased oxygen and nutrient availability in the central area of the thick construct.

Chapter 5
Conclusions

5.1 Conclusions

In this thesis, the technique for printing cell fibers is proposed and established. To enable the printing of cell fibers, a bioprinter is conceived and built up. The construction of the bioprinter covers detailed designs on its components as well as the practice of printer system assembly. Comparing to the existing bioprinting techniques, the cell fiber printing technique developed in this thesis is capable of rapidly printing densely cellularized tissue constructs. The cell fiber printing technique is then used to demonstrate the reconstruction of HepG2 cell fiber based tissue construct with *in-vivo* tissue-like morphology and function. In addition, as a proof-of-concept for using this technique to treat diseases such as acute liver failure, the HepG2 cell fiber based tissue construct was implanted into the abdomen of mouse; after 3 days of implantation, human albumin were detected in mouse blood samples, showing that the cell fiber based construct is a potentially useful short-term replacement tissue for the treatment of acute liver failures.

For the purpose of printing cell fibers, this thesis conceived and designed a bioprinter, starting from

each components of the bioprinter. First, the microfluidic printhead is designed and fabricated using stereolithography based approach; bench tests performed on the printhead shows that it is capable of generating core/shell hydrogel microfibers steadily, with controlled spinning velocity. Second, the syringe-vacuum substrate is designed and implemented, by combining a commercially available filter membrane with a perforated vacuum chamber fabricated using 3-D printer. The working principle of the vacuum substrate is then proposed and analyzed, with corresponding bench test experiments to find suitable working paramters. Then, the motion control system, pumping and tubing systems is discussed. Finally, the assembly of all the components into a whole system is described.

Following the detailed designs and implementation of the bioprinter, the the actual operation of the bioprinter was then demonstrated. First, by analyzing the relationship in between the many tunable parameters, the stable protocols for printing alginate microfibers is found out by several printing trials. Then, cell-laden core/shell microfibers are printed using the protocols. After printing, the viability of cells are tested, showing that more than 75% of cells are alive after being printed. Then, for the maturation of cell fibers inside the printed constructs, different culture methods are compared. As a result, we found that the static culture method was unable to maturate the printed core/shell cell-laden fibers into cell fiber, while rotary culture method was capable of forming cell fibers upon culture.

After the demonstration on the capability of the cell fiber bioprinter. The applicability of the cell fiber printing technique is further considered and experimented.

本段落は雑誌掲載の形での刊行 (5 年以内に出版予定) が予定されるため、非公開とする。

To summarize, this thesis starts with the fundamental designs and system implementation of the bioprinter which is capable of printing cell fibers, then established stable protocols for printing cell fibers using the bioprinter, and finally tested the applicability of the cell fiber printing technology.

5.2 Future outlooks

5.2.1 Printing system & culture system improvement

For the cell fiber based printing strategy, the cell fiber printing technology developed in this thesis will

be the first and foundational step towards the ultimate goal of building densely cellularized tissues.

Based on the technology developed in this thesis, further developments on both the printing system and the relative culture system can be expected. Regarding the printing system: first, the ability to print hollow fibers with endothelial cells encapsulated in the core region will have the potential to enable lumen structure reconstruction in the cell fiber based tissue construct; second, microfluidic fluid switching techniques could be integrated to enable the fabrication of heterogeneous cell fiber based construct with multiple types of cell fibers deposited with precise spatial control; finally, the combination of these two technology is able to fabricate heterogeneous tissue constructs with capillary vessel networks.

Alongside the development of printing system, the culture system development is also essentially important. Bioreactors with controlled oxygen delivery and the capability of perfusing the cell fiber based constructs will further increase the maturation speed of the cell fibers; in addition, the inletting and outletting system of the bioreactor actually mimics the major blood vessels which connect internal organs to circulation system, which will facilitate the practical usages of the in-vitro reconstructed tissues such as for implantation purposes.

5.2.2 Towards the applicable implantation graft

In this thesis, the proof-of-concept experiments of using the cell fiber based tissue construct as implantation graft is conducted. Based on the proof-of-concept work in this thesis, further developments towards real application of using the printed tissue constructs as implantation graft can be expected. For practical application, several improvements on the technique is required. First, the size of the printed construct should be able to scale up further to encapsulate more amount of cells, in order to be applied for larger animals comparing to mouse. Second, other types of hepatocytes should be adopted to replace HepG2 cells which are used in this thesis; as a cancer derived cell, HepG2 cell exhibit abnormal liver functions comparing to normal hepatocytes, the encapsulation of normal hepatocyte is expected to create tissue constructs with more native liver functions. Third, foreign body react which will attack the

implanted tissue graft shall be attenuated for longer survival of cells in the implanted graft; adjusting the alginate material which is used to encapsulate cells can be a possible method to attenuate the immune attack due to foreign body react.

Bibliography

[1] D. H. Freedman, “Layer by Layer,” MIT Technology Review, 19-Dec-2011.

[2] H. Lipson and M. Kurman, Fabricated: The New World of 3D Printing. John Wiley & Sons, 2013.

[3] R. Langer and J. P. Vacanti, “Tissue engineering,” Science, vol. 260, no. 5110, pp. 920–926, May 1993.

[4] N. Cubo, M. Garcia, J. F. Del Cañizo, D. Velasco, and J. L. Jorcano, “3D bioprinting of functional human skin: production and in vivo analysis,” Biofabrication, vol. 9, no. 1, p. 015006, Dec. 2016.

[5] V. Lee et al., “Design and fabrication of human skin by three-dimensional bioprinting,” Tissue Eng. Part C Methods, vol. 20, no. 6, pp. 473–484, Jun. 2014.

[6] C. Velasquillo, E. A. Galue, L. Rodriquez, C. Ibarra, and L. G. Ibarra-Ibarra, “Skin 3D bioprinting. Applications in cosmetology,” 2013.

[7] H.-W. Kang, S. J. Lee, I. K. Ko, C. Kengla, J. J. Yoo, and A. Atala, “A 3D bioprinting system to produce human-scale tissue constructs with structural integrity,” Nat. Biotechnol., vol. 34, no. 3, pp. 312–319, Mar. 2016.

[8] Y. Yu, Y. Zhang, J. A. Martin, and I. T. Ozbolat, “Evaluation of cell viability and functionality in vessel-like bioprintable cell-laden tubular channels,” J. Biomech. Eng., vol. 135, no. 9, p. 91011, Sep. 2013.

[9] H.-W. Kang, J. J. Yoo, and A. Atala, “Bioprinted Scaffolds for Cartilage Tissue Engineering,” Methods Mol. Biol., vol. 1340, pp. 161–169, 2015.

[10] S. J. Lee, I. K. Ko, C. Kengla, J. J. Yoo, and A. Atala, “A 3D bioprinting system to produce human-scale tissue constructs with structural integrity,” Nature, 2016.

[11] C. Colosi et al., “Microfluidic Bioprinting of Heterogeneous 3D Tissue Constructs Using Low-Viscosity Bioink,” Adv. Mater., vol. 28, no. 4, pp. 677–684, Jan. 2016.

[12] A. G. Tabriz, M. A. Hermida, N. R. Leslie, and W. Shu, “Three-dimensional bioprinting of complex cell laden alginate hydrogel structures,” Biofabrication, vol. 7, no. 4, p. 045012, Dec. 2015.

[13] D. B. Kolesky, R. L. Truby, A. S. Gladman, T. A. Busbee, K. A. Homan, and J. A. Lewis, “3D bioprinting of vascularized, heterogeneous cell-laden tissue constructs,” Adv. Mater., vol. 26, no. 19, pp. 3124–3130, May 2014.

[14] A. L. Rutz, K. E. Hyland, A. E. Jakus, W. R. Burghardt, and R. N. Shah, “A multimaterial bioink method for 3D printing tunable, cell-compatible hydrogels,” Adv. Mater., vol. 27, no. 9, pp. 1607–1614, Mar. 2015.

[15] Z. Wu, X. Su, Y. Xu, B. Kong, W. Sun, and S. Mi, “Bioprinting three-dimensional cell-laden tissue constructs with controllable degradation,” Sci. Rep., vol. 6, p. 24474, Apr. 2016.

[16] “Cyfuse Biomedical K.K. | 株式会社サイフューズ .” [Online]. Available: http://www.cyfusebio.com/. [Accessed: 27-May-2017].

[17] K. Jakab, C. Norotte, F. Marga, K. Murphy, G. Vunjak-Novakovic, and G. Forgacs, “Tissue engineering by self-assembly and bio-printing of living cells,” Biofabrication, vol. 2, no. 2, p. 022001, Jun. 2010.

[18] C. Norotte, F. S. Marga, L. E. Niklason, and G. Forgacs, “Scaffold-free vascular tissue engineering using bioprinting,” Biomaterials, vol. 30, no. 30, pp. 5910–5917, Oct. 2009.

[19] Y. Yu et al., “Three-dimensional bioprinting using self-assembling scalable scaffold-free ‘tissue strands’ as a new bioink,” Sci. Rep., vol. 6, p. 28714, Jun. 2016.

[20] H. Onoe et al., “Metre-long cell-laden microfibres exhibit tissue morphologies and functions,” Nat. Mater., vol. 12, no. 6, pp. 584–590, Mar. 2013.

[21] J. W. Nichol and A. Khademhosseini, “Modular Tissue Engineering: Engineering Biological Tissues from the Bottom Up,” Soft Matter, vol. 5, no. 7, pp. 1312–1319, 2009.

[22] D. L. Elbert, “Bottom-up tissue engineering,” Curr. Opin. Biotechnol., vol. 22, no. 5, pp. 674–680, Oct. 2011.

[23] H. Onoe and S. Takeuchi, “Cell-laden microfibers for bottom-up tissue engineering,” Drug Discov. Today, vol. 20, no. 2, pp. 236–246, Feb. 2015.

[24] Y. Morimoto, A. Y. Hsiao, and S. Takeuchi, “Point-, line-, and plane-shaped cellular constructs for 3D tissue assembly,” Adv. Drug Deliv. Rev., vol. 95, pp. 29–39, Dec. 2015.

[25] G. H. Lee, J. S. Lee, X. Wang, and S. Hoon Lee, “Bottom-Up Engineering of Well-Defined 3D Microtissues Using Microplatforms and Biomedical Applications,” Adv. Healthc. Mater., vol. 5, no. 1, pp. 56–74, Jan. 2016.

[26] M. W. Laschke and M. D. Menger, “Life is 3D: Boosting Spheroid Function for Tissue Engineering,” Trends Biotechnol., vol. 35, no. 2, pp. 133–144, Feb. 2017.

[27] B. G. Chung, K.-H. Lee, A. Khademhosseini, and S.-H. Lee, "Microfluidic fabrication of microengineered hydrogels and their application in tissue engineering," Lab Chip, vol. 12, no. 1, pp. 45–59, 2012.

[28] N. L' heureux, S. Pâquet, R. Labbé, L. Germain, and F. A. Auger, "A completely biological tissue-engineered human blood vessel," The FASEB Journal, vol. 12, no. 1, pp. 47–56, Jan. 1998.

[29] I. E. Hannachi, M. Yamato, and T. Okano, "Cell sheet technology and cell patterning for biofabrication," Biofabrication, vol. 1, no. 2, p. 022002, Jun. 2009.

[30] C. W. Hull, "Apparatus for production of three-dimensional objects by stereolithography," 4575330, 11-Mar-1986.

[31] J. Malda et al., "25th Anniversary Article: Engineering Hydrogels for Biofabrication," Adv. Mater., vol. 25, no. 36, pp. 5011–5028, Sep. 2013.

[32] M. Nakamura et al., "Biocompatible inkjet printing technique for designed seeding of individual living cells," Tissue Eng., vol. 11, no. 11–12, pp. 1658–1666, Nov. 2005.

[33] K. Arai, S. Iwanaga, H. Toda, C. Genci, Y. Nishiyama, and M. Nakamura, "Three-dimensional inkjet biofabrication based on designed images," Biofabrication, vol. 3, no. 3, p. 034113, Sep. 2011.

[34] T. Xu et al., "Viability and electrophysiology of neural cell structures generated by the inkjet printing method," Biomaterials, vol. 27, no. 19, pp. 3580–3588, Jul. 2006.

[35] T. Xu, H. Kincaid, A. Atala, and J. J. Yoo, "High-Throughput Production of Single-Cell Microparticles Using an Inkjet Printing Technology," J. Manuf. Sci. Eng., vol. 130, no. 2, p. 021017, Apr. 2008.

[36] V. Mironov, R. R. Markwald, and G. Forgacs, "ORGAN PRINTING: SELF-ASSEMBLING CELL AGGREGATES AS ' BIOINK,'" Science and Medicine, vol. 9, no. 2, pp. 69–71, 2003.

[37] A. Akkouch, Y. Yu, and I. T. Ozbolat, "Microfabrication of scaffold-free tissue strands for three-dimensional tissue engineering," Biofabrication, vol. 7, no. 3, p. 031002, Sep. 2015.

[38] X. Ma et al., "Deterministically patterned biomimetic human iPSC-derived hepatic model via rapid 3D bioprinting," Proc. Natl. Acad. Sci. U. S. A., vol. 113, no. 8, pp. 2206–2211, Feb. 2016.

[39] J. Liu, H. H. Hwang, P. Wang, G. Whang, and S. Chen, "Direct 3D-printing of cell-laden constructs in microfluidic architectures," Lab Chip, vol. 16, no. 8, pp. 1430–1438, 2016.

[40] W. Zhu et al., "Direct 3D bioprinting of prevascularized tissue constructs with complex

microarchitecture," Biomaterials, vol. 124, pp. 106–115, Apr. 2017.

[41] W. Liu et al., "Rapid Continuous Multimaterial Extrusion Bioprinting," Adv. Mater., Nov. 2016.

[42] D. B. Kolesky, K. A. Homan, M. A. Skylar-Scott, and J. A. Lewis, "Three-dimensional bioprinting of thick vascularized tissues," Proc. Natl. Acad. Sci. U. S. A., vol. 113, no. 12, pp. 3179–3184, Mar. 2016.

[43] "The 3D-Bioplotter by EnvisionTEC | A World Leading Bioprinter," EnvisionTEC. [Online]. Available: https://envisiontec.com/3d-printers/3d-bioplotter/. [Accessed: 23-May-2017].

[44] "Organovo: NovoGen MMX BioprinterTM — Life Sciences — Invetech." [Online]. Available: http://www.invetech.com.au/portfolio/life-sciences/3d-bioprinter-world-first-print-human-tissue/. [Accessed: 23-May-2017].

[45] "3D Bio-Printers - regenHU." [Online]. Available: https://www.regenhu.com/products/3d-bioprinting.html. [Accessed: 23-May-2017].

[46] "Bioprinter FABION." [Online]. Available: http://www.bioprinting.ru/en/investors/projects/fabion/. [Accessed: 23-May-2017].

[47] "Biobot 1 |." [Online]. Available: https://www.biobots.io/biobot-1/. [Accessed: 23-May-2017].

[48] "BioBot 2." [Online]. Available: https://www.biobot2.com/. [Accessed: 23-May-2017].

[49] C. Colosi et al., "Rapid prototyping of chitosan-coated alginate scaffolds through the use of a 3D fiber deposition technique," J. Mater. Chem. B Mater. Biol. Med., vol. 2, no. 39, pp. 6779–6791, Jul. 2014.

[50] M. Costantini et al., "3D bioprinting of BM-MSCs-loaded ECM biomimetic hydrogels for in vitro neocartilage formation," Biofabrication, vol. 8, no. 3, p. 035002, Jul. 2016.

[51] Y. S. Zhang et al., "Bioprinting 3D microfibrous scaffolds for engineering endothelialized myocardium and heart-on-a-chip," Biomaterials, vol. 110, pp. 45–59, Dec. 2016.

[52] S. H. Ahn, H. J. Lee, J.-S. Lee, H. Yoon, W. Chun, and G. H. Kim, "A novel cell-printing method and its application to hepatogenic differentiation of human adipose stem cell-embedded mesh structures," Sci. Rep., vol. 5, p. 13427, Aug. 2015.

[53] A. D. Augst, H. J. Kong, and D. J. Mooney, "Alginate hydrogels as biomaterials," Macromol. Biosci., vol. 6, no. 8, pp. 623–633, Aug. 2006.

[54] F. Pati et al., "Printing three-dimensional tissue analogues with decellularized extracellular matrix bioink," Nat. Commun., vol. 5, p. 3935, Jun. 2014.

[55] W. Jia et al., “Direct 3D bioprinting of perfusable vascular constructs using a blend bioink,” Biomaterials, vol. 106, pp. 58–68, Nov. 2016.

[56] C. Gentile, P. A. Fleming, V. Mironov, K. M. Argraves, W. S. Argraves, and C. J. Drake, “VEGF-mediated fusion in the generation of uniluminal vascular spheroids,” Dev. Dyn., vol. 237, no. 10, pp. 2918–2925, Oct. 2008.

[57] J. M. Pérez-Pomares, V. Mironov, J. A. Guadix, D. Macías, R. R. Markwald, and R. Muñoz-Chápuli, “In vitro self-assembly of proepicardial cell aggregates: an embryonic vasculogenic model for vascular tissue engineering,” Anat. Rec. A Discov. Mol. Cell. Evol. Biol., vol. 288, no. 7, pp. 700–713, Jul. 2006.

[58] S. F. Wong, D. Y. No, Y. Y. Choi, D. S. Kim, B. G. Chung, and S.-H. Lee, “Concave microwell based size-controllable hepatosphere as a three-dimensional liver tissue model,” Biomaterials, vol. 32, no. 32, pp. 8087–8096, Nov. 2011.

[59] H. Tekin, M. Anaya, M. D. Brigham, C. Nauman, R. Langer, and A. Khademhosseini, “Stimuli-responsive microwells for formation and retrieval of cell aggregates,” Lab Chip, vol. 10, no. 18, pp. 2411–2418, Sep. 2010.

[60] Y. T. Matsunaga, Y. Morimoto, and S. Takeuchi, “Molding cell beads for rapid construction of macroscopic 3D tissue architecture,” Adv. Mater., vol. 23, no. 12, pp. H90–4, Mar. 2011.

[61] M. Hospodiuk, M. Dey, D. Sosnoski, and I. T. Ozbolat, “The bioink: A comprehensive review on bioprintable materials,” Biotechnol. Adv., Jan. 2017.

[62] Y. Yu, Y. Zhang, and I. T. Ozbolat, “A Hybrid Bioprinting Approach for Scale-Up Tissue Fabrication,” J. Manuf. Sci. Eng., vol. 136, no. 6, p. 061013, Dec. 2014.

[63] W. Schuurman, V. Khristov, M. W. Pot, P. R. van Weeren, W. J. A. Dhert, and J. Malda, “Bioprinting of hybrid tissue constructs with tailorable mechanical properties,” Biofabrication, vol. 3, no. 2, p. 021001, Jun. 2011.

[64] T. K. Merceron et al., “A 3D bioprinted complex structure for engineering the muscle–tendon unit - IOPscience,” Biofabrication, vol. 7, no. 3, p. 035003, Jun. 2015.

[65] I. T. Ozbolat, “Bioprinting scale-up tissue and organ constructs for transplantation,” Trends Biotechnol., vol. 33, no. 7, pp. 395–400, Jul. 2015.

[66] R. G. Wells, “The role of matrix stiffness in regulating cell behavior,” Hepatology, vol. 47, no. 4, pp. 1394–1400, Apr. 2008.

[67] S. K. Bhatia, Engineering Biomaterials for Regenerative Medicine: Novel Technologies for Clinical Applications. Springer Science & Business Media, 2011.

[68] S. Even-Ram and K. M. Yamada, "Cell migration in 3D matrix," Curr. Opin. Cell Biol., vol. 17, no. 5, pp. 524–532, Oct. 2005.

[69] H.-B. Zhang, T.-L. Xing, R.-X. Yin, Y. Shi, S.-M. Yang, and W.-J. Zhang, "Three-dimensional bioprinting is not only about cell-laden structures," Chin. J. Traumatol., vol. 19, no. 4, pp. 187–192, Aug. 2016.

[70] R. Chang, K. Emami, H. Wu, and W. Sun, "Biofabrication of a three-dimensional liver micro-organ as an in vitro drug metabolism model," Biofabrication, vol. 2, no. 4, p. 045004, Dec. 2010.

[71] S. Knowlton, S. Onal, C. H. Yu, J. J. Zhao, and S. Tasoglu, "Bioprinting for cancer research," Trends Biotechnol., vol. 33, no. 9, pp. 504–513, Sep. 2015.

[72] J. I. Rodríguez-Dévora, B. Zhang, D. Reyna, Z.-D. Shi, and T. Xu, "High throughput miniature drug-screening platform using bioprinting technology," Biofabrication, vol. 4, no. 3, p. 035001, Sep. 2012.

[73] G. Pless, "Artificial and bioartificial liver support," Organogenesis, vol. 3, no. 1, pp. 20–24, Jan. 2007.

[74] B. Brandsaeter et al., "Fulminant hepatic failure: outcome after listing for highly urgent liver transplantation-12 years experience in the nordic countries," Liver Transpl., vol. 8, no. 11, pp. 1055–1062, Nov. 2002.

[75] A. M. Gañán-Calvo, R. González-Prieto, P. Riesco-Chueca, M. A. Herrada, and M. Flores-Mosquera, "Focusing capillary jets close to the continuum limit," Nat. Phys., vol. 3, no. 10, pp. 737–742, Sep. 2007.

[76] A. S. Utada, E. Lorenceau, D. R. Link, P. D. Kaplan, H. A. Stone, and D. A. Weitz, "Monodisperse double emulsions generated from a microcapillary device," Science, vol. 308, no. 5721, pp. 537–541, Apr. 2005.

[77] S. Takeuchi, P. Garstecki, D. B. Weibel, and G. M. Whitesides, "An Axisymmetric Flow-Focusing Microfluidic Device," Adv. Mater., vol. 17, no. 8, pp. 1067–1072, Apr. 2005.

[78] Y. Morimoto, K. Kuribayashi-Shigetomi, and S. Takeuchi, "A hybrid axisymmetric flow-focusing device for monodisperse picoliter droplets," J. Micromech. Microeng., vol. 21, no. 5, p. 054031, 2011.

[79] Y. Yu, H. Wen, J. Ma, S. Lykkemark, H. Xu, and J. Qin, "Flexible Fabrication of Biomimetic Bamboo-Like Hybrid Microfibers," Adv. Mater., vol. 26, no. 16, pp. 2494–2499, Apr. 2014.

[80] M. E. Kinahan et al., "Tunable silk: using microfluidics to fabricate silk fibers with

controllable properties," Biomacromolecules, vol. 12, no. 5, pp. 1504–1511, May 2011.

[81] W. Jeong, J. Kim, S. Kim, S. Lee, G. Mensing, and D. J. Beebe, "Hydrodynamic microfabrication via 'on the fly' photopolymerization of microscale fibers and tubes," Lab Chip, vol. 4, no. 6, pp. 576–580, Dec. 2004.

[82] Y. Jun, E. Kang, S. Chae, and S.-H. Lee, "Microfluidic spinning of micro- and nano-scale fibers for tissue engineering," Lab Chip, vol. 14, no. 13, pp. 2145–2160, Jul. 2014.

[83] E. Kang, S.-J. Shin, K. H. Lee, and S.-H. Lee, "Novel PDMS cylindrical channels that generate coaxial flow, and application to fabrication of microfibers and particles," Lab Chip, vol. 10, no. 14, pp. 1856–1861, Jul. 2010.

[84] J. Cheng, D. Park, Y. Jun, J. Lee, J. Hyun, and S.-H. Lee, "Biomimetic spinning of silk fibers and in situ cell encapsulation," Lab Chip, vol. 16, no. 14, pp. 2654–2661, May 2016.

[85] T. Cubaud and T. G. Mason, "Formation of miscible fluid microstructures by hydrodynamic focusing in plane geometries," Phys. Rev. E Stat. Nonlin. Soft Matter Phys., vol. 78, no. 5 Pt 2, p. 056308, Nov. 2008.

[86] Z.-J. Meng, W. Wang, R. Xie, X.-J. Ju, Z. Liu, and L.-Y. Chu, "Microfluidic generation of hollow Ca-alginate microfibers," Lab Chip, vol. 16, no. 14, pp. 2673–2681, May 2016.

[87] Y. Morimoto, W.-H. Tan, and S. Takeuchi, "Three-dimensional axisymmetric flow-focusing device using stereolithography," Biomed. Microdevices, vol. 11, no. 2, pp. 369–377, Apr. 2009.

[88] A. O. Ragheb, B. L. Bates, N. E. Fearnot, T. G. Kozma, and I. William D. Voorhees, "Coated implantable medical device," 5824049, 20-Oct-1998.

[89] T. Sun et al., "Magnetic assembly of microfluidic spun alginate microfibers for fabricating three-dimensional cell-laden hydrogel constructs," Microfluid. Nanofluidics, vol. 19, no. 5, pp. 1169–1180, Sep. 2015.

[90] A. Chambers, Modern Vacuum Physics. CRC Press, 2004.

[91] I. J. R. Aitchison, "The Vacuum and Unification," in The Philosophy of Vacuum, S. Saunders and H. R. Brown, Eds. Oxford University Press, 1991, pp. 159–196.

[92] N. Harris, "Modern vacuum practice," 2007.

[93] "Vacuum Pump | ULVAC | Products." [Online]. Available: https://www.ulvac.co.jp/products_e/components/vacuum-pump. [Accessed: 01-Jun-2017].

[94] "AF1 Dual - Vacuum & Pressure Controller - Elveflow," Elveflow. [Online]. Available: http://www.elveflow.com/microfluidic-flow-control-products/flow-control-system/high-accuracy-vacuum-pumps/. [Accessed: 01-Jun-2017].

[95] M. J. Akers, Sterile Drug Products: Formulation, Packaging, Manufacturing and Quality. CRC Press, 2016.

[96] J. Kee Paik, A. K. Thayamballi, and G. Sung Kim, "The strength characteristics of aluminum honeycomb sandwich panels," Thin-Walled Struct., vol. 35, no. 3, pp. 205–231, Nov. 1999.

[97] A.-J. Wang and D. L. McDowell, "In-Plane Stiffness and Yield Strength of Periodic Metal Honeycombs," J. Eng. Mater. Technol., vol. 126, no. 2, pp. 137–156, Apr. 2004.

[98] M. Nie and S. Takeuchi, "Microfluidics based synthesis of coiled hydrogel microfibers with flexible shape and dimension control," Sens. Actuators B Chem., vol. 246, pp. 358–362, 2017/7.

[99] S. Tottori and S. Takeuchi, "Formation of liquid rope coils in a coaxial microfluidic device," RSC Adv., vol. 5, no. 42, pp. 33691–33695, 2015.

[100] J. K. Nunes, H. Constantin, and H. A. Stone, "Microfluidic tailoring of the two-dimensional morphology of crimped microfibers," Soft Matter, vol. 9, no. 16, p. 4227, 2013.

[101] A. Y. Hsiao, T. Okitsu, H. Teramae, and S. Takeuchi, "3D Tissue Formation of Unilocular Adipocytes in Hydrogel Microfibers," Adv. Healthc. Mater., vol. 5, no. 5, pp. 548–556, Mar. 2016.

[102] A. Y. Hsiao et al., "Smooth Muscle-Like Tissue Constructs with Circumferentially Oriented Cells Formed by the Cell Fiber Technology," PLoS One, vol. 10, no. 3, p. e0119010, 2015.

[103] G. A. Somerville and R. A. Proctor, "Cultivation conditions and the diffusion of oxygen into culture media: the rationale for the flask-to-medium ratio in microbiology," BMC Microbiol., vol. 13, p. 9, Jan. 2013.

[104] A. G. Lee, C. P. Arena, D. J. Beebe, and S. P. Palecek, "Development of macroporous poly(ethylene glycol) hydrogel arrays within microfluidic channels," Biomacromolecules, vol. 11, no. 12, pp. 3316–3324, Dec. 2010.

Appendix A: Rotary culture protocols

The rotary culture protocol for maturation of cell fiber in the printed constructs is as follow:

1. Print the cell fiber based constucts following standard printing procedure.

2. Apply cationic particle containing solution to the printed tissue construct and soak for 1 min.

3. Remove cationic particle containing solution using water absorbent tissue paper.

4. Transfter the treated construct into thick petri dish (ThermoFisher, 60 mm), add 6 mL low glucose cell culture medium to the dish.

5. Set rotary mixer (Nissin, Rotary Shaker NA-301) and swith to speed 7.

6. Set the tissue construct containting dish on the rotary mixer and turn on the mixer.

7. Full volume culture medium are exchanged in a daily manner.

Appendix B: Cryosection

The protocol for cryosection are as follow:

1. Fix samples using 4% calcium containing Paraformaldehyde (PFA) and soak for more than 3 hours.

2. After the fixation of the samples, transfer the sample to calcium containing 10% sucrose (ca. 2 hours), 20% sucrose (ca. 2 hours), 30% sucrose (overnight)

3. Transfer the sample from 30% sucrose to OCT compound, soak for 1 hour at room temperature.

4. Transter the sample with OCT compund to plastic containers, and freeze the sample within containter using liquid nitrogen.

5. Cut freezed samples into 8 μm thick dissections using cryostat, transfer the dissections onto specially coated slide glass.

6. Dry the samples under dry condition for ca. 1 hour, then proceed to staining process. If not proceeding to the staining process, the samples shall be stored in hermetically sealed containers at -20 Celsius degree.

Appendix C: H & E staining

H & E staining protocol is as follow:

1. Wash the sample dissections using tap water for 20 times, this procedure is for the removal of OCT compounds.

2. Soak the sample dissections into Hematoxylin for 5 min.

3. Wash the dissections: transfer the dissections into a large container fully filled with constantly in-flow of fresh tap water and wait for 20 min.

4. Soak the sample dissections into eosin for 1 min with frequent shaking.

5. Wash the dissections by soaking into 99% ethanol with frequent shaking for ca. 10 seconds. Repeat the procedures 3 times.

6. Mount the samples using Entellan® new (EMD Millipore Corporation), cap with slide glasses and dry the mounted slides at dry condition overnight.

Appendix D: Coiled fiber fabrication

A method for flexible formation of coiled hydrogel microfibers is described here. The formation method of coiled pattern relies on the viscostiy and gelation rate tunning of the fiber spinning process, which is compatible with the fiber printing methods developed in this thesis; thus, it is possible to print coiled hydrogel fibers by combining the coiled fiber fabrication technique described here with the fiber printing technology.

Detailed description on the coiled fiber formation method is as follow:

1. Coiling phenomenon can be triggered inside the microfluidic tunnel due to viscous dragging force applied to core fluid thread by surrounding sheath fluid, as shown on left part; coiling phenomenon can also be triggered by vertically impinging the microfluidic-spun straight core fluid thread onto a flat horizontal surface (Fig. S1). The summary of synthesis conditions is given in Table S1.

2. Coiling formation and synthesis of coiled structure can be investigated and performed in microfluidic channel (Fig. S2).

3. Synthesis of pillar-like coiled structure with large amplitude can be achieved by triggering coiling on bottom surface of collection bath. (Fig. S3)

4. Synthesis of supercoiled structure can be achieved by triggering coiling both in microfluidic channels and on bottom surface of collection bath. (Fig. S4)

Shape	Dimension (Amplitude)	Fluids composition						Flowrate set ($\mu L/min$:$\mu L/min$)	Collection Bottom Type
		Core				Sheath			
		Alginate			Citrate concentration	$CaCl_2$ concenration	PEG-6000 concentration		
		Viscosity (cP)	concetration (wt%)	Molecular weight level					
Primarily coiled	Micro-scale ($\sim$ 850 μm)	$\sim$ 800	1%	Large ($\sim$ 800 cP @ 1wt%)	50 mM $\sim$ 150 mM	250 mM	N/A	20:75, 80:200, 160:400	Cone
Primarily coiled	Macro-scale (1.4 mm $\sim$ 2.6 mm)	$\sim$500	3%	Medium ($\sim$ 120 cP @ 1wt%)	250 mM	100 mM	80 g/L	10:1000, 10:1500, 10:2000	Flat
Secondarily coiled (Supercoiled)	Macro-scale ($\sim$ 3.6 mm)	$\sim$500	3%	Medium ($\sim$ 120 cP @ 1wt%)	200 mM	150 mM	80 g/L	20:300	Flat

Table S1 Summary table of experimental parameter sets in correspondence with the shape and dimension achieved by each set of parameters.

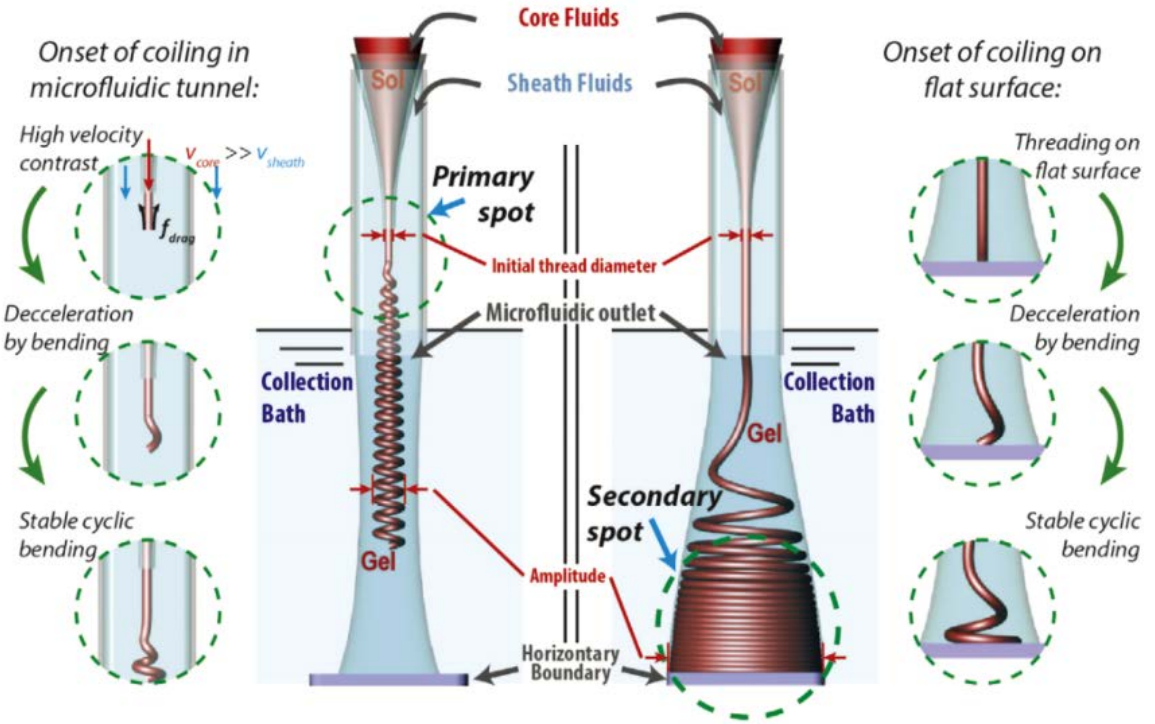

Fig. S1 Representative schematic sketch of the two methods for triggering the coiling phenomenon. © 2017 Elsevier B.V.

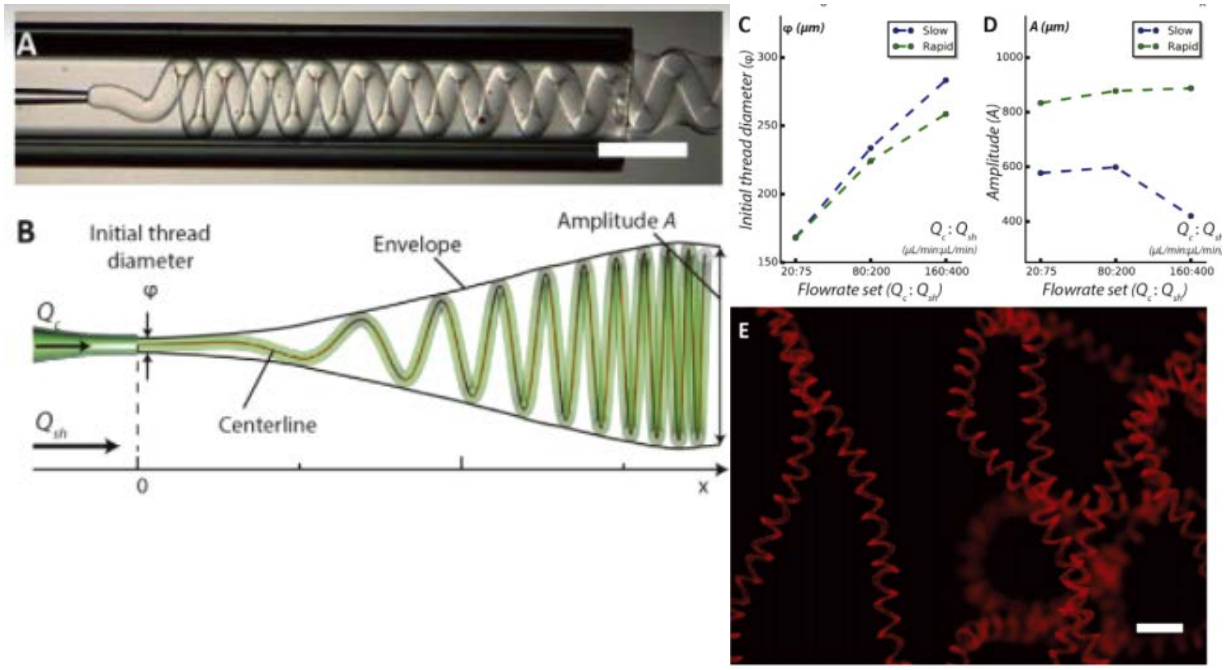

Fig. S2 Coiling formation and synthesis of coiled structure in microfluidic channel. Scale bars: (A and E) 1.5 mm. © 2017 Elsevier B.V.

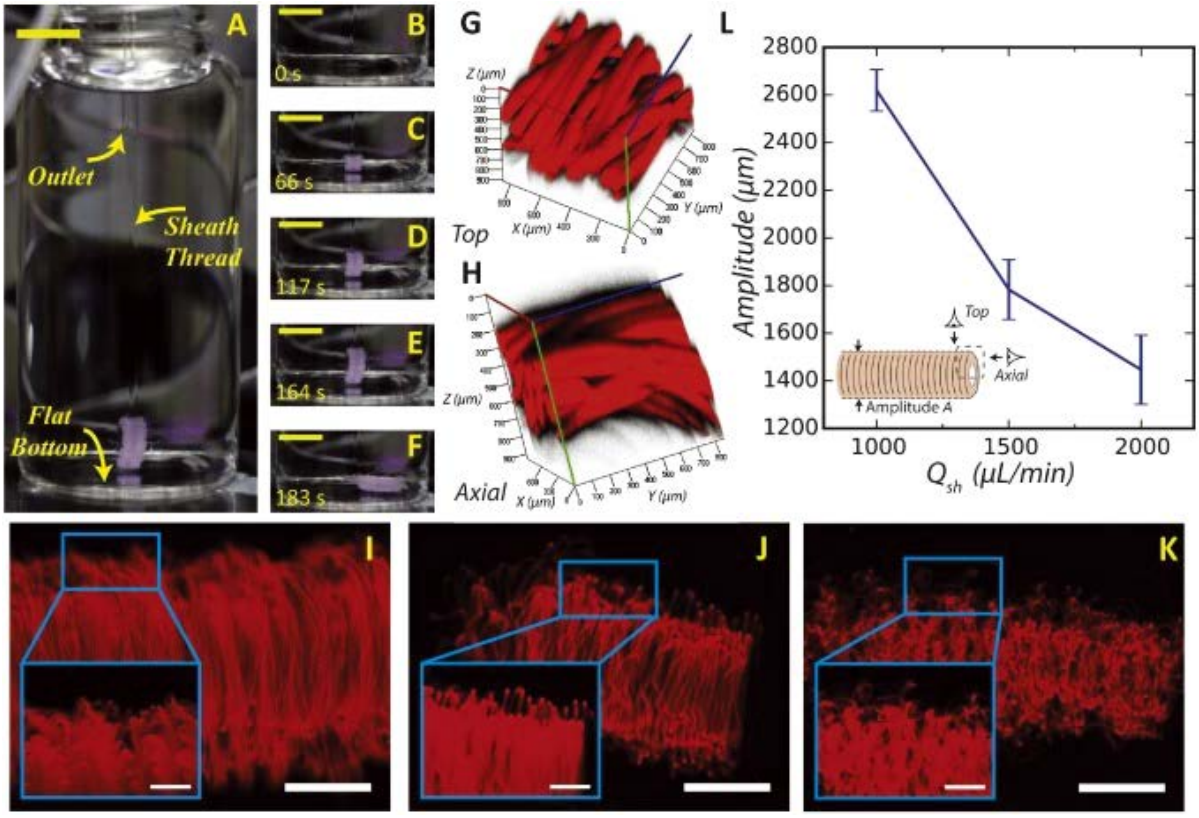

Fig. S3 Synthesis of pillar-like coiled structure with large amplitude by triggering coiling on bottom surface of collection bath. Scale bars: (A–F) 10 mm, (I–K) 1 mm (500 μm for the insets).

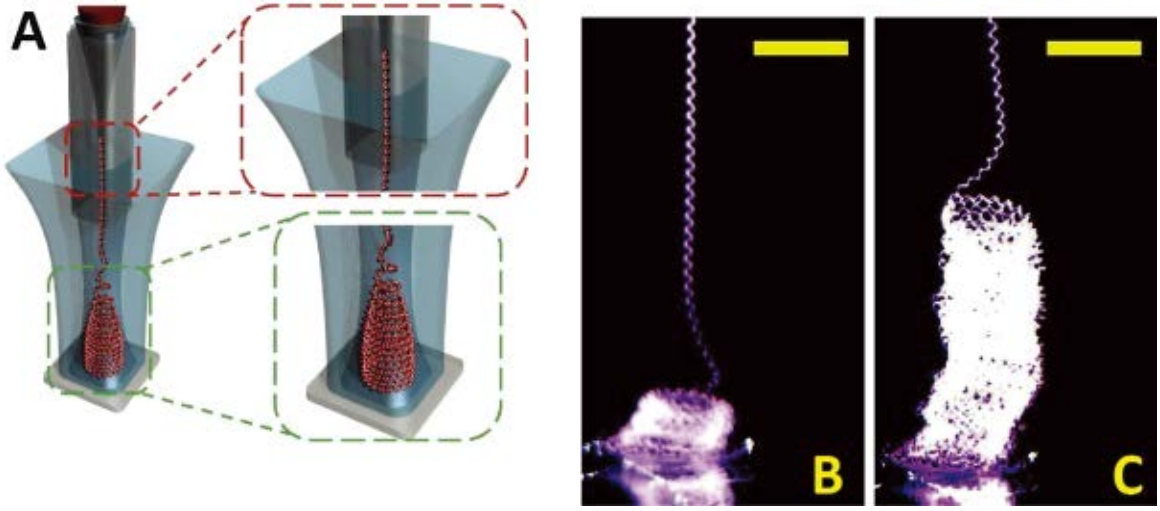

Fig. S4 Synthesis of supercoiled structure by triggering coiling both in microfluidic channels and on bottom surface of collection bath. Scale bar: 3.5 mm.

Acknowledgement

本項目は個人情報保護の観点から非公開とする

以上

博士論文

聶 銘昊

Nie Minghao